UNIVERSITAT POLITÈCNICA DE VALÈNCIA

Escuela de Doctorado

Programa de Doctorado en Infraestructuras de Transporte y Territorio

STUDY OF THE CLIMATE CHANGE EFFECT ON THE SNOW WATER RESOURCES IN THE SPANISH MOUNTAINS

DOCTORAL THESIS

Author

Eduardo Lastrada Marcén

Directors

Dr. Guillermo Cobos Campos

Dr. F. Javier Torrijo Echarri

Valencia, July 2022

A María, Inés y Álvaro

Ideale sind wie Sterne, man kann sie nicht erreichen, aber man kann sich an ihnen orientieren

Los ideales son como las estrellas, no se pueden alcanzar, pero te puedes orientar con ellas.

Carl Schurz

No basta con preguntarse qué planeta dejaremos a nuestros hijos, sino qué hijos dejaremos a nuestro planeta.

Pierre Rabhi

Agradecimientos / Acknowledgements

En primer lugar querría agradecer a aquellos visionarios, adelantados a su época, que hace 40 años iniciaron en nuestro país el programa de Evaluación de Recursos Hídricos procedentes de la INnivación (ERHIN), gracias al cual se dispone de un maravilloso registro histórico de datos y que son de gran ayuda para las investigaciones del presente y del futuro. Miguel Arenillas, Alfonso Pedrero, Eduardo Martínez de Pisón, César Ferrer y tantos otros.

Del mismo modo, quiero agradecer a los que a día de hoy han tomado el relevo del programa ERHIN y siguen impulsándolo con la misma pasión. Es el caso de Fernando Pastor, Francisco Javier Sánchez, Maria Luisa Moreno, Javier Sanromán y muchos más.

Mención especial merece Miguel Arenillas, con quién hace 15 años empecé a trabajar por primera vez en el glaciar de la Maladeta, mi primer flechazo con la alta montaña, experiencia que jamás se olvida.

No quiero olvidarme de mis compañeros José Agustín Collado (arquitecto del modelo ASTER), Julio Garzón o Fernando Gutiérrez, ni de los compañeros de campo o glaciar; Alfonso Pedrero Muñoz, Alberto Barseló, Miguel Motes y Paco Aguado, por la ayuda prestada siempre que ha sido requerida.

Quiero agradecer a mis directores de tesis, Francisco Javier Torrijo y Guillermo Cobos, por sus sabios y sosegados consejos y su inestimable guía en este arduo camino. Especialmente, a mi gran amigo Guillermo.

Por último, le doy las gracias a mi familia, por todo su apoyo y los valores y educación inculcados. A mi hermana Marta, a Carmina, mi madre y a José Eduardo, mi padre, allá donde estés te llevo en mi corazón todos los días de mi vida. A Jesús y a Toni.

Pero en especial, a María, mi compañera de viaje y amor de mi vida, por tantas cosas; y a mis hijos Inés y Álvaro, las estrellas que me orientan, por todos los ratos robados y tantas puertas abiertas de puntillas para poder ver a su padre, y con su sonrisa, darle la inspiración y la motivación para terminar esta tesis. Gracias.

Resumen

El cambio climático indudablemente afectará los eventos de nieve ya que se espera que la temperatura y la precipitación cambien en el futuro. Las montañas españolas se ven especialmente afectadas por esta situación, ya que el almacenamiento de nieve se concentra en periodos muy concretos del año hidrológico y juega un papel muy importante en la gestión de los recursos hídricos. En este estudio se realiza en primer lugar un análisis del comportamiento de los fenómenos complejos relacionados con la nieve en las cuatro principales regiones montañosas de España en los próximos 50 años. El modelo hidrológico ASTER se aplica utilizando como insumo básico datos de temperatura y precipitación, estimados bajo un escenario de cambio climático. Los resultados muestran diferentes cambios en los caudales máximos y promedio esperados, dependiendo de la muy diferente magnitud y signo de los cambios en la precipitación. Puede producirse un aumento de los episodios de inundación como consecuencia de una compleja relación entre los cambios en las precipitaciones y un aumento de las intensidades máximas de deshielo que oscilan entre el 2,1% en los Pirineos y el 7,4% en la Cordillera Cantábrica. Sin embargo, los patrones comunes se muestran en una menor duración de las reservas de masa de nieve, que se espera que ocurra 45 días antes para la Cordillera Cantábrica, y alrededor de 30 días para el resto de las regiones montañosas estudiadas. Los cambios observados también conducen a una disminución preocupante del efecto regulador de los fenómenos relacionados con la nieve en los ríos españoles, con una disminución de la acumulación media de nieve que oscila entre un 28% para Pirineos y Sierra Nevada y un 42% para el Sistema Central y la Cordillera Cantábrica. Se espera una disminución del caudal medio, que fluctúe desde el 2,4% en los Pirineos hasta el 7,3% en la Cordillera Cantábrica, aumentando únicamente en el Sistema Central un 4,0%, siendo necesario desarrollar nuevas medidas de adaptación al cambio climático.

Por otro lado, con el fin de lograr una mejor estimación del Equivalente de agua de nieve (SWE) utilizando una red meteorológica y de profundidad de nieve (SD) económica y extensa; y que mejore la calibración del modelo hidrológico ASTER, se proporcionan

nuevos modelos de regresión de densidad de nieve (SDEN). A partir del gran banco de datos de densidad de nieve (SDEN) existente para los Pirineos españoles, siendo una de las zonas más importantes y mejor monitorizadas del mundo, se evalúan modelos de regresión lineal simple y múltiple que relacionan SDEN con la intra-dependencia del tiempo anual y otros factores como la precipitación acumulada estacional, las temperaturas promedio de 7 días, la profundidad de la nieve (SD) y la elevación. La precipitación estacional acumulada presentó una influencia más dominante que la precipitación diaria, siendo usualmente el segundo factor determinante de SDEN, seguido por la temperatura. Las temperaturas medias mostraron el mejor ajuste a SDEN. Los resultados mostraron tasas de densificación similares que oscilaban ampliamente entre 0,7 x 10^{-3} kg/L/día y 2 x 10^{-3} kg/L/día sin mostrar un patrón espacial. La tasa de densificación para el conjunto de muestras manuales se fijó en 1,2 x 10^{-3} kg/L/día, muy similar al conjunto de medidas automáticas (1,3 x 10^{-3} kg/L/día). Los resultados aumentan el conocimiento sobre SDEN en los Pirineos, aunque hay que tener en cuenta la alta variabilidad espacial encontrada. Estimar una relación entre SDEN y varios factores climáticos nos permite además tener en cuenta el impacto de la variabilidad climática en SDEN.

Finalmente, como continuación a la metodología inicial, se estudian los efectos que el cambio climático puede tener en las inundaciones para un caso de estudio de una cuenca nival de la Cordillera Cantábrica. Las inundaciones son uno de los peligros naturales que más podría verse afectado por el cambio climático, causando grandes daños económicos y víctimas en el mundo. En diciembre de 2019 en Reinosa (Cantabria, España), tuvo lugar una de las peores inundaciones que se recuerdan. La implementación de la DIRECTIVA 2007/60/CE para la evaluación y gestión del riesgo de inundación en España permitió la detección de esta cuenca hidrográfica con un potencial riesgo de inundación significativo a través de una evaluación preliminar del riesgo de inundación, y se desarrollaron mapas de peligrosidad y riesgo de inundación. El objetivo principal de la parte final de este estudio es presentar una metodología para estimar los efectos del cambio climático sobre la peligrosidad y el riesgo de inundaciones, con Reinosa como caso de estudio. Esta cuenca fluvial se ve afectada por el fenómeno de las nieves, siendo aún más sensible al cambio climático. Usando diferentes modelos climáticos, considerando un escenario de emisiones de gases de efecto invernadero comparativamente altas (RCP8.5), con datos diarios de temperatura y precipitación entre los años 2007-2070, y comparando los resultados en términos relativos, se estiman el caudal y la variación del riesgo de inundación debido al cambio climático. En el caso concreto de Reinosa, el modelo climático MRI-CGCM3 muestra que el cambio climático provocará un aumento significativo de habitantes potenciales afectados y daños económicos por riesgo de inundaciones. Esta evaluación nos permite definir acciones de mitigación en términos de análisis de coste-beneficio y priorizar las que deben incluirse en los planes de gestión del riesgo de inundaciones.

Abstract

Climate change undoubtedly will affect snow events as temperature and precipitation are expected to change in the future. Spanish mountains are especially affected by that situation, since snow storage is there focussed on very specific periods of the hydrological year and plays a very important role in the management of water resources. In this study, an analysis of the behaviour of the complex snow-related phenomena in the four main mountain regions of Spain in the next 50 years is conducted. The ASTER hydrological model is applied using temperature and precipitation data as basic input, estimated under a climate change scenario. Results show different changes in the maximum and average expected flows, depending on the very different magnitude and sign of changes in precipitation. An increase of flooding episodes may occur as a result of a complex relation between changes in precipitation and an increase in maximum snowmelt intensities that range from 2.1% in the Pyrenees to 7.4% in the Cantabrian Mountains. However, common patterns are shown in a shorter duration of the snow bulk reserves, expected to occur 45 days earlier for the Cantabrian Mountains, and about 30 days for the rest of the studied mountain regions. Changes observed also lead to a concerning decrease in the regulatory effect of the snow-related phenomena in the Spanish rivers, with a decrease in the average snow accumulation that ranges from about 28% for the Pyrenees and Sierra Nevada to 42% for the Central System and the Cantabrian Mountains. A decrease in average flow is expected, fluctuating from 2.4% in the Pyrenees to 7.3% in Cantabrian Mountains, only increasing in the Central System by 4.0%, making all necessary to develop new adaptation measures to climate change.

In order to achieve a better estimation of Snow Water Equivalent (SWE) using an economical and extensive snow depth (SD) and meteorological network that leads to improve the calibration of ASTER hydrological model, new snow density (SDEN) regression models are given in this work. Based on the most significant dataset of snow

density (SDEN) in the Spanish Pyrenees for on-site manual samples and automatic measurements, as one of the most important and best monitored areas in the world, single and multiple linear regression models are evaluated that relate SDEN with intra-annual time dependence and other drivers such as the seasonal accumulated precipitation, 7-day average temperatures, snow depth (SD) and elevation. The seasonal accumulated precipitation presented a more dominant influence than daily precipitation, usually being the second most dominant SDEN driver, followed by temperature. Average temperatures showed the best fitting to SDEN. The results showed similar densification rates ranging widely from 0.7×10^{-3} kg/L/day to 2×10^{-3} kg/L/day without showing a spatial pattern. The densification rate for the set of manual samples was set to 1.2×10^{-3} kg/L/day, very similar to the set of automatic measurements (1.3×10^{-3} kg/L/day). The results increase knowledge on SDEN in the Pyrenees, although the high spatial variability that has been found must be regarded. Estimating a relationship between SDEN and several climate drivers enables us to take into account the impact of climate variability on SDEN.

Finally, as a continuation of the initial methodology, the effects that climate change can have on floods are studied for a case study of a snow basin in the Cantabrian Mountains. Floods are one of the natural hazards that could be most affected by climate change, causing great economic damage and casualties in the world. On December 2019 in Reinosa (Cantabria, Spain), took place one of the worst floods in memory. Implementation of DIRECTIVE 2007/60/EC for the assessment and management of flood risks in Spain enabled the detection of this river basin with a potential significant flood risk via a preliminary flood risk assessment, and flood hazard and flood risk maps were developed. The main objective of the final part of this study is to present a methodology to estimate climate change's effects on flood hazard and flood risk, with Reinosa as the case study. This river basin is affected by the snow phenomenon, even more sensitive to climate change. Using different climate models, regarding a scenario of comparatively high greenhouse gas emissions (RCP8.5), with daily temperature and precipitation data from years 2007–2070, and comparing results in relative terms, flow rate and flood risk variation due to climate change are estimated. In the specific case of Reinosa, the MRI-CGCM3 climate model shows that climate change will cause a significant increase of potential affected inhabitants and economic damage due to flood risk. This evaluation enables us to define mitigation actions in terms of cost–benefit analysis and prioritize the ones that should be included in flood risk management plans.

Resum

El canvi climàtic afectarà indubtablement els esdeveniments de neu ja que s'espera que la temperatura i la precipitació canvien en el futur. Les muntanyes espanyoles estan especialment afectades per aquesta situació, ja que l'emmagatzematge de neu es concentra en períodes molt concrets de l'any hidrològic i juga un paper molt important en la gestió dels recursos hídrics. En aquest estudi es fa una anàlisi del comportament dels fenòmens complexos relacionats amb la neu a les quatre principals regions muntanyoses d'Espanya en els propers 50 anys. El model hidrològic ASTER s'aplica utilitzant com a insum bàsic dades de temperatura i precipitació, estimades sota un escenari de canvi climàtic. Els resultats mostren diferents canvis en els cabals màxims i la mitjana esperada, depenent de la molt diferent magnitud i signe dels canvis en la precipitació. Es pot produir un augment dels episodis d'inundació com a conseqüència d'una relació complexa entre els canvis en les precipitacions i un augment de les intensitats màximes de desglaç que oscil·len entre el 2,1% als Pirineus i el 7,4% a la Serralada. Cantàbrica. Tot i això, els patrons comuns es mostren en una menor duració de les reserves de massa de neu, que s'espera que ocórreguen 45 dies abans per a la Serralada Cantàbrica, i al voltant de 30 dies per a la resta de les regions muntanyoses estudiades. Els canvis observats també condueixen a una disminució preocupant de l'efecte regulador dels fenòmens relacionats amb la neu als rius espanyols, amb una disminució de l'acumulació mitjana de neu que oscil·la entre un 28% per als Pirineus i Sierra Nevada i un 42% per al Sistema Central i la Serralada Cantàbrica. S'espera una disminució del cabal mitjà, que fluctua des del 2,4% als Pirineus fins al 7,3% a la Serralada Cantàbrica, augmentant únicament al Sistema Central un 4,0%, i cal desenvolupar noves mesures d'adaptació al canvi climàtic.

D'altra banda, per tal d'aconseguir una estimació millor de l'Equivalent d'aigua de neu (SWE) utilitzant una xarxa meteorològica i de profunditat de neu (SD) econòmica i extensa que condueix a millorar el calibratge del model hidrològic ASTER, en aquest document es proporcionen nous models de regressió de densitat de neu (SDEN). A partir del banc de dades més significatiu de densitat de neu (SDEN) als Pirineus espanyols, i sent una de les zones més importants i millor monitorizades del mon per a mostrejos manuals in situ i mesures automàtiques, s'avaluen models de regressió lineal simple i múltiple que relacionen SDEN amb intra-dependència del temps anual i altres factors com la precipitació acumulada estacional, les temperatures mitjana de 7 dies, la profunditat de la neu (SD) i l'elevació. La precipitació estacional acumulada va presentar una influència més dominant que la precipitació diària, sent usualment el segon factor determinant de SDEN més dominant, seguit per la temperatura. Les temperatures mitjanes van mostrar el millor ajustament a SDEN. Els resultats van mostrar taxes de densificació similars que oscil·laven àmpliament entre 0,7 x 10^{-3} kg/L/dia i 2 x 10^{-3} kg/L/dia sense mostrar un patró espacial. La taxa de densificació per al conjunt de mostres manuals es va fixar en 1,2 x 10^{-3} kg/L/dia, molt semblant al conjunt de mesures automàtiques (1,3 x 10^{-3} kg/L/dia). Els resultats augmenten el coneixement sobre SDEN als Pirineus, encara que cal tindre en compte l'alta variabilitat espacial trobada. Estimar una relació entre SDEN i diversos factors climàtics ens permet tindre en compte l'impacte de la variabilitat climàtica a SDEN.

Finalment, com a continuació a la metodologia inicial, s'estudien els efectes que el canvi climàtic pot tindre en les inundacions per a un cas d'estudi d'una conca nival de la Serralada Cantàbrica. Els efectes que el canvi climàtic pot tindre en les inundacions són un dels perills naturals que més es podria veure afectat pel canvi climàtic, causant grans danys econòmics i víctimes al món. El desembre del 2019 a Reinosa (Cantàbria, Espanya), va tenir lloc una de les pitjors inundacions que es recorden. La implementació de la DIRECTIVA 2007/60/CE per a l'avaluació i la gestió del risc d'inundació a Espanya va permetre la detecció d'aquesta conca hidrogràfica amb un risc d'inundació significatiu potencial a través d'una avaluació preliminar del risc d'inundació, i es van desenvolupar mapes d'amenaça i risc d'inundació. L'objectiu principal de la part final d'aquest estudi és presentar una metodologia per a estimar els efectes del canvi climàtic sobre l'amenaça i risc d'inundacions, amb Reinosa com a cas d'estudi. Aquesta conca fluvial es veu afectada pel fenomen de les neus, sent encara més sensible al canvi climàtic. Usant diferents models climàtics, considerant un escenari d'emissions de gasos d'efecte hivernacle comparativament altes (RCP8.5), amb dades diàries de temperatura i precipitació dels anys 2007-2070, i comparant els resultats en termes relatius, la taxa de flux i la variació del risc d'inundació degut al canvi climàtic són estimat. En el cas concret de Reinosa, el model MRI-CGCM3 mostra que el canvi climàtic provocarà un augment significatiu d'habitants potencials afectats i danys econòmics per risc d'inundacions. Aquesta avaluació ens permet definir accions de mitigació en termes d'anàlisi de cost-benefici i prioritzar les que s'han d'incloure als plans de gestió del risc d'inundació.

Table of Contents

List of Figures

List of Tables

List of Acronyms

AEMET – Agencia Estatal de METeorología

ANA – Analogic downscaling method

AR5 – Fifth Assessment Report

CMIP – Coupled Model Intercomparison Project

CRN – Cosmic-Ray Neutron

CV – Coefficient of variation

EFAS – European Flood Awareness

ERHIN – Evaluación de Recursos Hídricos procedentes de la INnivación

FRA – Flood Risk Assessments

GCM – Global Climate Models

IPCC – International Panel on Climate Change

MITECO – MInisterio para la Transición ECOlógica

MLRs – Multiple linear regressions

MRI – Meteorological Research Institute

NSE – Nash-Sutcliffe parameter

NWSRFS – National Weather Service River Forecast System

PREEMPT – Policy-relevant assessment of economic and social effects of hydro-meteorological disasters

RCP – Representative Concentration Pathways

SD – Snow Depth

SDEN – Snow DENsity

SWE – Snow Water Equivalent

TNMs – Telenivometers

Chapter 1
Introduction

1.1. Content

This doctoral thesis is presented in the form of a compendium of articles.

The content of the doctoral thesis has been organized in different chapters, after which the references are cited in the document and different appendices are provided.

- Chapter 1 describes the content, objectives and main contributions of the doctoral thesis.

- Chapter 2 analyses the state of the art, describes the materials and methods applied to achieve the objectives and includes the results of the article:
    - "*A decrease in the regulatory effect of snow-related phenomena in Spanish mountain areas due to climate change*". https://doi.org/10.3390/w13111550

- Chapter 3 analyses the state of the art, describes the materials and methods applied to achieve the objectives and includes the results of the article:
    - *"Seasonal variability of snow density in the Spanish Pyrenees".* https://doi.org/10.3390/w13111598

- Chapter 4 analyses the state of the art, describes the materials and methods applied to achieve the objectives and includes the results of the article:

- *"Analysis of Climate Change's Effect on Flood Risk. Case Study of Reinosa in the Ebro River Basin"*. https://doi.org/10.3390/w12041114

- Chapter 5 contains a discussion for the different results of the three articles, as well as a global discussion.

- Chapter 6 includes the conclusions of this study and a suggestion of future researches.

- Chapter 7 contains the final conclusion of the doctoral thesis.

The original articles are included as three appendices. Supplementary material for these studies can be found online in the original articles[1].

[1]https://doi.org/10.3390/w13111550
https://doi.org/10.3390/w13111598
https://doi.org/10.3390/w12041114

1.2. Context

The ERHIN program was started in the 1980s (ERHIN programme, 2021), implementing an extensive measurement network that currently provides a valuable historical record of data for improving knowledge of the snow phenomenon in Spain, thanks to visionary experts such as Miguel Arenillas and Eduardo Martínez de Pisón, in the Department of Geotechnical Engineering of the Polytechnic University of Valencia. These studies were continued with the doctoral theses of Ramiro Martínez (Martínez, 1988), defining the areas to be monitored, Isidro Cantarino (Cantarino I. , 1994), setting the fundamentals of ASTER hydrological model and Guillermo Cobos (Cobos, 2004), configuring a geostatistical model to quantify the snow water resources based on the monitoring network that would additionally serve to calibrate the ASTER hydrological model. All these studies form the foundations of the doctoral thesis presented in this document, carried out from 2018 to 2022.

In the last decades, other researchers have analysed the phenomenon of snow and its contribution to flooding in Spain. It is worth mentioning the assessment of a decrease in winter precipitation in the last 50 years that cause a decrease in both winter and spring discharges (López Moreno & García-Ruiz, 2004); estimating the contribution of snowmelt for a case study in one of the most important extreme events in the Pyrenees (Corripio & López-Moreno, 2017); characterizing mountain river regimes in the Spanish Pyrenees and assessing the significance of snow accumulation and snowmelt on the timing of daily river flows (Sanmiguel_Vallelado, Morán-Tejeda, Alonso-González, & López-Moreno, 2017); estimating daily gridded snowpack for the Iberian Peninsula from 1980 to 2014 (Alonso-González, et al., 2018) or characterizing the major floods in Spanish mountain rivers, with 47% of 250 major floods having a snow contribution higher than 10%, and of 18% in average terms (Morán-Tejeda, et al., 2019).

The overall object and specific objectives of this work are described in the next section.

1.3. Objectives

The object of this thesis is the study of the climate change effects on the snow water resources in the Spanish mountains. This is achieved by addressing three different specific objectives:

(1) The study of the effect of climate change on the regulatory effect of snow in Spanish mountain areas.
(2) The assessment of seasonal and spatial variability of snow density in the Spanish Pyrenees.
(3) The study of the effect of climate change on flood risk in basins where the snow phenomenon is significant, with the case study of Reinosa in the Ebro river basin.

Firstly, in this doctoral thesis, the expected behaviour of the snow-related phenomena in Spain in a future scenario considering the effect of climate change and their consequences in the regulatory effect that snow has on Spanish rivers are assessed. The main variables that control the snow-related phenomena are studied: temperature, precipitation, snowfall, snow accumulation, snowmelt and flow produced. Four Spanish mountain regions are analysed: the Pyrenees, Sierra Nevada, the Central System and the Cantabrian Mountains. The results of this work contribute to improve the knowledge about the effect of climate change on water resources in the form of snow in the main mountain regions of Spain, with few previous similar studies in the same region (Morán-Tejeda, Lorenzo-Lacruz, López-Moreno, Rahman, & Beniston, 2014) .

In this work, those variables that control the snow-related phenomena are obtained using the hydrological model ASTER (Cantarino I. , 1998); (Cobos & Collado, 2019); (Cobos, 2004); (Cobos, Francés, & Arenillas, 2010), a model applied in several countries and implemented by Spanish water authorities as an accurate model in river basins with strong snow phenomena. The obtained results enable establishing both the actual state and the future scenario, considering forecasts given by climate models approved by the IPCC (AEMET, 2021) .

In the near future, a more efficient consumption of water will be required to allow a sustainable life system over time. The management of water resources in a country like Spain, where those resources are scarce, will be more complex. The study on how the snow-related hydrological processes evolve in the main mountainous areas of Spain is therefore decisive to quantify its regulatory effect and establish future management plans.

Secondly, from the different parameters defining snow-related phenomena, snow density (SDEN) relates snow depths (SDs) with the snow water equivalent (SWE). Since SD measurements are much more frequent and accurate than the available SWE data, better knowledge and parameterization of SDEN will enable the achievement of a better estimation of the SWE based on SD measurements. Moreover, as wind data become more available, hydrological models can determine a more accurate estimation of forced-

convection snowmelt and snow transport, for which SDEN is needed. However, SDEN is a complex parameter that can vary temporally, spatially and even within the snowpack profile in the vertical direction.

The novelty of this study remains in the definition of SDEN variability in the Spanish Pyrenees, using the vast amount of data from the ERHIN program obtained from manual sampling and non-destructive automatic measurements. A series of relationships are established with other parameters, and its temporal and spatial variability is characterized. To achieve this goal, a series of single and multiple linear regressions are conducted, relating SDEN with the time evolution variability and the most important climate drivers (seasonal accumulated precipitation, SD, elevation and average temperatures).

Finally, using a study case in Reinosa, a new methodology is set to estimate flow and flood risk variation due to climate change regarding a scenario of comparatively high greenhouse gas emissions (RCP8.5), with daily temperature and precipitation data.

1.4. Contributions of the doctoral thesis

Firstly, the expected behaviour of the snow-related phenomena in Spain in a future scenario considering the effect of climate change and their consequence in the regulatory effect that snow has on Spanish rivers are assessed, considering forecasts given by climate models approved by the IPCC.

Additionally, a series of single and multiple linear regressions are conducted, relating SDEN with the time evolution variability, seasonal accumulated precipitation, SD, elevation and average temperatures in the Spanish Pyrenees.

Finally, a new methodology to estimate flow and flood risk variation due to climate change has been set, giving specific results for Reinosa, in the Cantabrian Mountains.

Chapter 2

A decrease in the regulatory effect of snow-related phenomena in Spanish mountain areas due to climate change

Lastrada, E.; Garzón-Roca, J.; Cobos, G.; Torrijo, F.J. A Decrease in the Regulatory Effect of Snow-Related Phenomena in Spanish Mountain Areas Due to Climate Change. *Water* 2021, *13*, 1550. https://doi.org/10.3390/w13111550

2.1. Introduction.

In the current era, where society demands sustainable development together with a respectful treatment of the environment, the availability of water resources is an essential issue both qualitatively and quantitatively. The quantification of water resources in the form of snow is therefore of high interest as it corresponds to a natural system for regulating the flow of water.

Researches showed the connection between the timing and volume of snow accumulation and snowmelt in hydrological systems (Barry, 1992); (Beniston, 1997); (Nijssen, B., O'Donell, G.M., Hamlet, A. F., & Lettenmaier, D.P., 2001) . Snow melting creates a set of water resources which need to be controlled and quantified, establishing their flow contribution to the rivers. Forecasting both variables, snowmelt and flow contribution, is important for the ordinary management that each Basin Organization performs and acquires great relevance for managing extreme hydrological phenomena, i.e., droughts and flooding, especially when trying to envisage and mitigate the damage they may cause (Lastrada, Cobos, & Torrijo, 2020); (Soulsby, Helliwell, Ferrier, Jenkins, & Harriman, 1997); (Moore, Hamilton, & Scibek, 2002); (Krasovskaia & Gottschalk, 2002); (Ye, Yang, & Kaine, 2003).

In Spain, the meteorological conditions of mountainous areas, as well as their geographical and geomorphological characteristics, cause the snow-related phenomena to be focussed on very specific periods of the hydrological year, mainly between December and May, while presenting great variability in time and location (Arenillas, Cobos, G., & Navarro, 2008). Accumulated precipitations in the form of snow take place in these areas between November and April, while snowmelt is centred in spring, in the March–June period. This aspect implies an important regulatory effect of water resources (López Moreno & García-Ruiz, 2004), as the incorporation of the snowfalls into the fluvial channels are delayed during winter - at that time, snow is accumulated in the mountains. Additionally, snow plays an important role in the infiltration of water resources (Mora Alonso-Muñoyerro, 2015)

Snowmelt in the highest parts of Spanish basins starts in spring and accelerates between the end of March and April, even continuing until July in the highest areas of the Pyrenees (Arenillas, Cobos, G., & Navarro, 2008); (López Moreno & García-Ruiz, 2004). Normally this melted snow is gradually incorporated into the river networks and the reservoirs as runoff (ordinary regulation). Therefore, snow regulates the water resources of the country as it ensures a base flow in the rivers during the beginning of the summer period, which is characterized by low precipitation, high evapotranspiration and significant water demand. However, in certain specific weather conditions, such as a rapid increase in temperature combined with rains, significant melting of snow in short periods may occur, leading to high flows in river channels and causing flooding (Lastrada, Cobos, & Torrijo, 2020).

Changes in the snow patterns in mountains and ranges are undoubtedly one of the clearest indicators that climate change is taking place on our planet since snow is extremely sensitive to changes in global meteorological conditions (Jaagus, 1997); (Henderson & Leathers, 2010); (Szwed, Pinskwar, Kundzewicz, Graczyk, & Mezghani, 2017); (Klein, Vitasse, & Rixen, 2016); (Beniston, Keller, & Goyette, 2003); (Vincent, et al., 2004); (Zemp, et al., 2015). Snow depends on the type of precipitation, i.e., in the form of snow or liquid, and water resources associated also depend on the duration of snow in mountains and the speed of snowmelt, which leads snow to disappearing as a stored water resource, being integrated into the river network. Both aspects are related among other factors to temperature (Ye & Lau, 2017). An increment in temperature, as

expected in climate change scenarios, will reduce precipitation in form of snow and considerably affect snowmelt by accelerating it, affecting not only water flow, but also water infiltration (Mora Alonso-Muñoyerro, 2015).

The Pyrenees, Sierra Nevada, the Central System and the Cantabrian Mountains were the Spanish mountain regions selected to be studied in this work. Those areas are defined by Spanish Institutions (ERHIN programme, 2021) as regions where the snow-related phenomena reach a special relevance. These four regions also match with areas occupied by ice during the last ice age.

The Pyrenees extends about 490 km between Spain and France and its highest altitude corresponds to the peak of Aneto with 3404 m. The set of headwaters of the main rivers of the Spanish Pyrenees were simulated, covering an area of 10,300 km^2 with an average elevation of around 1400 m.

Sierra Nevada extends about 80 km to the south of Spain and its highest altitude is the Mulhacen with 3479 m. In this region there are two delimited areas: the Guadalquivir river basin and the Mediterranean basin; the simulation covers an area of 1253 km^2 with an average elevation of around 1500 m.

The Central System extends about 600 km in the central area of the Iberian Peninsula, just north of the 40th parallel, and its highest altitude corresponds to the peak of Almanzor with 2592 m. This mountain range is in fact a succession of ranges separated by valleys or mountain passes. Gredos, Guadarrama and Ayllon are some of those ranges. In this region, the simulation covers an area of 7,758 km^2 with an average elevation of around 1069 m. Unlike the two previous regions, the snow-related phenomena in the Central System have unequal importance that depends on each basin since their average levels vary between 850 m and 1500 m.

The Cantabrian Mountains extend about 480 km in the north of Spain, parallel to the Cantabrian Sea (Bay of Biscay) and their highest altitude is the Torre Cerredo with 2648 m; this range is the most western one in Europe. In this region, there are two main areas: the Duero river area and the Cantabrian Sea area. In total, the simulation covers an area of 14,099 km^2 with an average elevation of around 1169 m. Snow is especially important in the cloud fronts coming from the north since this mountain range is the first orographic obstacle found by these fronts in their movement from north to south. The fronts discharge significant precipitations in the form of snow, making the Cantabrian Mountains the largest snow-covered surface of Spain.

Table 2.1 lists the number of basins analysed in each region as well as some statistical values regarding their size along with the actual average values of temperature and precipitation (time period 2007–2018). The location of the regions in Spain and the set of basins studied in each region are displayed in Figure 2.1.

Table 2.1. Basins on each region analysed.

Mountain Range	No. Basins	Total Area [km²]	Basin Area [km²]			Avg. Temperature [°C]	Avg. Precipitation [mm]
			Min	Max	Avg.		
Pyrenees	11	10,300	295	2186	936	5.8	1115
Sierra Nevada	2	1253	177	1076	627	8.5	558
Central System	11	7758	247	1848	775	9.9	1107
Cantabrian Mountains	30	14,099	154	1851	728	7.3	1220

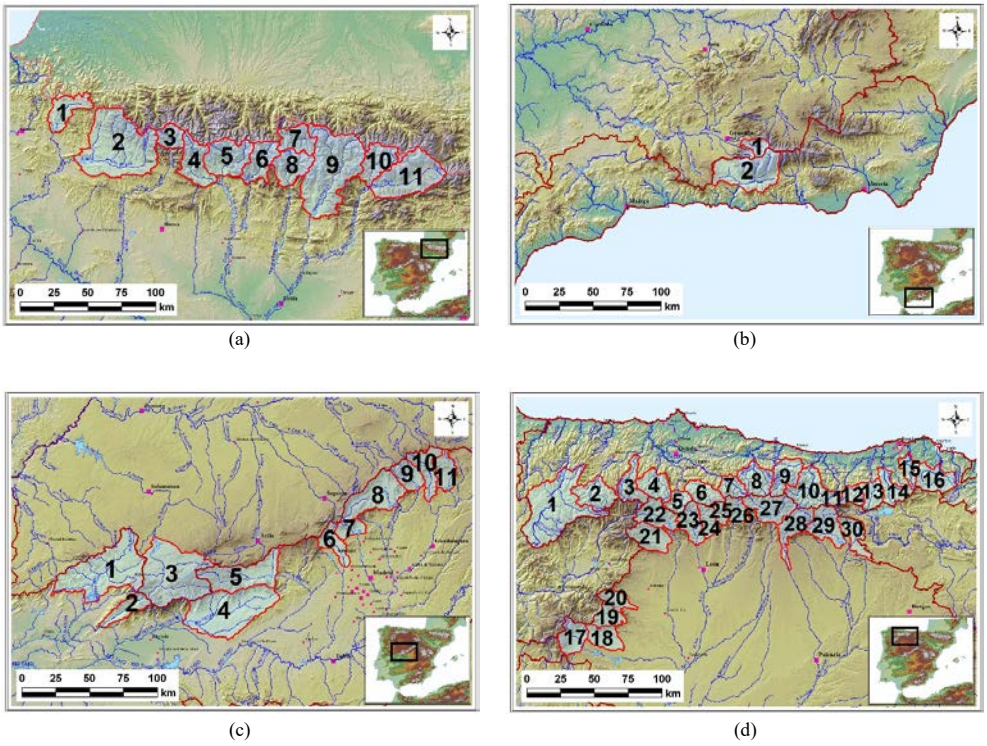

Fig. 2.1. Location of the Spanish mountain regions studied and set of basins analysed on each region: (a) Pyrenees; (b) Sierra Nevada; (c) Central System; (d) Cantabrian Mountains.

2.2. Materials and Methods.

2.2.1. Variables Analysed

The main variables that control the snow-related phenomena and their contribution in terms of water resources are temperature, precipitation, snowfall, snow accumulation, snowmelt and flow produced.

Temperature fluctuation over a year affects the precipitation in form of snow as well as melting period and speed. Temperature evolution is essential to define what will be the change in the importance of snow in each region and what will be the change in the way in which this resource becomes part of the flows in rivers (melting).

Precipitation may be in form of snow or water, with the threshold temperature between these two varying from +2 °C to −2 °C according to several atmospheric conditions. Thus, precipitation refers to the total precipitation while snowfall refers to the precipitation in form of snow. Precipitations evolution will affect the snow-related phenomena, as the more total precipitation the more snowfall, although temperature also influences the latter.

The temperatures and the precipitations (both rainfall and snowfall) are the inputs required by the ASTER model to predict the snow accumulation, the snowmelt and the flow (model outputs).

Snow accumulation refers to the water resources accumulated in the basin in form of snow. These water resources will be incorporated into the river networks (flow) by snowmelt. Usually, snow starts to melt practically at the same time as the first snowfall begins, especially in the lower areas of the basin during the first months.

Later, with the increment of temperatures in spring, melting starts in the highest areas where snow was accumulated throughout the winter. This leads to a rapid increase in the contributions (flow) due to this phenomenon. Thus, the alteration in the temperature regime could cause melting in a basin to be advanced, making it coincide with raining periods and increasing the flows of liquid water in the rivers, raising the risk of flooding and affecting the current management of a basin.

2.2.2. ASTER Hydrological Model

ASTER is a continuous simulation distributed hydrological model that simulates the hydrological behaviour of a high mountain sub-basin and calculates the expected stream flow in a river and the equivalent volume of water stored at any time in the studied basin using precipitation and temperature as the main inputs variables. This model, used currently by Spanish water authorities (Cobos & Collado, 2019); (Cobos, 2004) was specially developed for basins with steep reliefs, with very marked meteorological changes in time and space (Mora, Ferrer, Arenillas, & Cobos, 2004); (Morin, Fortin, Lardeau, Sochanska, & Paquette, 1981). Some remarkable features of the ASTER model include the possibility of choosing different spatial and temporal series for the simulation, the fragmented treatment of precipitation and temperature variables and the

specific and distributed analysis of the snow-related phenomena. In this work a daily time resolution was used, matching the time series resolution provided by the climate models. The daily accumulated precipitation and the average daily temperature were the input variables of the model, from which the evolution of the snow-related phenomena and the daily flows were obtained.

ASTER model calculation algorithm follows the classical hydrological models based on quasi—distributed continuous simulation deposits similar to the Canadian CEQUEAU model (Anderson, 1968), with a variable temporal operating scale. The snowmelt routine is based on the studies carried out by Anderson (Anderson, 1973) and applied in the US model NWSRFS of the National Weather Service (Anderson, 1976), 1976; (Anderson, 2006); (Garijo & Mediero, 2018). Particularly, the model calculates snowmelt and snow accumulation making use of an energy balance equation (Cobos & Collado, 2019); (Cobos, 2004).

For defining the snow accumulation, quantification of snowfall is conducted based on a given temperature named "rain/snow temperature" $T_{rain/snow}$ which is defined for each basin, a typical value being around 1.5 °C. For that value, half precipitation is considered to fall as snow and half as water. If precipitation temperature is greater than $T_{rain/snow}$ by 2 °C, all the precipitation is considered as liquid form. If precipitation temperature is lower than $T_{rain/snow}$ by -2 °C, all the precipitation is considered to fall as snow. A linear interpolation is made between the previous values.

Snowmelt is equal to the result of two components: snowmelt due to precipitation (M_p) and snowmelt without rainfall (M_c).

The snowmelt due to precipitation (M_p) is the snowmelt produced by the precipitation energy and it is calculated using Equation (2.1), assuming the snow surface temperature is equal to 0 °C (Anderson, 1973):

$$M_p = 0.0125 \cdot P \cdot f_p \cdot T_p \qquad \textbf{Equation 2.1}$$

Where, P is the precipitation, in mm; T_p is the temperature of the precipitation, in °C; and f_p is a coefficient that estimates the fraction of precipitation in the form of rain, its value being set to 0.5 for $T_{rain/snow}$. Besides the precipitation energy, other secondary terms like radiation and condensation energy may be added to calculate snowmelt when precipitation occurs.

The snowmelt without rainfall (M_c) corresponds to the snowmelt on a dry day and is calculated using Equation (2.2), which is based on non-forced convection (note that this kind of estimations are commonly used in hydrological models along with other empirical relations depending on air temperature since estimating wind speed is difficult) (Anderson, 2006):

$$M_c = M_f \cdot (T_a - T_{mi}) \qquad \textbf{Equation 2.2}$$

Where, T_a is the air temperature, in °C; T_{mi} is the snowmelt temperature in the basin, in °C; and M_f is the melt factor, in mm/°C, which varies seasonally and depends on several implicit factors, mainly on radiation (latitude, orientation, slope, albedo and vegetation cover), exposition and wind. This factor may be expressed by Equation (2.3) in terms of the maximum melt factor on 21st June ($M_{F,MAX}$) and the minimum melt factor on 21st December ($M_{F,MIN}$), both given in mm/°C/24 h [35,36]:

$$M_f = \frac{M_{F,MAX}+M_{F,MIN}}{2} + sin\left(\frac{n\cdot 2\pi}{366}\right)\cdot\frac{M_{F,MAX}-M_{F,MIN}}{2} \qquad \textbf{Equation 2.3}$$

Where, n is the number of days from 21st March. It should be noted that the value T_{mi} (snowmelt temperature) may be different from 0 °C. For instance, on calm and clear days, when solar radiation dominates the energy balance, melting can occur below 0 °C, while on clear nights, when the long wave radiation emitted is significant, there would be no melting until air temperature exceeds 0 °C. Therefore, T_{mi} needs to be calibrated in each case analysed.

By using the previous equations, the amount of water incorporated in the river networks can be obtained and added to the one directly produced by rain (precipitations in form of water) to estimate the flow expected on each period of the year.

2.2.3. Selection of the Climate Model

The input data required by the ASTER hydrological model are the temperatures and the precipitations (see Section 2.2.1), stemming from climate models.

In this work, temperature and precipitations time series provided by the Spanish Agency of Meteorology AEMET (AEMET, 2021) are considered. In particular, among the 24 climate models made available by AEMET, ANA-MRI-CGCM3-rcp85 was selected for conducting the present study. This model provides regionalized climate projections from the CMIP5 (Coupled Model Intercomparison Project phase 5), according to the IPCC and framed within the greenhouse gas emission scenario (RCP 8.5), by using an analogic downscaling method (ANA).

The motivation for using the ANA-MRI-CGCM3-rcp85 model results is twofold: (i) previous experience; and (ii) current validation (Figure 2.2). Previous experience refers to a previous work carried out by the authors (Lastrada, Cobos, & Torrijo, 2020), where the analyses showed that this climate model achieved a good fit with real annual-average daily-flow-rates. Besides, before using the model again for this study, the authors checked and demonstrated, for the particular case of the Arga river basin (see Figure 2.2), that the validity of the ANA-MRI-CGCM3-rcp85 model predictions still stands.

Figure 2.2 shows the results of a thorough simulation study on the extreme rainfall predictions of several climate models (provided by AEMET), over the period 2011–2017 on the Arga river basin. In the figure, the results of the numerical study are compared

with experimental data measured by the local authorities. According to Ebro Water Authority, Arga river basin is one of the best monitored basins in the region, being the experimental data reliable and thus suitable for validation purposes. From Figure 2.2, it can be concluded that ANA-MRI-CGCM3-rcp85 is the most accurate model and it is thus used as reference climate model for this work.

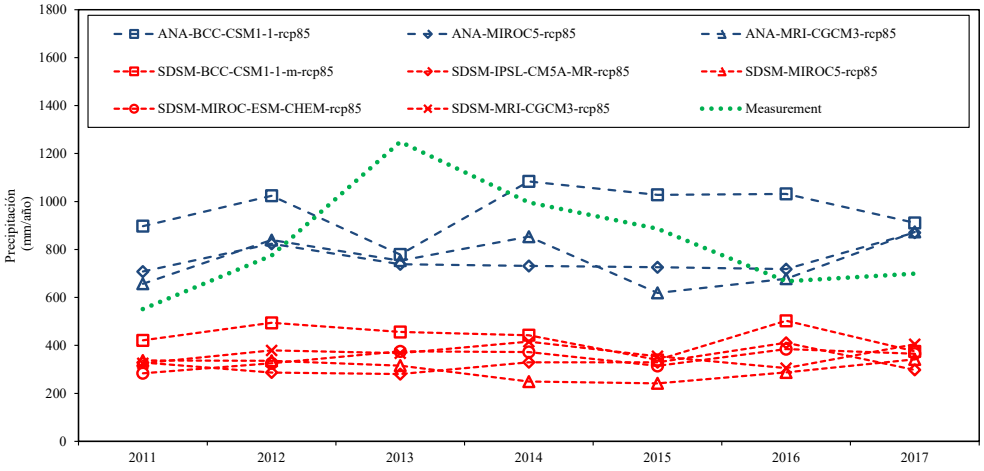

Fig. 2.2. Estimated precipitation in the Arga river basin using several climate models provided by AEMET for the time period 2011–2017 against the real observations measured by local authorities at that period.

2.2.4. Calibration and Validation of the ASTER Model

For each hydrological basin studied in this work, the calibration of the ASTER hydrological model is done against the flow data measured at each of the rivers defining each of the hydrological basins studied, obtained from the recorded level-flow data in gauging stations (flow control points) for the reference time period, which in this case it extended from 1st October 2006 to 30th September 2010. The model is calibrated defining the hydrological parameters that make it possible to optimize the correlation coefficient and the Nash-Sutcliffe parameter (NSE) by statistically analysing the observed flow series and those estimated by the ASTER model. The resulting model is then validated by comparing the flow model predictions from 1st October 2010 to 30th September 2018 with the corresponding available measured data.

Not only the flow, but also the snow accumulation predicted by the ASTER hydrological model in the four regions under analysis is confirmed with measured snow depth and snow density gathered from campaigns carried out three times per year at the snow poles network during the last 30 years (ERHIN programme, 2021).

Table 2.2 shows a summary of the model parameters resulting from the calibration process. The calibration and validation carried out in a previous work for a longer period

(1950–2005) in all the basins of the Pyrenees (Arenillas, Cobos, G., & Navarro, 2008), showed a good consistency of the model to the variability that might be associated with climate change. However, several uncertainties still remain associated with changing climate conditions, such as infiltration due to evolution of vegetation, which may not be easy to predict and may be influenced as well by other anthropic effects non-related with climate change. As snowmelt is calculated based on temperature, other uncertainties associated with changes in incoming radiation or other parameters will result in temperature changes that will be taken into account by the model. As a distributed model, spatial interpolation and temperature and precipitation elevation gradients enable to transform grid data from climate models over complex terrain.

Table 2.2. Calibration parameters.

Parameter	Value	Pyrenees	Sierra Nevada	Central System	Cantabrian Mountains
$M_{F,MAX}$ [mm/°C/24 h]	Minimum	2.00	3.00	1.00	0.74
	Maximum	7.30	6.00	10.00	5.00
	Average	4.60	4.50	4.90	3.15
$M_{F,MIN}$ [mm/°C/24 h]	Minimum	0.10	1.00	0.10	0.10
	Maximum	5.00	2.00	5.00	3.00
	Average	1.35	1.50	1.38	1.60
Snowmelt temperature T_{mi} [°C]	Minimum	−0.25	1.00	0.00	0.10
	Maximum	1.60	2.00	3.00	3.00
	Average	0.65	1.50	1.12	1.17
Rain/snow temperature $T_{rain/snow}$ [°C]	Minimum	0.00	0.00	0.00	−1.70
	Maximum	1.48	2.50	3.10	4.00
	Average	0.88	1.25	0.96	0.67
Altimetry temperature gradient [°C/1000 m]	Minimum	−6.10	−6.50	−8.00	−6.00
	Maximum	−3.00	−6.30	−4.00	−1.77
	Average	−4.70	−6.40	−5.98	−4.37

2.3. Results.

2.3.1. Results of the Validation of the ASTER Model

Table 2.3 shows the results of the validation of the ASTER model from 1st October 2010 to 30th September 2018, for several basins, representing the four studied mountain regions and for two different periods (the complete period and the snowmelt period). The average observed flow and the average flow that is calculated by the ASTER model are presented along with the coefficient of determination (R^2) and the Nash-Sutcliffe parameter (NSE), suggesting good predictive skills for the ASTER hydrological model.

Table 2.3. Validation results of the ASTER model from 1st October 2010 to 30th September 2018 for the complete period (1st January to 1st December) and for the snowmelt period (1st March to 31st May).

		Complete Period (1st January to 31st December)				**Snowmelt Period (1st March to 31st May)**			
		Observed	**Calculated**			**Observed**	**Calculated**		
Regions	**Basins**	**Flow (m^3/s)**	**Flow (m^3/s)**	**R^2**	**NSE**	**Flow (m^3/s)**	**Flow (m^3/s)**	**R^2**	**NSE**
Pyrenees	No.2	44.6	42.4	0.93	0.85	75.8	71.4	0.90	0.78
	No.11	12.2	11.8	0.89	0.78	24.2	24.0	0.87	0.78
	No.5	27.4	25.2	0.9	0.8	44.0	45.0	0.85	0.82
Sierra Nevada	No.1	2.2	2.2	0.85	0.7	4.7	4.5	0.82	0.68
Central System	No.1	21.6	19.2	0.9	0.81	39.4	35.3	0.91	0.83
	No.2	9.6	10.2	0.92	0.8	19.4	16.0	0.91	0.85
	No.9	4.5	4.8	0.9	0.82	9.9	8.7	0.93	0.85
Cantabrian Mountains	No.18	12.9	10.8	0.83	0.66	19.6	11.4	0.81	0.51
	No.16	22.08	21.6	0.89	0.8	26.4	23.8	0.90	0.79
	No.23	8.6	8.9	0.82	0.65	16.6	15.1	0.77	0.56

2.3.2. Results of the Projections for the Selected Climate Model

Using the values reported in Table 2.2 and the temperature and precipitations given by the ANA-MRI-CGCM3-rcp85 climate model, the ASTER hydrological model was used

for conducting a future projection of the snow-related phenomena in the period 2041–2070.

Table 2.4 shows the resulting values of the temperature, precipitation, snowfall, snow accumulation, snowmelt and flow in the four regions analysed. For each parameter, the maximum and average values are listed, both in terms of the present-day scenario (from 2006 to 2018) and the future scenario, along with its relative change (Rel. change) as a percentage following Equation (2.4):

$$relative\ change = \frac{V_{fut} - V_{act}}{V_{act}} \cdot 100 \qquad \textbf{Equation 2.4.}$$

Where, V_{act} is the actual value of a parameter and V_{fut} is the future estimated value.

Maximum values represent the highest daily values found in the present-day scenario (from 2006 to 2018). Those maximum values cannot be directly compared with the ones corresponding to the future scenarios: the difference in the length of both periods may lead the maxima in the future scenario to representing much more rare events (once in 30 years) than those during the present-day period (once in 13 years). Consequently, a homogenization procedure was conducted for the future scenario results consisting of considering only the last 13 years of the climate projection (from 2058 to 2070) for computing the maximum values (highest daily values found in that period). Average values were not affected by that procedure and were computed for the whole 30-year period (from 2041 to 2070).

Table 2.4. Snow-related phenomena evolution.

Parameter	Value	Measure	Pyrenees	Sierra Nevada	Central System	Cantabrian Mountains
Temperature [°C]	Maximum value	Actual	23.20	23.81	28.47	18.87
		Future	24.50	23.07	28.05	21.25
		Rel. change	5.79%	−3.11%	−1.48%	12.61%
	Average value	Actual	5.80	8.48	9.87	7.29
		Future	7.30	9.82	11.42	8.63
		Rel. change	25.86%	15.80%	15.70%	18.38%
Precipitation [mm]	Maximum value	Actual	32.50	46.46	45.25	31.26
		Future	29.19	48.29	41.83	24.74

Parameter	Value	Measure	Pyrenees	Sierra Nevada	Central System	Cantabrian Mountains
Snowfall [mm]	Average value	Rel. change	−10.11%	3.93%	−7.55%	−20.86%
		Actual	3.10	1.53	3.03	3.34
		Future	3.20	1.61	3.18	3.26
		Rel. change	3.23%	5.23%	4.95%	−2.40%
	Maximum value	Actual	27.40	23.28	20.48	15.82
		Future	27.03	24.33	19.91	20.55
		Rel. change	−1.45%	4.50%	−2.78%	29.91%
	Average value	Actual	1.30	0.46	0.46	0.83
		Future	1.20	0.43	0.40	0.70
		Rel. change	−7.69%	−6.52%	−13.04%	−15.66%
Snow accumulation [hm^3]	Maximum value	Actual	4037.70	216.72	774.96	2072.12
		Future	3580.92	187.13	423.11	1476.73
		Rel. change	−11.31%	−13.67%	−45.40%	−28.73%
	Average value	Actual	858.6	49.38	77.94	333.02
		Future	621.00	35.10	45.40	190.10
		Rel. change	−27.62%	−28.95%	−41.74%	−42.91%
Snowmelt [hm^3]	Maximum value	Actual	190.86	13.61	94.6	381.24
		Future	194.91	9.52	101.64.9	280.25
		Rel. change	2.12%	−30.05%	7.44%	−26.49%
	Average value	Actual	12.64	0.56	3.53	11.63
		Future	11.80	0.50	3.05	9.80
		Rel. change	−6.6%	−12.0%	−13.6%	−15.7%

Parameter	Value	Measure	Pyrenees	Sierra Nevada	Central System	Cantabrian Mountains
Flow [m^3/s]	Maximum value	Actual	845.60	76.04	1952.31	1783.68
		Future	918.98	120.83	1990.74	1656.25
		Rel. change	7.98%	58.90%	1.97%	−7.14%
	Average value	Actual	205.0	9.90	148.5	342.0
		Future	200.0	9.50	154.3	317.0
		Rel. change	−2.44%	−4.04%	3.88%	−7.31%

2.3.2.1 Pyrenees

Temperatures in the Pyrenees show a great increase in annual average values, with a moderate increase in the maximum value. Precipitations are expected to show a slight increase in terms of average values but a decrease in the maximum values. Both average and maximum snowfall values decrease due to the increment in average temperatures and the decrease of maximum precipitations.

Figure 2.3 shows average values for precipitation, accumulated snow, snowmelt and flow in the Pyrenees. Figure 2.3.a confirms the slight increase in precipitations and it also reveals a change in the precipitation pattern, decreasing in summer-autumn and increasing in winter and spring. Figure 2.3.b shows that the average accumulated snow decreases throughout the year. Even though the average snowmelt decreases for the whole year, the increase in temperatures results in an increase in snow meltdowns from January to April as displayed in Figure 2.3.c. This also means a change in the snowmelt pattern, which will be forwarded in time and will take place more than a month before to the present-day scenario. Average flow decreases along the year too, but the increase in precipitations and snowmelt during the mentioned period leads to an increase in the flow stream to rivers during the first months of the year (Figure 2.3.d). Advance in snowmelt and the decrease in precipitations in summer also result in decreasing the average flow between the months of June and October.

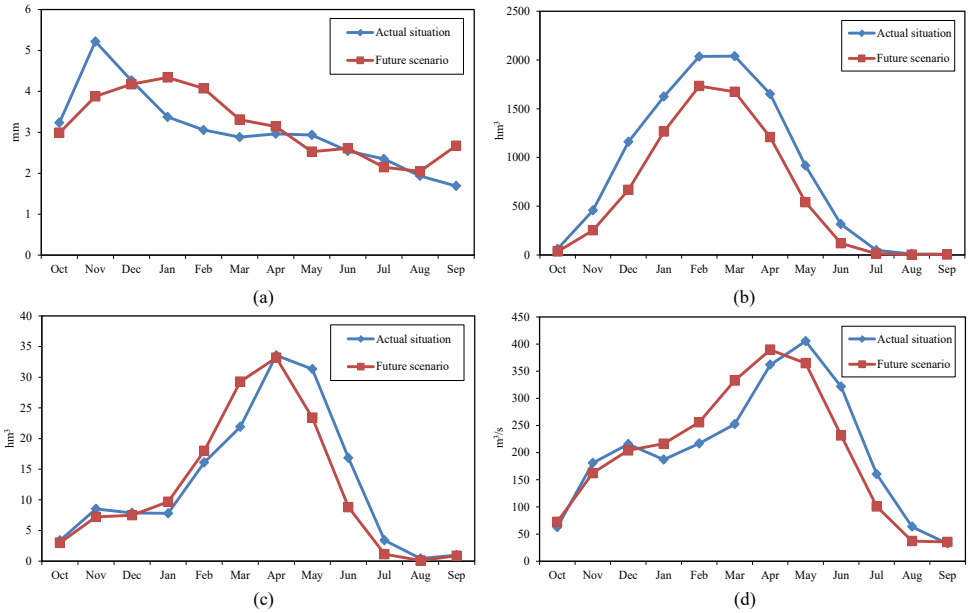

Fig. 2.3. Average values for the snow-related phenomena evolution for a standard year in the Pyrenees. Actual situation (blue) and future scenario (red) simulated: (a) average precipitation; (b) average accumulated snow; (c) average snowmelt; (d) average flow.

Figure 2.4 shows the evolution of the previous variables in terms of maximum values. Figure 2.4.a displays the increase in maximum precipitations during winter, matching the increase in average values indicated above, especially from December to February, a period where currently maximum precipitation values are low. The maximum accumulated snow shows a slight decrease with respect to the actual values between the months of February and May (Figure 2.4.b). This also leads to having strong maximum snowmelt values in the same period (Figure 2.4.c), confirming the change in the melting pattern and giving rise to an increase in the maximum flow values. As Figure 2.4.d shows, maximum flow values experience a clear increase during winter and early spring.

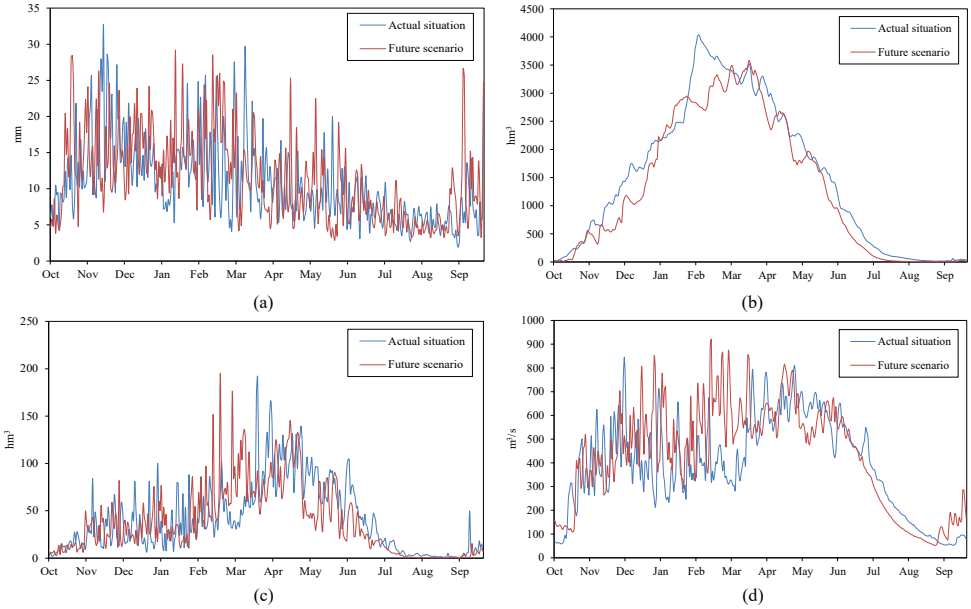

Fig. 2.4. Snow-related phenomena evolution for a standard year in the Pyrenees. Actual situation (blue) and future scenario (red) simulated: (a) maximum precipitation; (b) maximum accumulated snow; (c) maximum snowmelt; (d) maximum flow.

2.3.2.2. Sierra Nevada

Temperatures in Sierra Nevada show a great increase in annual average values, while a slight decrease is observed in the maximum values. Precipitations increase, the increment being moderate for both the average and the maximum values. Maximum snowfall slightly increases in line with the total precipitation, although the average snowfall decreases due to the increment in average temperatures.

Figure 2.5 shows average values for precipitation, accumulated snow, snowmelt and flow in Sierra Nevada. Figure 2.5.a displays how precipitations are concentrated in autumn in the present-day scenario, while in the future scenario precipitations will occur mainly in winter and early spring. This will cause a decrease in the accumulated precipitations in summer and autumn and reveals a change in the precipitation pattern. Average accumulated snow (Figure 2.5.b) decreases throughout the year. Snowmelt average value decreases for the whole year, but Figure 2.5.c shows a clear increase in average snowmelt from January to April, also leading to an advance in the snowmelt pattern (in the actual time, snowmelt mainly occurs in spring) due to the increase in temperatures similar to what was observed in the Pyrenees. A decrease in average annual flow is expected but also showing a pattern change: flow will decrease from June to January and increase in late winter and spring (Figure 2.5.d).

Figure 2.6 shows the evolution of the previous variables in terms of maximum values. Figure 2.6.a confirms the increase of precipitations along the year with some of the

highest maximum values expected in winter. Maximum accumulated snow is expected to decrease in the future scenario (Figure 2.6.b) while the maximum snowmelt values will increase in the middle of the winter period (Figure 2.6.c). This confirms the advance in the snowmelt pattern. As Figure 2.6.d displays, the maximum flow will considerably increase along the year, and especially during the months of March to May, as a consequence of the forwarding of the snowmelt, thus confirming the tendency observed for average values.

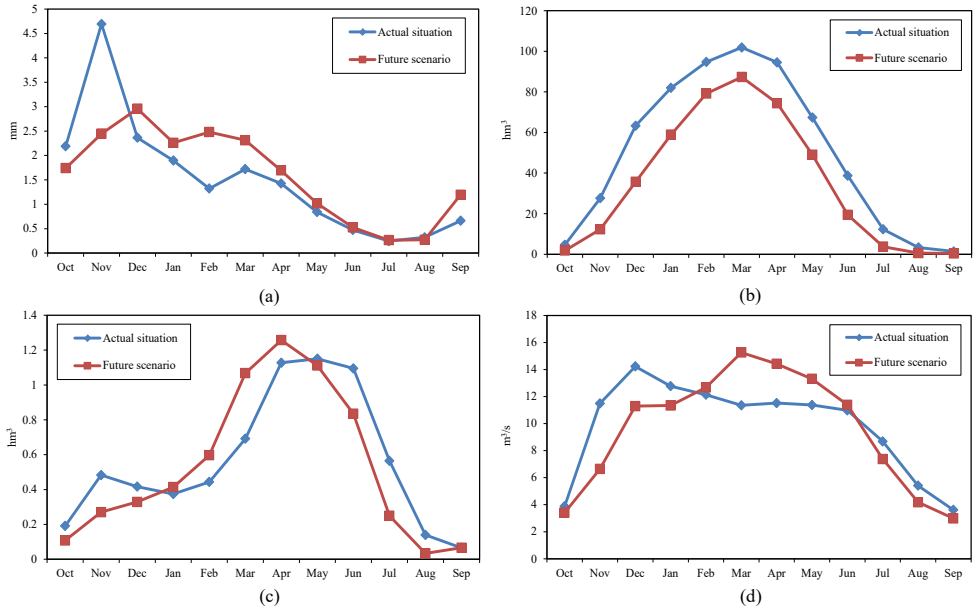

Fig. 2.5. Average values for the snow-related phenomena evolution for a standard year in Sierra Nevada. Actual situation (blue) and future scenario (red) simulated: (a) average precipitation; (b) average accumulated snow; (c) average snowmelt; (d) average flow.

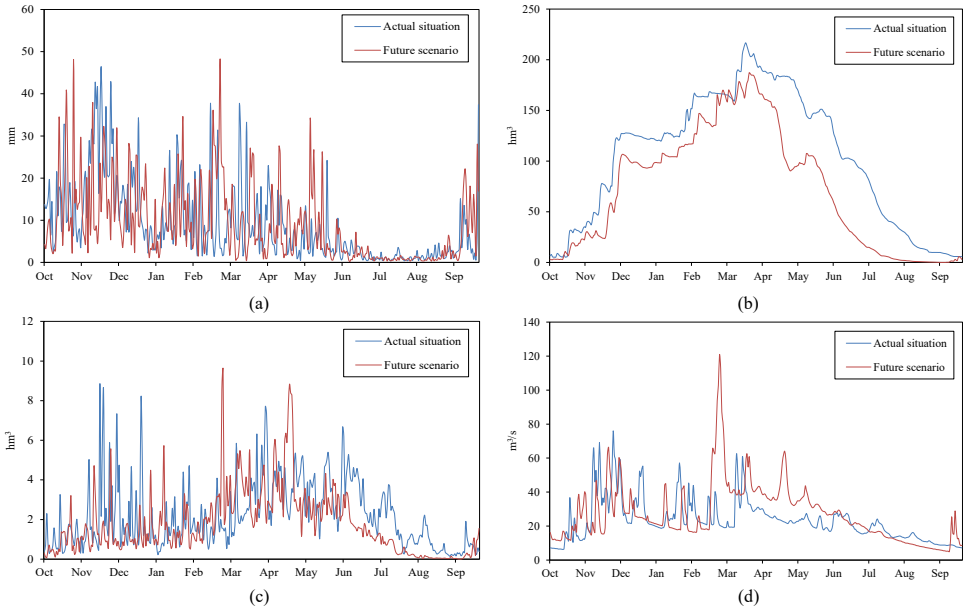

Fig. 2.6. Snow-related phenomena evolution for a standard year in Sierra Nevada. Actual situation (blue) and future scenario (red) simulated: (a) maximum precipitation; (b) maximum accumulated snow; (c) maximum snowmelt; (d) maximum flow.

2.3.2.3. Central System

Temperatures in the Central System show a great increase in average values and a slight decrease in maximum values. Similarly, a moderate increase in average precipitations is expected while maximum values will show a decrease. Snowfall decreases both in terms of maximum and average values due to the increment in average temperatures.

Figure 2.7 shows average values for precipitation, accumulated snow, snowmelt and flow in the Central System. Figure 2.7.a reveals a change in the precipitation pattern with precipitations decreasing in autumn and increasing along the months of January to April. Consequently, snow accumulations and flow rates will experience significant changes in both magnitude and temporal location with respect to the actual values. Figure 2.7.b shows that the average accumulated snow decreases throughout the year, while Figure 2.7.c displays an increase in snowmelt from January to March due to the increase in temperatures. Average annual flow experiences a slight increase, especially in months between January and April caused by the increase in snowmelt (Figure 2.7.d).

Figure 2.8 shows the evolution of the previous variables in terms of maximum values. According to Figure 2.8.a, maximum precipitation values in the future scenario will be higher in winter. Figure 2.8.b shows that maximum snow accumulation will decrease throughout the whole year. Maximum snow accumulations will reach their peak in winter and will start decreasing from March, evidencing a change in the melting pattern which is also confirmed in Figure 2.8.c. In the present-day scenario, the maximum

snowmelt occurs in spring while in the future scenario is expected to take place in winter and decrease in the months of April and May. Therefore, melting will be forwarded and accelerated with respect to the actual situation. A moderate increase in the maximum flow value is detected and as Figure 2.8.d shows in the Central System winter will favor the increase of flow due to the early melting expected to occur in those months. The advancement in the meltdown pattern together with the increase in total precipitations in the first half of the year will result in increasing the maximum flow in this period. The maximum flow is expected to decrease in autumn as a consequence of the decrease in precipitations and the increase in temperatures.

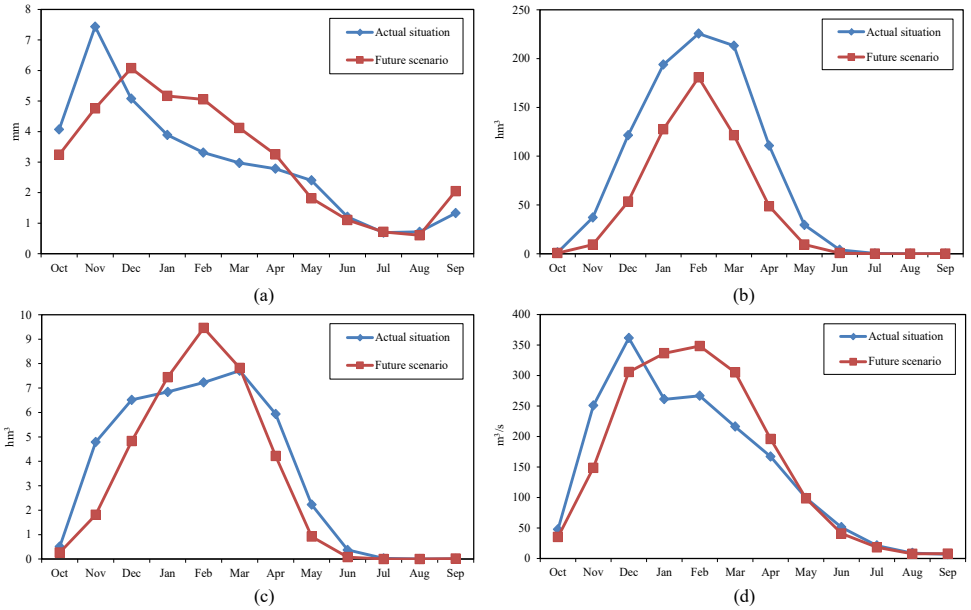

Fig. 2.7. Average values for the snow-related phenomena evolution for a standard year in the Central System. Actual situation (blue) and future scenario (red) simulated: (a) average precipitation; (b) average accumulated snow; (c) average snowmelt; (d) average flow.

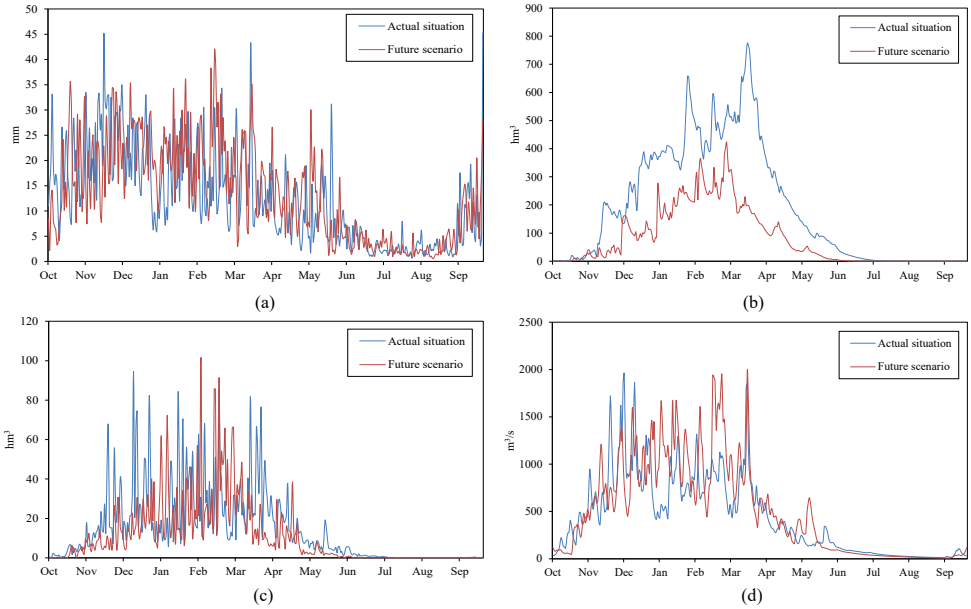

Fig. 2.8. Snow-related phenomena evolution for a standard year in the Central System. Actual situation (blue) and future scenario (red) simulated: (a) maximum precipitation; (b) maximum accumulated snow; (c) maximum snowmelt; (d) maximum flow.

2.3.2.4. Cantabrian Mountains

Temperatures in the Cantabrian Mountains show an increase in both annual average and maximum values. Precipitations show a slight decrease in average values and a great decrease in maximum values. Average snowfall decreases due to the increment in average temperatures and the decrease in average precipitations, but maximum snowfall increases, which indicates that important heavy snowfalls are expected to occur in the future scenario.

Figure 2.9 shows average values for precipitation, accumulated snow, snowmelt and flow in the Central System. Figure 2.9.a displays a change in the precipitation pattern similar to the ones observed in the previous regions studied, with precipitations decreasing in autumn and increasing in winter. Figure 2.9.b confirms that the increase in temperatures and the decrease in average snowfall results in a significant decrease in the accumulated snow throughout the year. A change in the melting pattern is also observed in Figure 2.9.c, as the highest average snowmelt values move from spring (present-day situation) to winter (future situation). Therefore, melting will be forwarded and accelerated with respect to the actual situation. A shorter duration of the snow mantle is also evidenced (difference length of the "plateaus" observed in Figure 2.9.c). Figure 2.9.d shows a clear change in the average flow pattern and how flow increases during the first months of the year as a result of snowmelt, despite the slight decrease in precipitations.

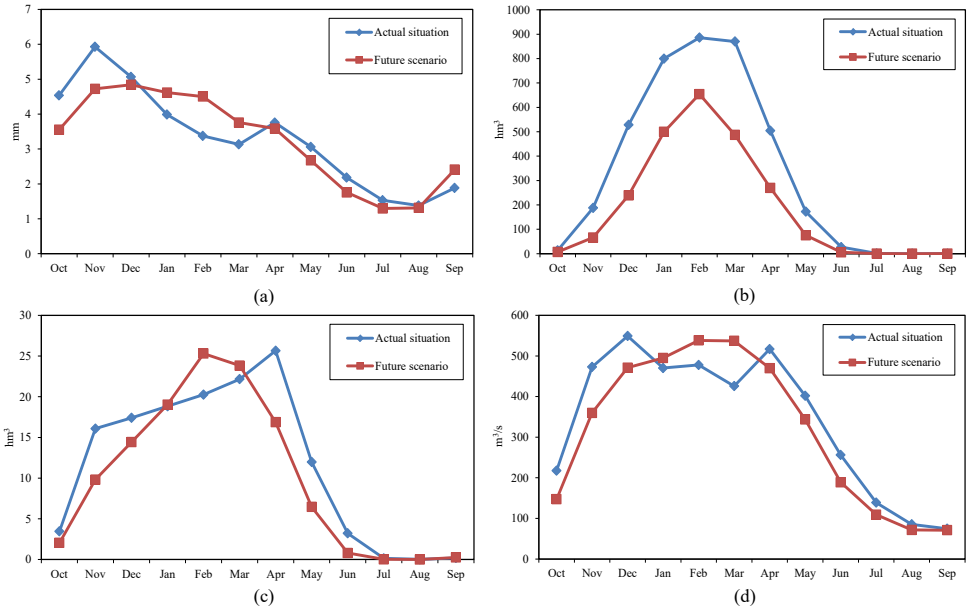

Fig. 2.9. Average values for the snow-related phenomena evolution for a standard year in the Cantabrian Mountains. Actual situation (blue) and future scenario (red) simulated: (a) average precipitation; (b) average accumulated snow; (c) average snowmelt; (d) average flow.

Figure 2.10 shows the evolution of the previous variables in terms of maximum values. Figure 2.10.a confirms the decrease in maximum precipitation. Figure 2.10.b shows that the maximum accumulated snow also decreases throughout the whole year. The large increase in the maximum snowfall but the decrease in accumulated snow, points to a change in the snow pattern in which heavy snowfall will be favored but their permanence on the peaks will be shorter due to the significant increase in temperatures. According to Figure 2.10.c, the maximum snowmelt is expected to increase between January and April and decrease along the months of April and May. That confirms the change in the melting pattern observed with average values. As both the maximum snowmelt and maximum precipitation decrease, the maximum flow also decreases. Figure 2.10.d shows how the flow will increase during the first months of the year as a result of snowmelt, despite the slight decrease in precipitations, which evidences that the maximum flow will be influenced by snowmelt in a greater proportion than in the present time.

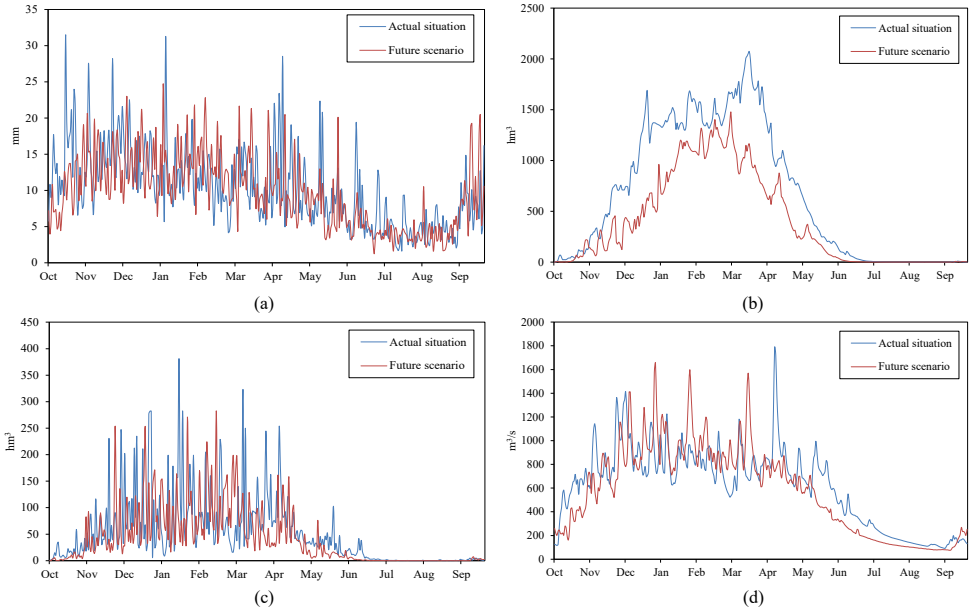

Fig. 2.10. Snow-related phenomena evolution for a standard year in the Cantabrian Mountains. Actual situation (blue) and future scenario (red) simulated: (a) maximum precipitation; (b) maximum accumulated snow; (c) maximum snowmelt; (d) maximum flow.

Chapter 3
Seasonal variability of snow density in the Spanish Pyrenees

Lastrada, E.; Cobos, G.; Garzón-Roca, J.; Torrijo, F.J. Seasonal Variability of Snow Density in the Spanish Pyrenees. Water 2021, 13, 1598. https://doi.org/10.3390/w13111598

3.1. Introduction.

As aforementioned, snow in Spain plays a key role in water resource management and occurs essentially in mountainous areas due to Spanish latitudes and meteorological conditions (Morán-Tejeda, et al., 2019); (López Moreno & García-Ruiz, 2004); (Morán-Tejeda, Lorenzo-Lacruz, López-Moreno, Rahman, & Beniston, 2014); (Mandal & Sharma, 2020); (Corripio & López-Moreno, 2017) (Mellor, 1964). One of the most important Spanish mountain regions is the Pyrenees, which extends, as already mentioned, about 490 km between Spain and France, connecting the Atlantic Ocean at its eastern limit with the Mediterranean Sea at its western limit (both of which influence the climate of the Pyrenees), and with Aneto Peak as its highest point (3404 m altitude).

From the different parameters defining snow-related phenomena, snow density (SDEN) relates snow depths (SDs) with the snow water equivalent (SWE). Since SD measurements are much more frequent than the available SWE data, better knowledge and parameterization of SDEN will enable the achievement of a more accurate estimation of the SWE based on SD measurements. Moreover, as wind data become more available, hydrological models can determine a more accurate estimation of forced-convection snowmelt and snow transport, for which SDEN is needed. However, SDEN is a complex parameter that can vary temporally, spatially and even within the snowpack profile in the vertical direction.

The density of freshly fallen snow depends on three main climatic conditions: temperature, wind and humidity. Typical proposed density values for recently fallen snow are found between 0.07 and 0.15 kg/L, with 0.1 kg/L being the most common value (Mellor, 1964); (Sommerfeld & LaChapelle, 1970); (Gartska, 1964). The density of the new snow can also be estimated linearly, based on air temperature between −15 °C and 0 °C ((Anderson, 1976); (Gray & Male, 2004). However, as SDEN depends on the liquid and snow form proportions, a higher SDEN can be given for fresh snow.

The aggregation of the ice grains begins as soon as snow touches the surface, increasing the snow cover density (Dingman, 2002). This process is known as sintering and plays an important role in snow densification. There are two distinct types of snow metamorphism: constructive metamorphism-recrystallization by vapour diffusion and destructive metamorphism-equilibrium growth (Colbeck, 1982). A temperature gradient of about 10 °C/m is considered a threshold for the initiation of constructive metamorphism (Akitaya, 1974); (Armstrong, 1980). Liquid water causes destructive metamorphism to take place at a faster rate. Moreover, daily melting cycles associated with solar radiation and atmospheric temperature cause snow crystal metamorphism. This leads to a gradual loss of voids and an irreversible increase in the density of the snow layer over time (Anderson, 1968). At the same time, SDEN affects shortwave radiation penetration in snow. About 80% of this energy is absorbed in the first 5 to 15 cm of the snowpack (Colbeck, 1982). The range depends on SDEN (Anderson, 2006). Compaction due to gravity should also be considered for SDs above 1 m (Lantarón, 2007). In the Spanish Pyrenees, as the SD is deep for high elevations, this effect may not be negligible. In addition, precipitation over the snow-pack will also increase SDEN (Brun, 1989). These cycles can repeat until the whole snow layer is melted and frozen, turning into ice with an average density of 0.917 kg/L. However, defining an accurate proportion for each of these processes in the densification rate is not easy.

Different techniques were used to measure or estimate SDEN worldwide (Bilello, 1984); (Onuchin & Burenina, 1996); (Sturm & Holmgren, 1998); (Kershaw & McCulloch, 2007); (Meloysund, Leira, Hoiseth, & Liso, 2007). Common techniques include conventional on-site manual sampling, the non-destructive snow water equivalent (SWE) determination based on cosmic-ray neutron attenuation (CRN) (Paquet, et al., 2007); (Kodama, Nakai, Kawasaki, & Wada, 1979), acoustic signal delays (Kinar & Pomeroy, 2009) and stepped-frequency continuous-wave radar, recently used at the

AEMET Formigal-Sarrios test site (Spanish Pyrenees) and implemented in a coherent software-defined radio in the range from 150 MHz to 6 GHz (Alonso, del Pozo, Buisán, & Álvarez, 2021). The use of SWE products derived from satellite microwave radiometer-based measurements, combined with SD measurements, is another alternative technique, but the low spatial resolution of these products may not be suitable for mountainous and complex small catchments (Collados-Lara, Pulido-Velázquez, Pardo-Igúzquiza, & Alonso-González, 2020); (López-Moreno & Nogués-Bravo, 2006) . Snow pillows are also used for the non-destructive monitoring of SDEN, but they have a complex installation process, maintenance and have uncertainties associated with low SD and irregular snowmelt drainage (López-Moreno, Quirós, Latron, & Fassnacht, 2010).

Several studies (Onuchin & Burenina, 1996); (Anderton, White, & Alvera, 2004); (Elder, Dozier, & Michaelsen, 1991); (Mizukami & Perica, 2008); (Rohrer, Braun, & Lang, 1994) estimated linear density-time functions or densification rates, providing links to the physical processes. However, density models still need to cope with a high SDEN variability at low SD values, as it can range from low-density new snow to high-density slush. Regarding SDEN's relationship with time, it shows a gradual increase throughout the winter season. Across the western United States, SDEN was found to be location-dependent during early and midwinter, although the snowpack densification daily rate was nearly fixed regardless of the location. Considerable intra-annual variability in SDEN was also reported, with densification trends generally linear, but significantly less year-to-year variation (Mizukami & Perica, 2008). The low intra-annual variability of SDEN was also observed in southern Canada (Brown, 2000). In the Swiss Alps, SDEN was found to depend on the season, SD, elevation and location. Elevation had only a minor direct effect (Jonas, 2009), as higher SDs at higher sites imply higher SDEN due to compaction in winter, while melting cycles at lower elevations and in the late winter season induce a compensating effect (Sturm & Holmgren, 1998); (Mizukami & Perica, 2008); (Jonas, 2009). For the alpine regions in the former Soviet Union and the US, precipitation was the dominant climate variable, followed by average temperature (Bormann, Westra, Evans, & McCabe, 2013) .

In the Iberian Peninsula, snow observations and a validated daily gridded snowpack dataset were simulated from downscaled reanalysis (Alonso-González, et al., 2018), calculating SDEN for each time step with different maximum thresholds: 0.3 kg/L for cold (non-isothermal) and 0.5 kg/L for melting (isothermal) snow conditions (Essery, 2015). In the central Pyrenees, statistically significant correlations between the SD and other topographic variables with SDEN were found, but they showed a great variability among sites and surveys. The absolute error in the SWE estimated from the computed SDEN was less than 15% and was similar to that obtained by relating SDEN directly to SD (López-Moreno, et al., 2013).

The Spanish Pyrenees hold more than one hundred snow poles and up to thirteen automatic snow monitoring devices, or telenivometers (TNMs), operating since 2008.

This instrumentation allows for the study of the seasonal variability of snowfall events (Navarro-Serrano & López-Moreno, 2007). Additionally, the Spanish and Ebro Water Authority have been carrying out on-site SDEN measurements since the early 1990s through the ERHIN program ("Estudio de Recursos Hídricos procedentes de la INnivación"—Study of Snow Water Resources) (Cobos, Francés, & Arenillas, 2010). TNM data show significant variability in annual SD. Western regions (Atlantic Ocean weather) give the most annual accumulation in the winter months, while eastern regions (Mediterranean weather types) show more homogenous accumulation over winter, spring and late autumn. It is interesting to note that western TNMs also show behaviours similar to that observed for the western coast of the US, which is characterized by plenty of precipitation and relatively high air temperatures, both possible contributors to early season high SDEN (Serreze, Clark, Armstrong, McGinnis, & Pulwarty, 1999).

The ERHIN program (Arenillas, Cobos, G., & Navarro, 2008) started in 1986, studying snow phenomena in river basins in the mountainous regions of the Pyrenees, Sierra Nevada, the Central System and the Cantabrian Mountains. In this framework, on-site manual SDEN measurements were carried out and a dense network of snow poles and TNMs (SWE and SD non-destructive measurements) were installed. The Pyrenees is the densest region monitored, with 13 TNMs and more than 100 snow poles (Figure 3.1). The TNMs cover a range about 200 km long in the Pyrenees and are numbered from west to east.

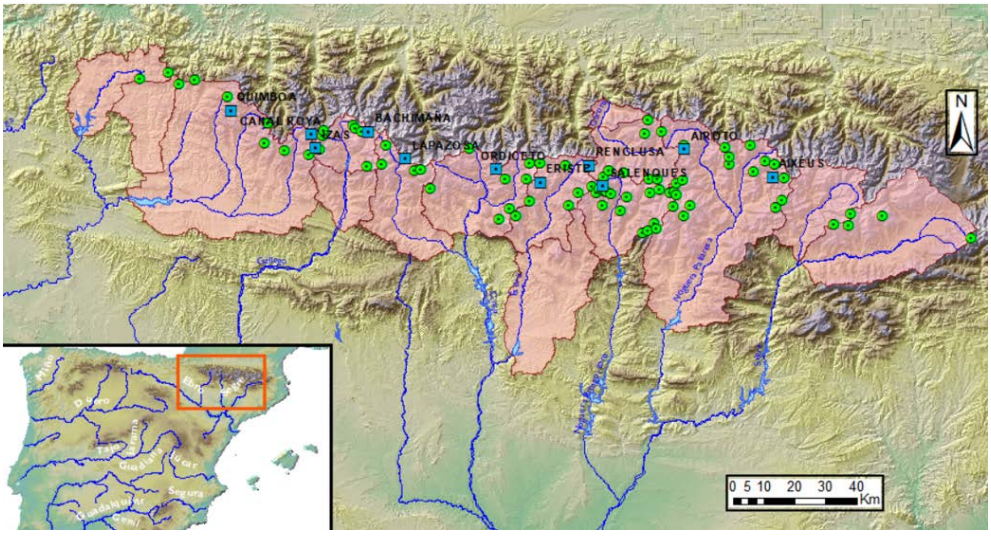

Fig. 3.1. Snow poles (green) and telenivometers (TNM) (blue) network from the ERHIN program in the Pyrenees.

3.2. Materials and Methods.

3.2.1. On-Site Manual Sampling and Measurements

Since 1987, on-site manual SDEN measurements have been carried out at certain snow poles. At the same time, SD measurements were taken for the whole snow pole network. Sampling elevations range from 1440 m to 2615 m and cover up to three seasonal campaigns between December and May.

Figure 3.2 shows a 0.8 m stackable sampling tube of constant 53.8 mm diameter inside a section (22.72 cm2) and 2.5 mm thick, with up to 4 m of maximum penetration depth. This SWE tube was handmade in 1986 at the Polytechnic University of Valencia. Knowing the weight and dimensions of the core, and therefore its volume, by directly weighing it on a precision weighing scale, the net weight of the snow core is obtained, and the density is calculated.

(a)

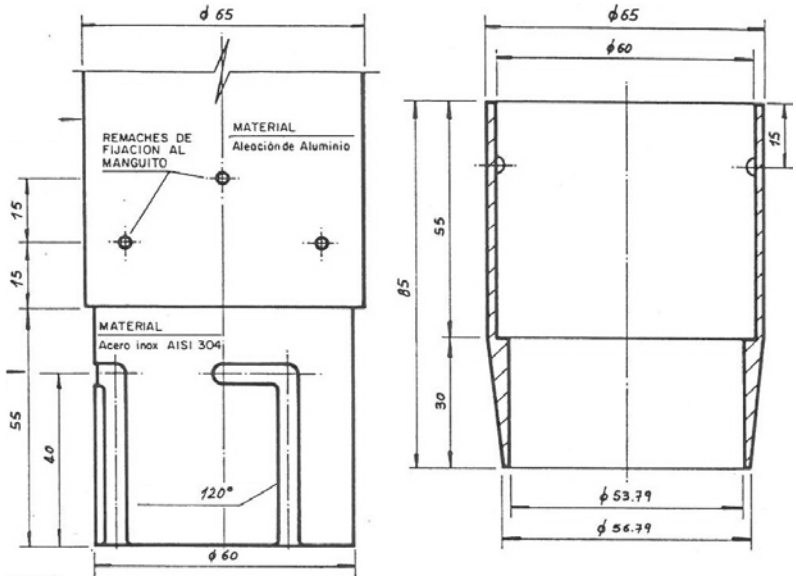

(b)

Fig. 3.2. On-site manual sampling. (a) Snow tubes. (b) Nozzle dimensions.

Table 3.1 shows the on-site manual sampling and elevation for sites in the same locations as 11 TNM sites. The number of samples is also included. The complete list of 35 snow pole sites and the number of samples are given as supplementary data. Figure 3.3 shows

the elevation distribution for all of the samples taken, ranging from 1810 m to 2615 m for snow pole sites.

Table 3.1. On-site manual sampling sites. Snow poles are in the same locations as the TNM sites.

Name	X COORDINATE ETRS89H30	Y COORDINATE ETRS89H30	Elevation (m)	No. Samples	Sampling Period (Years)
1. Quimboa	682,767	4,748,419	1,810	13	1998–2019
2. Izas	710,308	4,736,177	2,080	9	2007–2012
3. Canal Roya	708,779	4,740,716	1,860	17	1987–2019
4. Bachimaña	727,394	4,741,571	2,220	61	1987–2019
5. Lapazosa	739,424	4,732,777	2,115	11	2009–2019
6. Ordiceto	768,642	4,729,429	2,380	65	1987–2015
7. Renclusa	799,030	4,730,578	2,180	32	1987–2017
8. Salenques	803,363	4,723,843	2,600	13	2008–2014
9. Eriste	783,155	4,725,107	2,350	7	2009–2014
10. Airoto	829,803	4,735,946	2,380	60	1987–2019
11. Aixéus	858,381	4,726,892	2,400	66	1987–2019
Total samples				354	

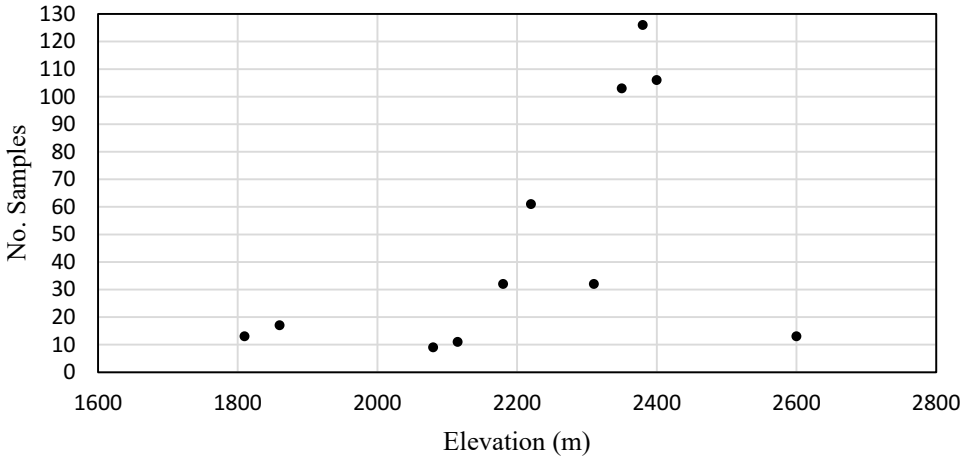

Fig. 3.3. Number of snow density (SDEN) manual samples and elevation distribution.

3.2.2. On-Site Non-Destructive Measurements

First Cosmic-Ray Neutron (CRN) attenuation telenivometers (TNMs) were installed in 2008 along the Spanish Pyrenees (Figure 3.4), and two more were recently installed in 2015 and 2018. TNMs allow the acquisition of SWE high time resolution data (15 min) and SD vertical data (1 cm resolution). From those values, SDEN can be estimated according to Equation (3.1):

$$SDEN = \frac{SWE}{SD} \qquad \textbf{Equation 3.1}$$

Table 3.2 shows the name, situation, elevation, number of daily samples and sampling period for each TNM, which were located above 1800 m elevation and with 2600 m as the maximum elevation. It should be noted that SDEN calculated according to Equation (3.1) is not sensitive to a higher time resolution. Figure 3.1 shows the situation of the TNMs in the Pyrenees, (named from west to east), while Figure 3.5 shows the elevation distribution for the automatic TNM measurements. It is interesting to mention that the Eriste TNM is located at approximately the same distance from the Atlantic Ocean and the Mediterranean Sea.

Although the TNMs have been operating for a shorter period than the period covered by manual samples, daily data were registered, with more than 20,000 samples and officially provided by the Ebro Water Authority (http://www.saihebro.com/saihebro/index.php?url=/datos/usos/mapa:TNG/tipoestacion:TN accessed on 4 June 2021). Additionally, the maximum, average and minimum daily temperatures were available.

Fig. 3.4. TNM and on-site manual sampling for the snow pole sampler

Table 3.2. On-site non-destructive measurements. TNM sites.

Name	X COORDINATE ETRS89H30	Y COORDINATE ETRS89H30	Elevation (m)	No. Data	Data Period (Years)
1. Quimboa	682648	4748214	1810	1465	2008–2021
2. Izas	710243	4735937	2080	2107	2008–2021
3. Canal Roya	708660	4740541	1971	1661	2008–2021
4. Bachimaña	727282	4741345	2220	2086	2008–2021
5. Lapazosa	739388	4732579	2140	1676	2008–2021
6. Ordiceto	768527	4729209	2380	2043	2008–2021
7. Renclusa	798925	4730377	2175	1737	2008–2020
8. Salenques	803294	4723655	2600	263	2008–2010
9. Eriste	783048	4724896	2350	2049	2009–2021
10. Airoto	829707	4735723	2380	2004	2008–2021
11. Aixeus	858269	4726759	2400	2010	2008–2021
14. Sarrios-Formigal	713384	4737624	1800	643	2015–2021
15. Besurta	799420	4731387	1930	317	2018–2021
Total samples				21257	

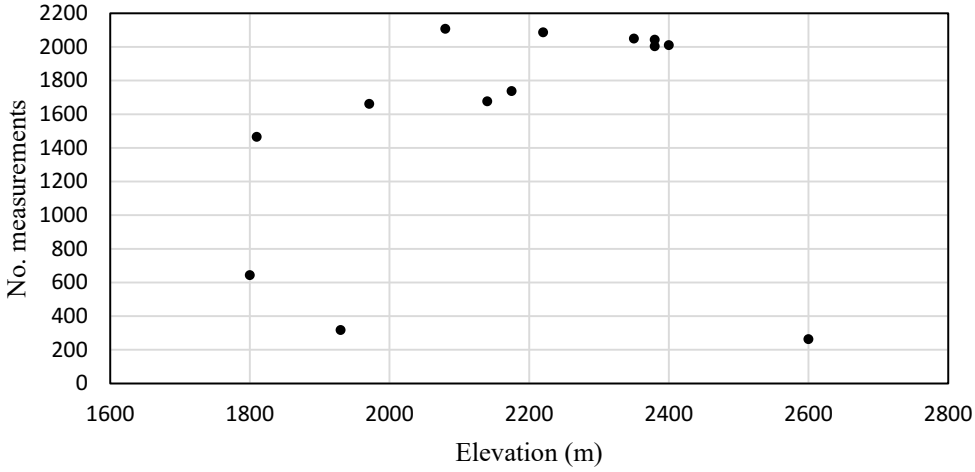

Fig. 3.5. Number of SDEN automatic TNM measurements and elevation distribution

3.2.3. Other Data and Sources of Error

Supplementary Materials are provided for both on-site manual sampling and on-site non-destructive (TNM) daily measurements.

The daily data for precipitation from the closest meteorological stations within the same period as the TNM measurements are also given in the Supplementary Material.

The sources of error and uncertainties associated with snow sampling include the loss of part of the sample due to snowpack collapse when the sampler encounters hard layers. When the sampler is extracted from the snowpack for weighing, snow can also be lost (Dixon & Boon, 2012) or stuck to the outside of the sampler. These errors may be increased by a snow-pack with ice layers that give the false perception of reaching the ground, basal ice and layers of depth hoar and non-cohesive crystals. New snow or wet snow can also increase sampling errors, especially if the observer is collecting core samples to be weighed later rather than using a spring balance and tube cradle. The experience of the observer plays an important role in reducing potential errors due to human failure. Depending on the temperature, new and wet snow will tend to stick in the tube, and this will result in an underestimation of the SWE, which could exceed 10%. Smaller diameter cutters (down to 20 cm2) were more prone to plugging as they encountered ice lenses, and they were more likely to induce the collapse of non-cohesive layers under the cutter, resulting in an underestimation of the total SWE) (World Meteorological Organization, 2018). The ideal cutter area was about 30 cm^2, demonstrated by the low error percentage of the ESC30 sampler, which ranged from a 5% overestimation to a 2% underestimation (Farnes, Goodison, Peterson, & Richards, 1982). The uncertainty of density measurements in non-ideal snow conditions is approximately within 10 to 15% (López-Moreno, et al., 2020). As a control measure, random validation tests were carried out for manual samples and measurement protocols were followed (World Meteorological Organization, 2018).

Errors in TNM measurements can occur due to non-environmental issues such as instrument malfunction and incorrect instrument calibration (or calibration drift), CRN uncertainties due to changes in mid-season soil moisture levels and the undervaluation of precipitation and gaps or false null data from other meteorological variables. In this regard, TNM data are periodically calibrated with manual sampling during late snow conditions (Cobos, Francés, & Arenillas, 2010).

3.2.4. Analysis Methodology

A previous screening process was carried out, with the identification of outliers (a range check for reasonable values between zero and the maximum possible SDEN for the site), gaps and null data, discarding sites with little information or information that was not representative.

TNM measurements are fully automated and, even though they are frequently calibrated, are not quality controlled. Thus, the calculated SDEN values that significantly exceeded

the expected maximum and minimum values at each site were removed. The number of samples for each TNM is given after quality-control procedures. All negative and null values were eliminated from the records, for both the SWE and SD, which are necessary to estimate SDEN. Consequently, TNMs numbers 8, 14 and 15 (Salenques, Sarrios-Formigal and Besurta) were discarded.

Manual samples, much less prone to uncertainties (Bormann, Westra, Evans, & McCabe, 2013), underwent a similar screening process. On-site manual sample sites with enough data in the same location as TNM sites were selected and pooled. The previous screening process reduced 35 on-site manual sites with 841 samples to five on-site manual sites matching TNM sites with 284 samples. SDEN statistics were calculated for both manual samples and automatic measurements during the entire year (annual period), as well as for the accumulation period (winter snow, until 21 March) and for the melting period (spring snow, from 21 March).

Automatic TNM sites with a significant correlation between SDEN and the day of the year (time evolution) were selected and grouped (the set of TNMs) for automatic TNM measurements, where day 1 corresponds to 1 October. The results were compared with the SDEN–day of the year correlation for manual samples.

Independent variables were analysed for the selected automatic TNM sites. The dominant climatological drivers of annual SDEN variability were extracted by establishing single linear regressions between each of the predictor terms and SDEN. The selected climate and spatial predictors include the time evolution, precipitation, accumulated precipitation, SD and average temperature.

Multiple linear regressions (MLRs) between SDEN and these predictors were studied for automatic measurements and compared with manual samples. The effect of elevation on the grouped series (the set of TNMs) was evaluated. Predictors were added progressively in the MLR model from more to less dominant with a significance threshold of 0.05.

3.3. Results.

In this section, the SDEN results are analysed, identifying dominant climatological variables and studying MLR models for SDEN. Results from both the manual and automatic measurements are presented.

3.3.1. SDEN Statistics.

Table 3.3 shows a summary of the SDEN statistics obtained by on-site manual data for two annual periods, winter or early season (until 21 March) and spring or late season (21 March–30 June). The word "set" refers to all grouped data.

Table 3.3. SDEN statistics for the most representative manual samples in the same location as TNM sites and for the set of samples.

Name	Average (Annual)	C. V. (Annual)	Average (Winter)	C. V. (Winter)	Average (Spring)	C. V. (Spring)
4. Bachimaña	0.396	1.82%	0.351	1.82%	0.442	0.90%
6. Ordiceto	0.396	1.72%	0.349	1.23%	0.451	0.93%
7. Renclusa	0.368	1.96%	0.306	0.88%	0.437	0.71%
10. Airoto	0.382	1.60%	0.344	1.69%	0.427	0.68%
11. Aixéus	0.386	1.53%	0.337	0.92%	0.427	1.05%
Set of Manual Samples	0.394	1.75%	0.348	1.47%	0.443	0.93%

The average SDEN and coefficient of variation (C.V.) were very similar among sites for every period, without spatial patterns from east to west locations. Renclusa showed the lowest average SDEN and the highest C.V. due to a very low winter average SDEN and very marked differences between early and late season snow. Bachimaña and Ordiceto showed the highest average SDEN. As expected, the average SDEN value was greater for the late season (spring) than for the early season (winter). The C.V. is small for all sites studied and the set of samples, being the greatest during the early season (winter).

Table 3.4 shows a summary of the SDEN statistics obtained from TNM data for two annual periods, winter or early season (until 21 March) and spring or late season (21 March–30 June). The set of TNMs refers to TNMs numbers 1, 2, 4, 6, 7 and 9.

Table 3.4. SDEN statistics for TNM data and for data from the set of TNMs.

Name	Average (Annual)	C. V. (Annual)	Average (Winter)	C. V. (Winter)	Average (Spring)	C. V. (Spring)
1.Quimboa	0.389	3.80%	0.344	3.17%	0.511	1.04%
2. Izas	0.36	1.97%	0.309	1.04%	0.435	0.80%

Name	Average (Annual)	C. V. (Annual)	Average (Winter)	C. V. (Winter)	Average (Spring)	C. V. (Spring)
3. Canal Roya	0.348	1.67%	0.325	1.32%	0.400	1.40%
4. Bachimaña	0.368	2.53%	0.332	2.11%	0.455	0.95%
5. Lapazosa	0.364	3.13%	0.334	2.81%	0.438	1.92%
6. Ordiceto	0.385	4.60%	0.312	2.66%	0.512	1.29%
7. Renclusa	0.365	2.52%	0.326	1.47%	0.462	1.43%
9. Eriste	0.435	2.23%	0.398	1.61%	0.508	1.63%
10. Airoto	0.383	3.55%	0.357	3.31%	0.449	2.67%
11. Aixeus	0.386	3.83%	0.360	4.36%	0.440	1.95%
Set of TNMs	0.384	3.07%	0.337	2.26%	0.480	1.44%

As for manual samples, except for Eriste, the TNM data showed very similar SDEN averages among sites for every period, without spatial patterns from east to west locations. Eriste showed the highest average SDEN, while Canal Roya's average SDEN was the lowest; the C.V. is again small, with all TNMs below 5%, but there were some differences among sites, since the amount of data between them is variable. The Ordiceto TNM showed the greatest C.V. Once again, the C.V. was usually greater for the early season (winter) than for the late season (spring).

A comparison of statistics between manual and automatic data (see Table 3.5) showed small differences in terms of the average SDEN, although the C.V. values are higher for the automatic data. The set of manual samples and the set of TNM data show small differences for the average SDEN, especially for the annual and early-season periods. Renclusa showed the lowest annual SDEN average for both the manual and automatic data, while the highest annual average SDEN was represented by different locations for each technique.

Table 3.5. SDEN statistics comparison between automatic data for TNM sites in the same location as manual samples

Name	Average (Annual)	C. V. (Annual)	Average (Winter)	C. V. (Winter)	Average (Spring)	C. V. (Spring
4. Bachimaña	107.6%	71.9%	105.7%	86.3%	97.1%	94.7%
6. Ordiceto	102.9%	37.4%	111.9%	46.2%	88.1%	72.1%
7. Renclusa	100.8%	77.8%	93.9%	59.9%	94.6%	49.7%
10. Airoto	99.7%	45.1%	96.4%	51.1%	95.1%	25.5%
11. Aixeus	100.0%	39.9%	93.6%	21.1%	97.0%	53.8%
Set of TNMs	102.6%	57.0%	103.3%	65.0%	92.3%	64.6%

3.3.2. Most Representative Automatic TNM Sites

The most representative automatic TNM sites were selected and grouped (the set of TNMs) for the automatic TNM data, with a significant correlation between SDEN and the day of the year (intra-annual time dependence), where day 1 corresponds to 1 October. An intra-annual time dependence for SDEN was found using Equation (3.2):

$$SDEN = A \cdot day + B \qquad \textbf{Equation 3.2}$$

The coefficients A and B are given in Table 3.6 along with the site elevation of each TNM and the average elevation of the set of TNMs, with the coefficient of determination (R^2) being computed in each case. The relationship found is important as it describes SDEN when data from other climatic variables are not available. The coefficient A represents the densification rate, ranging from 0.7 x 10^{-3} kg/L/day to 2 x 10^{-3} kg/L/day; the coefficient B represents the initial SDEN, ranging from 0.1 kg/L to 0.3 kg/L. Neither of the two parameters shows a spatial pattern.

Automatic TNM sites with a significant coefficient of determination (R^2) were selected and grouped (the set of TNMs) for automatic TNM measurements. The densification rate for the data from the set of TNMs is set to 1.3 x 10^{-3} kg/L/day, with an initial SDEN of 0.196 kg/L. Ordiceto, placed in the central Pyrenees, showed the highest densification rate and coefficient of determination (R^2) and the lowest initial SDEN. Aixeus, in the eastern part of the Pyrenees, showed the lowest densification rate and coefficient of determination (R^2), while the highest initial SDEN was found in Eriste. Canal Roya, Bachimaña, Lapazosa, Eriste, Airoto and Aixeus showed low densification rates and high initial SDENs, while Quimboa, Izas, Ordiceto and Renclusa showed the opposite behaviour. Therefore, no spatial pattern can be observed.

Regarding (R^2), TNMs numbers 1, 2, 4, 6, 7 and 9 are selected. TNM number 9 (Eriste) is selected as the most representative of the eastern part of the Pyrenees. Figure 3.6 shows the SDEN intra-annual time dependence for the selected TNMs and the trend line for the set of TNMs.

Table 3.6. SDEN intra-annual time dependence for automatic measurements. Bold letters are used for selected sites for the Set of TNMs.

Name	A (day)	B	Elevation (m)	R^2	Sampling Period (Years)
1.Quimboa	0.0020	0.112	1810	0.61	2008–2021
2. Izas	0.0012	0.177	2080	0.64	2008–2021
3. Canal Roya	0.0007	0.252	1971	0.18	2008–2021
4. Bachimaña	0.0011	0.224	2220	0.4	2008–2021

Name	A (day)	B	Elevation (m)	R^2	Sampling Period (Years)
5. Lapazosa	0.0009	0.242	2140	0.17	2008–2021
6. Ordiceto	0.0020	0.090	2380	0.73	2008–2021
7. Renclusa	0.0018	0.1	2175	0.15	2008–2020
9. Eriste	0.0009	0.303	2350	0.27	2009–2021
10. Airoto	0.0008	0.280	2380	0.13	2008–2021
11. Aixeus	0.0007	0.285	2400	0.10	2008–2021
Set of TNMs	0.0013	0.196	2187	0.44	2008–2020

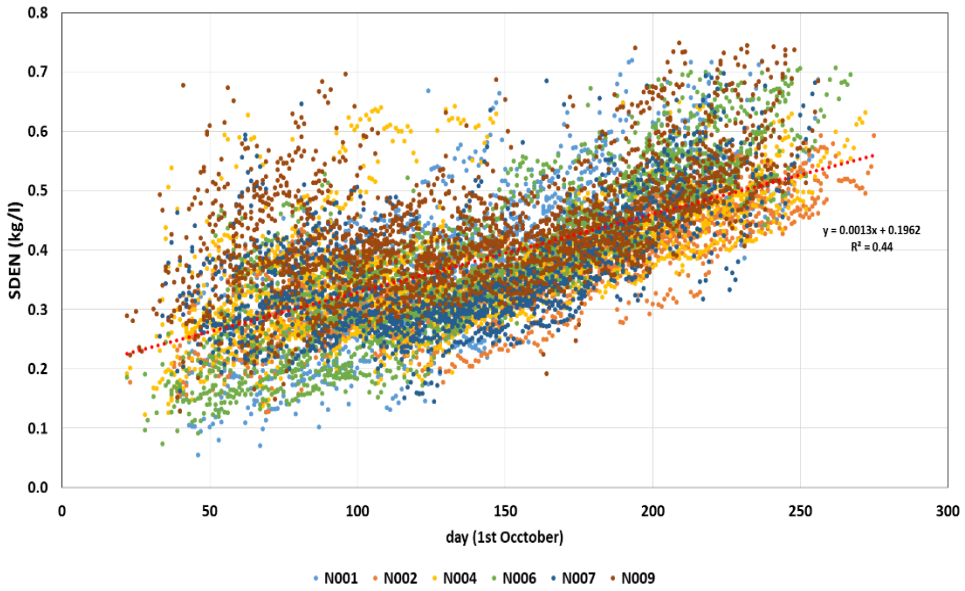

Fig. 3.6. SDEN intra-annual time dependence for selected TNM measurements. Red trend line for the set of TNMs.

Table 3.7 shows the values of the coefficients A and B for manual sampling in the most representative TNM sites and the set of manual samples, which enables the establishment of the intra-annual time dependence of SDEN using Equation (3.2). The average elevation for the set of manual samples and the coefficient of determination (R^2) are shown, too. For manual samples, the densification rates and an initial SDEN range have less variability than the automatic measurements, from 1.1 x 10^{-3} kg/L/day to 1.8 x 10^{-3} kg/L/day and from 0.13 kg/L to 0.19 kg/L, respectively. The densification rate from the set of manual samples is set to 1.2 x 10^{-3} kg/L/day, with an initial SDEN of 0.189 kg/L,

showing values very similar to but lower than the values of the automatic measurements. Common sites for both manual and TNM data are Bachimaña, Ordiceto and Renclusa. Bachimaña showed the same coefficient of determination but a higher densification rate and a lower initial SDEN for manual samples than for automatic data. Ordiceto showed a lower coefficient of determination and densification rate, but a higher initial SDEN for the manual samples than for the automatic data. Renclusa had a higher coefficient of determination and the same densification rate, but a lower initial SDEN.

Table 3.7. SDEN intra-annual time dependence for manual sampling in the most representative TNM sites and the set of manual samples. Bold letters are used for manual samples in the same locations as selected TNM sites.

Name	A (day)	B	Elevation (m)	R^2	No. Samples
4. Bachimaña	0.0013	0.157	2220	0.4	61
6. Ordiceto	0.0016	0.126	2380	0.57	65
7. Renclusa	0.0018	0.054	2180	0.73	32
10. Airoto	0.0011	0.188	2380	0.35	60
11. Aixéus	0.0011	0.180	2400	0.34	66
Set of Manual samples	0.0012	0.189	2268	0.34	840

Figure 3.7 displays the linear time dependence of SDEN for the set of manual samples.

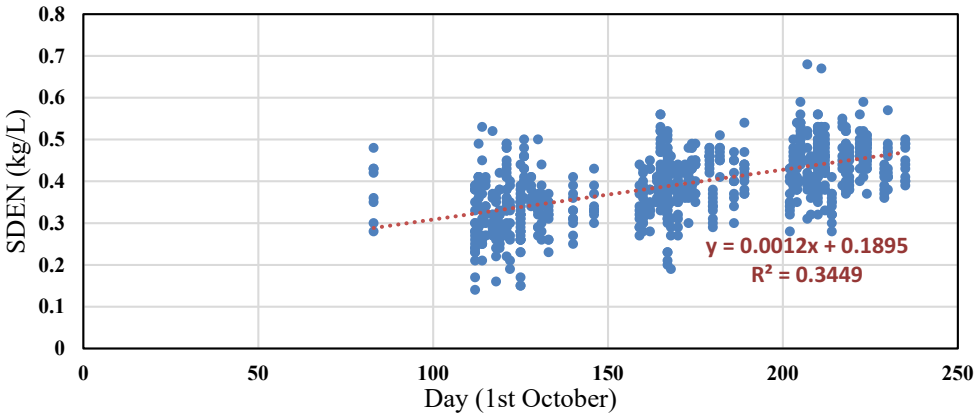

Fig. 3.7. SDEN time dependence for on-site manual sampling. Trend line for the set of manual samples.

3.3.3. Identification of Dominant Variables

In addition to the time dependence, the selected predictors included the SD (cm), seasonal accumulated daily precipitation (PP_{acum} (mm)) and 7-day average temperature

(Tave7d) (°C/7 days). The seasonal accumulated precipitation was taken into account from the first day that snow accumulation starts and presented a more dominant influence than the daily precipitation, as SDEN depends on historical intra-annual evolution. The 7-day average temperatures have shown the best fitting to SDEN. SDEN depends on punctual temperatures for the accumulation process, but during melting cycles, average temperatures may describe it better (Mizukami & Perica, 2008). The effects of the maximum and average daily temperatures were similar, while the minimum daily temperature was less dominant. Average daily temperatures were chosen, as they may be more available. Table 3.8 shows the correlation values, with the intra-annual time dependence and seasonal accumulated precipitation being the most dominant variables.

Table 3.8. SDEN correlation coefficients (R^2) for TNM selected sites.

Name	Time dependence (day)	PP_{acum} (mm)	T_{ave7d} (°C/7 days)	SD (cm)
1. Quimboa	0.61	0.58	0.18	0
2. Izas	0.64	0.47	0.37	0.03
4. Bachimaña	0.4	0.21	0.20	0
6. Ordiceto	0.73	0.44	0.21	0.14
7. Renclusa	0.15	0	0.38	0
9. Eriste	0.27	0.13	0.19	0.07
Set of TNMs	0.44	0.25	0.19	0

For the Quimboa TNM, the PP_{acum} driver was the most dominant, while T_{ave7d} was the most dominant for the Renclusa TNM. For the rest of the selected TNMs (Izas, Bachimaña, Ordiceto and Eriste), the intra-annual time dependence was the main variable.

The SDEN linear correlation with SD is almost negligible, except for the Ordiceto and Eriste TNMs. However, it may give useful information, as the significance threshold of SDEN is reduced for high SD values. Figure 3.8 represents SDEN's variability on SD for the set of TNMs, divided into an early-mid season snowpack and mid-late season snowpack. As observed, SDEN has a wide range of values with low SD, especially for the early season snowpack, reducing SDEN variability as SD increases.

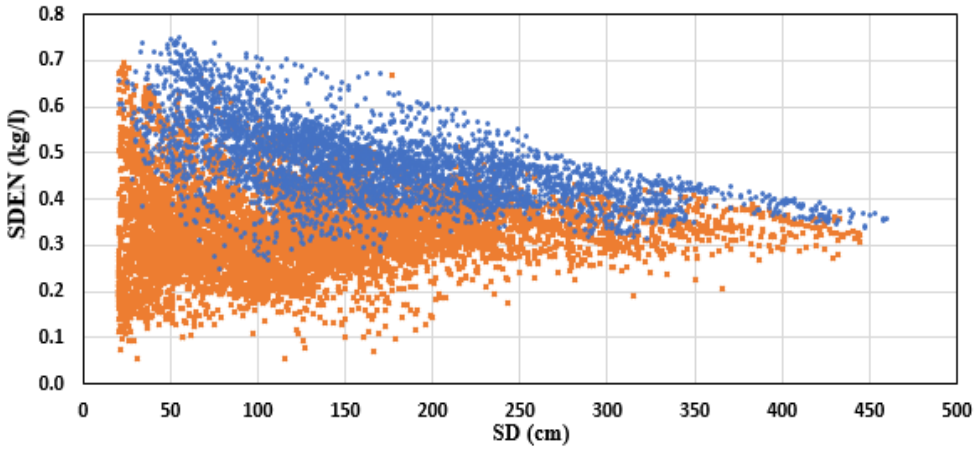

Fig. 3.8. SDEN variability with SD for the set of TNMs. Blue, front—Late season snowpack (21 March–21 June); Orange, back—Early season snowpack (21 October–21 March).

3.3.4. Multiple Linear Regressions (MLRs)

The MLRs between SDEN and the evaluated predictors were studied for the automatic measurements and compared with the manual samples. Those MLRs follow Equation (3.3):

$$SDEN = A_1 \cdot day + A_2 \cdot PPacum + A_3 \cdot Tave7d + A_4 \cdot SD + B \qquad \textbf{Equation 3.3}$$

The coefficients Ai are given in Table 3.9 for each site studied. As mentioned before, predictors were added progressively in the MLR model from more to less dominant, indicating the incrementally adjusted correlation coefficient (adjusted R^2). Moreover, the effect of elevation for the data from the set of TNMs was also evaluated as a driver, thus the MLR followed Equation (3.4):

$$SDEN = A_1 \cdot day + A_2 \cdot PPacum + A_3 \cdot Tave7d + A_4 \cdot SD + A_5 \cdot elevation + B \qquad \textbf{Equation 3.4}$$

Therefore, (R^2) for A4 (SD) represents the adjusted correlation coefficient for the MLR model and Equation (3.3), while (R^2) for A5 (Elevation) represents the adjusted correlation coefficient for the MLR model and Equation (3.4).

Table 3.9. Optimum SDEN multiple linear regression model for TNM selected sites and the set of TNMs (TNMs Nos. 1, 2, 4, 6, 7 and 9). Regression coefficients [A_i, B] and the incrementally adjusted correlation coefficient (Ri^2). Bold letters are used for the final adjusted correlation coefficient (R^2) for Equations (3.3) and (3.4).

Name	A_1 (day)	A_2 (PP_{acum})	A_3 (T_{ave7d})	A_4 (SD)	A_5 (Elevation)	B
1.Quimboa	$[1.056\cdot10^{-3}]$ (0.606)	$[0.205\cdot10^{-3}]$ (0.648)	$[4.783\cdot10^{-3}]$ (0.681)	$[-0.190\cdot10^{-3}]$ **(0.691)**	-	[0.187]
2. Izas	$[0.788\cdot10^{-3}]$ (0.641)	$[0.078\cdot10^{-3}]$ (0.652)	$[5.520\cdot10^{-3}]$ (0.732)	$[-0.057\cdot10^{-3}]$ **(0.735)**	-	[0.218]
4. Bachimaña	$[1.282\cdot10^{-3}]$ (0.396)	$[0.020\cdot10^{-3}]$ (0.414)	$[2.317\cdot10^{-3}]$ (0.468)	$[-0.480\cdot10^{-3}]$ **(0.542)**	-	[0.257]
6. Ordiceto	$[2.295\cdot10^{-3}]$ (0.733)	$[0.035\cdot10^{-3}]$ (0.780)	$[3.287\cdot10^{-3}]$ (0.803)	$[-0.440\cdot10^{-3}]$ **(0.825)**	-	[0.096]
7. Renclusa	$[1.267\cdot10^{-3}]$ (0.152)	-	$[7.242\cdot10^{-3}]$ (0.514)	$[-0.694\cdot10^{-3}]$ **(0.631)**	-	[0.271]
9. Eriste	$[1.263\cdot10^{-3}]$ (0.271)	$[0.0475\cdot10^{-3}]$ (0.280)	$[2.505\cdot10^{-3}]$ (0.356)	$[-1.005\cdot10^{-3}]$ **(0.600)**	-	[0.365]
Set of TNMs	$[1.268\cdot10^{-3}]$ (0.459)	$[0.0685\cdot10^{-3}]$ (0.460)	$[4.266\cdot10^{-3}]$ (0.503)	$[-0.352\cdot10^{-3}]$ **(0.562)**	$[0.0482\cdot10^{-5}]$ **(0.568)**	[0.130]

The MLR models improve the correlation compared with the single linear regression for intra-annual temporal dependence (A1), especially for those with a low adjusted R^2, such as the Renclusa and Eriste TNMs. The adjusted R^2 ranges from 0.54 for the Bachimaña TNM to 0.83 for the Ordiceto TNM. The seasonal accumulated precipitation (PP_{acum}) improves the correlation for the Quimboa and Ordiceto TNMs. The 7-day average temperature (Tave7d) plays a key role in describing SDEN for the Renclusa TNM and influences SDEN moderately for the Izas and Eriste TNMs. SD had an important effect in describing SDEN for the Bachimaña, Renclusa and especially the Eriste TNMs, and consequently, in the overall set of TNMs. The set of TNMs shows an adjusted R^2 of 0.57. However, adding elevation showed very little improvement, as the SD and elevation had a great collinearity.

Chapter 4
Analysis of climate change's effect on flood risk. Case study of Reinosa in the Ebro river basin

Lastrada, E.; Cobos, G.; Torrijo, F.J. Analysis of Climate Change's Effect on Flood Risk. Case Study of Reinosa in the Ebro River Basin. Water 2020, 12, 1114. https://doi.org/10.3390/w12041114

4.1. Introduction

Finally, as a continuation of the initial methodology, the effects that climate change can have on floods are studied for a case study of a snow basin in the Cantabrian Mountains.

Floods are natural hazards that produce great material damage and human losses worldwide (European Environmental Agency, 2010). The increasing population density and infrastructure on river banks contribute to increased floodplain vulnerability, which can result in severe social, economic and environmental damage (MITECO, accessed on 2019).

The fourth of the nine essential rules of flood risk management indicates that it should be taken into account that "The future will be different from the past. Climate and

societal change as well as changes in the condition of structures can all profoundly influence flood risk" (Yuanyuan, et al., accessed on 2020).

For all these reasons, it is essential to design methodologies that enable one to estimate flow regime variations and evaluate flood risk modification due to climate change (Doroszkiewicz, Romanowicz, & Kiczko, 2019); (Zhu, Lund, Jenkins, Marques, & Ritzema, 2007); (Nyaupane, Thakur, Kalra, & Ahmad, 2018). Flood Risk Assessment recent methodologies can be classified in three major categories, being the present study focused on the assessment of the sources of uncertainties in FRA (Díez-Herrero & Garrote, 2020).

The technical document of the IPCC IV forecasts a probable increase in the frequency and intensity of precipitation episodes, as well as a decrease in average values in summer for mid-latitudes countries as Spain. The Fifth Assessment Report (AR5) of the IPCC (2013–14), points out that it is probable that the frequency or intensity of intense rainfall has increased in Europe, and in relation to future changes, that extreme precipitation events over most of the mid-latitude lands will most likely be more intense and more frequent (Intergovernmental Panel on Climate Change, 2019). Additionally, climate change can specially affect those regions in which the snow phenomenon is relevant in hydrological behaviour.

As a matter of these facts, the 2019 flash flood European notifications beat the last 7 years of notifications clearly (European Flood Awareness (EFAS), accessed on 2019) , and Reinosa (Cantabria, Spain) suffered two important floods on January and December 2019, the second one being one of the worst floods in memory. This flood was caused by the Elsa storm, on December 19 and 20, which came from the southwest and was accompanied by very strong winds and very high temperatures for that time of the year, causing the melting of the snow-cover in the highest part of the catchment. A203 gauging station, recorded on 12/20/2019 at 1:00 a.m., 246 m3/s instant (15 minutes period) flow, while the maximum ever recorded was 100 m^3/s (02/27/2010). The daily flow rate recorded by A203 for this event was 83 m3/s and the return period has been estimated approximately as Tr = 300 years. This flood caused great damage in Reinosa, affecting residential areas (Figure 4.1).

Fig. 4.1. Reinosa (Cantabria, Spain). 20th December 2019.

Reinosa (Cantabria, Spain) is located in the north of the Iberian Peninsula, in the junction of Hijar, Ebro and Izarilla rivers, immediately upstream the Ebro reservoir. Hijar catchment, with 27.6 km length and 147.6 km^2 surface, drains the highest area of Cantabrian mountain range that belongs to the Ebro river basin. The catchment height ranges between 865 and 2023 m above sea level, with a mean height of 1351 m. A203 gauging station is located in Hijar river, immediately upstream of Reinosa, with a time of concentration of approximately 15 hours.

The average rainfall of the head of the Ebro for the period 1920–2002 was 1190 mm/year, concentrated in autumn and winter, characteristic of an Atlantic climate, with some continental patterns producing 33 L/s/km^2. The average annual temperature is 8.9 ºC in Reinosa. The main land uses in the catchment are forest and scrub. Figure 4.2 shows Hijar river basin overall and site map.

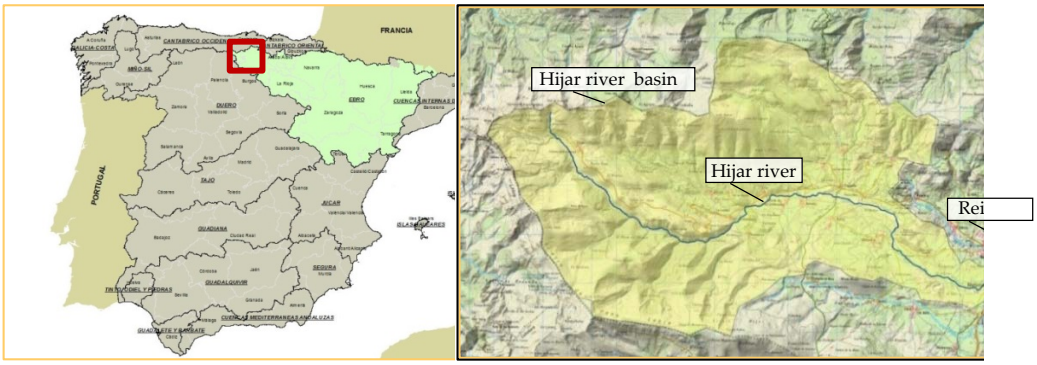

(a) (b)

Fig. 4.2. Hijar river basin. (a) Overall Site map. (b) Detailed Site map.

Reinosa belongs to the Hijar river basin, and had potential significant flood risk (ES091_HIJ_01_02_04_05_06) during the implementation of DIRECTIVE 2007/60/EC, as shown in Figure 4.3.

Fig. 4.3. Hijar potential significant flood risk (ES091_HIJ_01_02_04_05_06). http://iber.chebro.es/SitEbro/sitebro.aspx.

DIRECTIVE 2007/60/EC implies an objective quantification of flood risk, for low (500 years return period), medium (100 years return period) and high probabilities (10 years return period), that will allow the efficient development of flood risk management plans by implementing a set of combined actions to reduce floods' consequences (European Commision Directive 2007/60/Ec, 2007).

To evaluate different climate change scenarios, the Spanish Meteorological Agency (AEMET) regionalized a set of global climate models, by using two statistical downscaling methods. The usefulness of this regionalization was assessed by their fitting to the observed data in the control period (1961–2000). A comparison based on a set of statistics show that although the fit is good for annual mean values, annual maximum values for both regionalization methods are not adequately simulated, since they provide lower extremes with a smaller variability. However, different fitting was observed depending on the Spanish region (Garijo & Mediero, 2018).

Although results might show a decrease in the magnitude of extreme floods for climate model projections downscaled by AEMET (Garijo, Mediero, & Garrote, 2018), a different pattern might be concluded, when taking into account snowmelt, if the melting flow rate's increase due to higher temperatures is bigger than the decrease caused by less snow accumulation.

4.2. Materials and Methods.

4.2.1. Overall methodology.

According to DIRECTIVE 2007/60/EC, Spanish hazard and flood risk maps can be downloaded at https://sig.mapama.gob.es/snczi/, regarding the following scenarios: (a) floods with a low probability, or extreme event scenarios (return period ≥ 500 years); (b) floods with a medium probability (likely return period ≥ 100 years); (c) floods with a high probability (return period ≥ 10 years).

By relating flow rates in A203 gauging station with hazard and risk maps, correlations with flooding surface, economic damage and casualties can be achieved.

In order to evaluate climate change, projections of a series of climatic variables are entered as input data in a calibrated hydrological model in the study basin. The ASTER® model is a distributed hydrological model that calculates snowmelt and accumulation regarding energy balance (Cantarino I. , 1998); (Cobos & Collado, 2019).

Two global climate models (GCM), downscaled by the Spanish Meteorological Agency (AEMET), have been selected; being validated with real flow rates from the control period (1961 to 2000) and used under the highest greenhouse gas emissions pathway (RCPs 8.5) from the Fifth Assessment Report of the Intergovernmental Panel on Climate Change.

The relationship between calculated daily flow rates and instant (15 minutes period) flow rates is not necessary for these downscaled climate models, as climate change's effect will be calculated in relative terms comparing climate models in the calculation period in two equal length stages (2007–2038) and (2039–2070).

Once the flow rate variation for the climate projection is estimated and applied on real flow, new impacts on hazard and risk maps can be established. Figure 4.4 shows the overall methodology scheme.

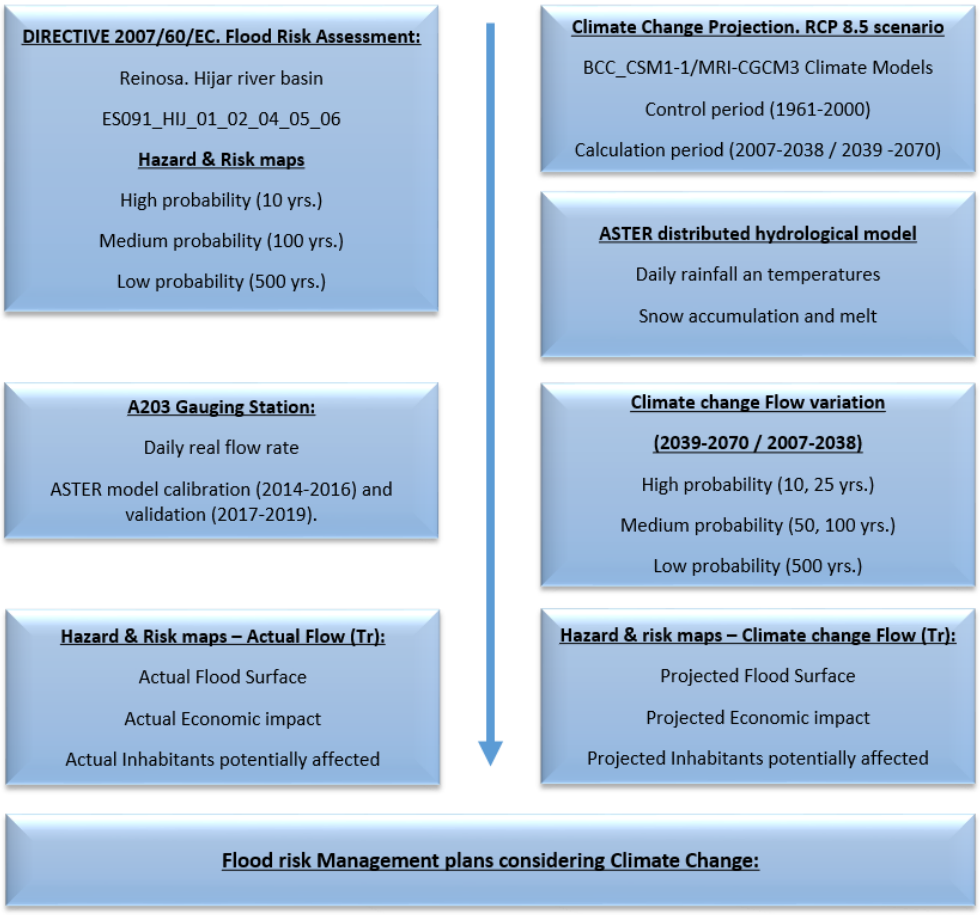

Fig. 4.4. Overall methodology scheme

4.2.2. Hazard and risk maps.

Hazard maps are the result of two-dimensional hydraulic models, indicating flooded area, flood depths and flood velocities. Return periods were given by Spanish Authority in the framework of DIRECTIVE 2007/60/EC implementation by "Maximum Flow Maps" software, based on a regionalized gauging station study (Jiménez, Montañés, Mediero, Incio, & Garrote, 2018).

Flood risk maps shall show the potential adverse consequences associated with flood scenarios, and express, among other things, terms of the indicative numbers of inhabitants potentially affected and the type of economic activity of each area potentially affected. Additionally, economic damage can be estimated.

According to DIRECTIVE 2007/60/EC, these maps serve as a tool for establishing priorities and for making additional technical, economic and political decisions related to flood risk management. Measures to be implemented in the at-risk areas can be prioritized, depending on the results of the cost-benefit analysis. They also allow the evaluation of the climate change's effects. The risk associated with flood events is established based on the vulnerability of the threatened element and the hazard to which it is exposed. The estimation of indicative number of inhabitants potentially affected depends on updated census data. The Spanish Water Authority has also established a methodology to estimate the economic value of flood damage partially based on the PREEMPT project (MITECO, accessed on 2019); (PREEMPT, accessed on 2019).

Finally, a relationship, as shown in Table 4.1, between flow rates for different return periods in Hijar, A203, and hazard and risk maps can be estimated, and subsequently a trend line, as shown in Figure 4.5, can be fitted:

Table 4.1. Instant (15 minute) flow rate, flood surface, inhabitants potentially affected and economic damage[1].

Instant Flow rate (m3/s)	Return Period (years)	Surface (km2)	Inhabitants	Economic value (€)
138	10	2.783	346	29194901
214	100	3.843	982	56806383
273	500	4.620	1484	90791074

[1] Obtained for overall ES091_HIJ_01_02_04_05_06 potential significant flood risk area, including the Spanish Public Water Domain (RDPH).

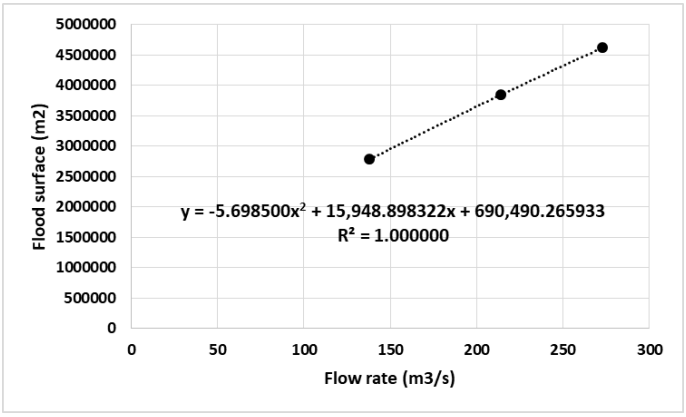

(a)

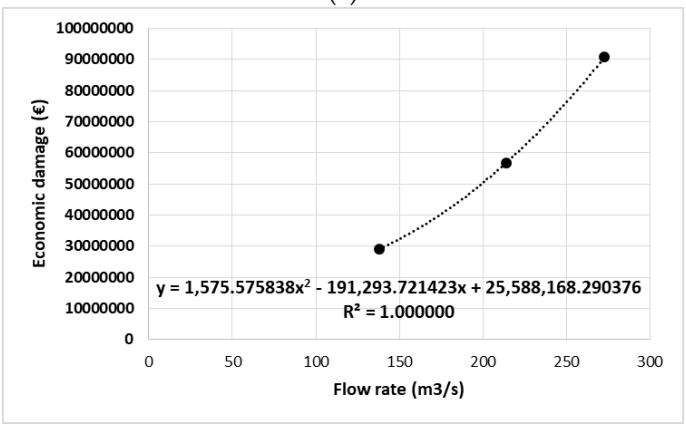

(b)

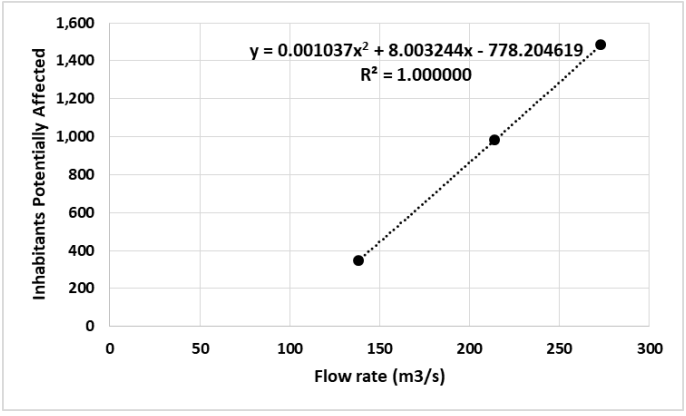

(c)

Fig. 4.5. (a) Flood surface, (b) inhabitants potentially affected and (c) economic damage value in terms of flow rate in A203 Hijar in Reinosa Gauging Station

4.2.3. Hydrological model. Hijar basin model.

A 500 by 500 m grid and daily time resolution distributed hydrological model has been built for the Hijar river basin (Figure 4.6), with A203 in Reinosa as the outlet and calibration point, 2014–2016 as the calibration period and 2017–2019 as the validation period.

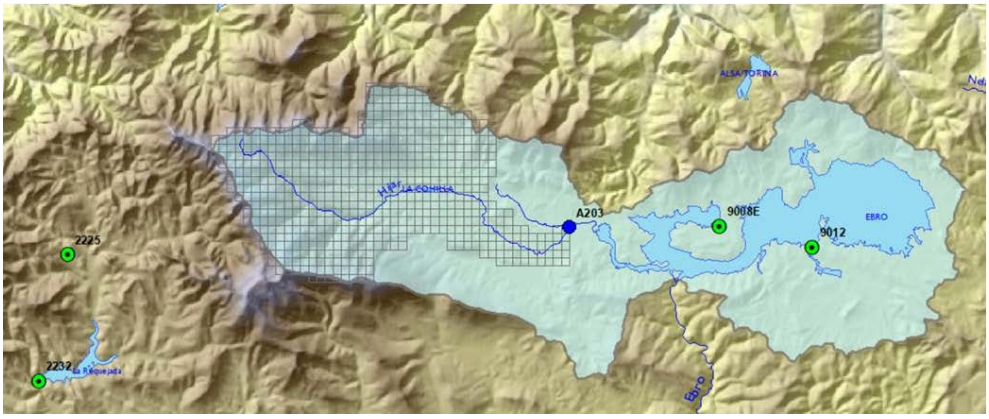

Fig. 4.6. ASTER hydrological model. Hijar river basin mesh (grey grid), Gauging Station (A203), rainfall stations (9008E, 9012) and temperature stations (2225, 2232)

ASTER® is a distributed hydrological model that calculates stream flow in a river using rainfall, temperature, wind speed and radiation as climate inputs. It has been applied in several countries and implemented by Spanish water authorities as an accurate model in river basins with strong snow phenomena, as in our case study (Hijar catchment) (Cobos, 2004); (Cobos, Francés, & Arenillas, 2010). Figure 4.7 shows the snow–water equivalent for two consecutive days in Hijar model.

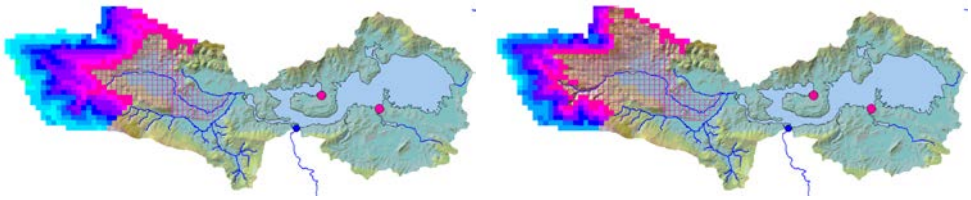

(a) (b)

Fig. 4.7. ASTER hydrological model snow accumulation (snow–water equivalent) (a) Day 1, (b) Day 2. Hijar model (ranging from 1 mm – pink to 215 mm – cyan).

4.2.4. Snow accumulation and Snow melt routine.

See Section 2.2.2.

4.2.5. Model calibration and validation.

Calibration and validation have been carried out, comparing real daily flow rates, in A203 Hijar in Reinosa Gauging Station with the ASTER model daily flow rates being calculated with real meteorological data. The available continuous period for the observed daily flow rate ranges from 2014 to 2019, defining the calibration period as October 1st 2014 to September 30th 2016 and the validation period from October 1st 2017 to December 22nd 2019, including the aforementioned extraordinary event.

Figure 4.8, shows results during the calibration period, with a correlation coefficient of 0.90 and a Nash index (NSE) of 0.78. The maximum observed daily flow rate was 23.6 m^3/s, and the maximum calculated daily flow rate was 23.5 m^3/s. Total observed runoff was 189 hm^3 and calculated runoff was 200.7 hm^3, with 27 hm^3 of overall snow–water equivalent accumulation.

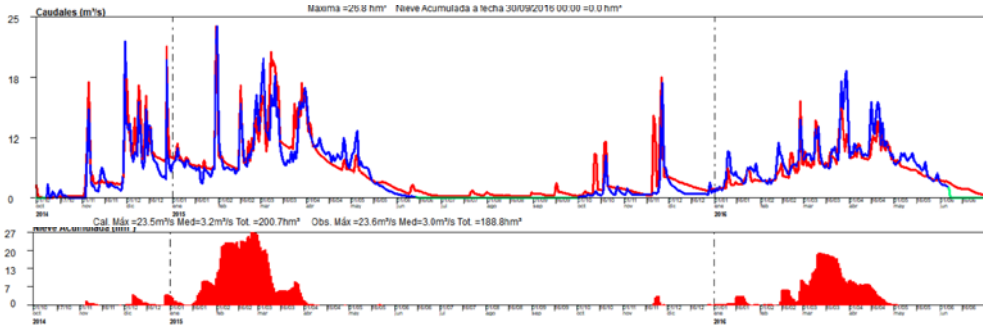

Fig. 4.8. Upper level. Real (blue) and calculated (red) daily flow rates in A203. Lower level. Snow water equivalent in the catchment for the calibration period.

The main calibration parameters of the model are:

- M_{FMAX} = 5.5 (mm/ºC/24 h);
- M_{FMIN} = 1.46 (mm/ºC/24 h);
- T_{mi} = -0.35 (ºC);
- Rain/Snow temperature = -0.53 (ºC);
- Altimetry temperature gradient = -3.1 (ºC/1000 m).

Figure 4.9 shows results during the validation period, with a correlation coefficient of 0.90 and a Nash index (NSE) of 0.80. The maximum observed daily flow rate was 83 m^3/s, and the maximum calculated daily flow rate was 69 m^3/s. Total observed runoff was 231 hm^3 and calculated runoff was 289 hm^3, with 20 hm^3 of overall snow–water equivalent accumulation.

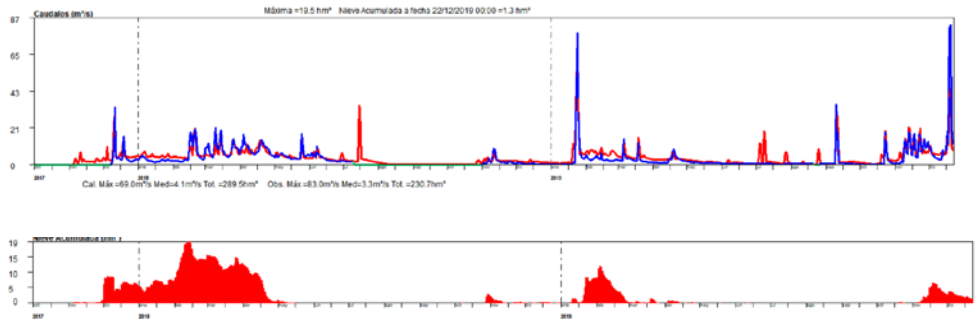

Fig. 4.9. Upper level. Real (blue) and calculated (red) daily flow rates in A203. Lower level. Snow water equivalent in the catchment for the validation period.

4.2.6. Climate projection.

Daily rainfall and temperature data from two regionalized climate models (analog method—ANA and statistical regionalization method—SDSM) can be obtained from AEMET website (http://www.aemet.es/es/serviciosclimaticos/cambio_climat) for RCP 8.5.

Two climate models have been selected from 24, to analyse the combination of rainfall and temperature:

- ANA—BCC-CSM1-1 (BCC);
- ANA—MRI-CGCM3 (MRI).

These two models have been pre-selected as generating the highest rainfalls. To evaluate their suitability, daily flow rates for the control period (1961–2000) have been calculated with ASTER for real meteorological data and both climate models. Figure 4.10 (a) shows that annual maximum real daily flow rates are above climate models, and the trend line shows a higher increase as well. Figure 4.10 (b) shows that annual mean real daily flow rates fit the MRI better at the beginning of the control period, while a fit better with BCC is shown at the end of the control period. Supplementary Materials for rainfall stations (9008E, 9012) and temperature stations (2225, 2232) is given.

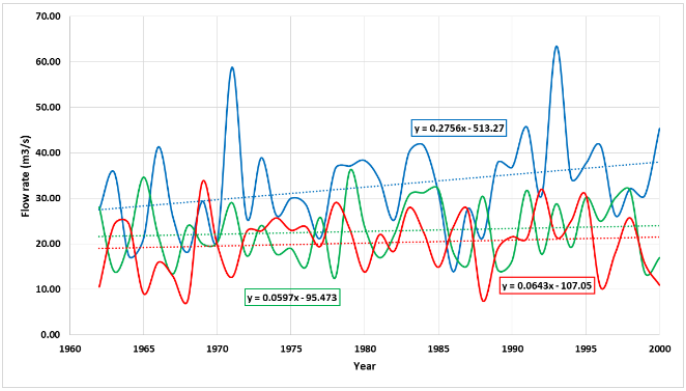

(a)

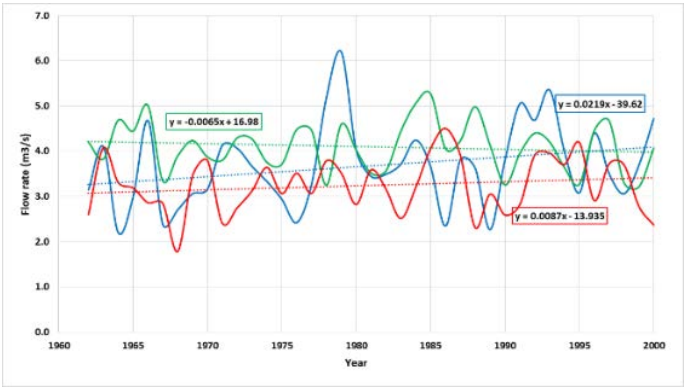

(b)

Fig. 4.10. Daily flow rate evolution during control period (1961–2000) for real data (blue), BCC (green) and MRI (red). (a) Annual maximum, (b) annual mean.

4.2.7. Calculation of flow rates for different return periods.

Daily flow rates for the calculation period (2007 to 2070) have been estimated with ASTER model for both climate projections (BCC and MRI). Calculation period has been divided in two equal length stages (2007 to 2038) and (2039–2070) and a probability distribution of extreme values has been estimated using the Gumbel distribution, presenting the best fit goodness (Equation 4.1):

$$X = u - \beta \cdot \mathrm{Ln}\left(-Ln\left(\frac{Tr-1}{Tr}\right)\right) \qquad \textbf{Equation 4.1.}$$

Where,

u = location parameter; β = scale parameter; T_r = Return period

Finally, daily flow rates and instant (15 minute period) flow rates observed in A203 can be fitted in a linear relationship. As climate projections flow rates are being studied in relative terms with observed flow rates, transformation from daily flow rates into instant flow rates is not necessary.

4.3. Results.

4.3.1. Flow rate evolution (RCP 8.5).

Table 4.2 and Figure 4.11 show results and trend lines from percentile analysis for both calculated climate models. For BCC-CSM1-1 a small decrease in flow rate projection due to climate change is estimated, with small variability for different probabilities, while for MRI-CGCM3 bigger increase is predicted, showing a smooth variability for different probabilities, describing a more extreme climate.

Table 4.2. Return period, daily flow rate projection, 1st Stage (2007–2038); daily flow rate projection ratio, 2nd Stage (2039–2070); and flow rate ratio (2nd Stage/1st Stage).

ANA—BCC-CSM1-1

Tr (years)	Flow rate Projection 2007–2038 (m3/s)	Flow rate Projection 2039–2070 (m3/s)	2039–2070 / 2007–2038[1] (%)
10	28.13	27.00	96.0%
25	31.92	30.62	95.9%
50	34.73	33.30	95.9%
100	37.52	35.96	95.9%
500	43.96	42.11	95.8%

ANA—MRI-CGCM3

Tr (years)	Flow rate Projection 2007–2038 (m3/s)	Flow rate Projection 2039–2070 (m3/s)	2039–2070 / 2007–2038[1] (%)
10	27.36	31.05	113.5%
25	31.99	36.51	114.1%
50	35.43	40.57	114.5%
100	38.85	44.59	114.8%
500	46.74	53.88	115.3%

[1] Column 3 divided by column 2.

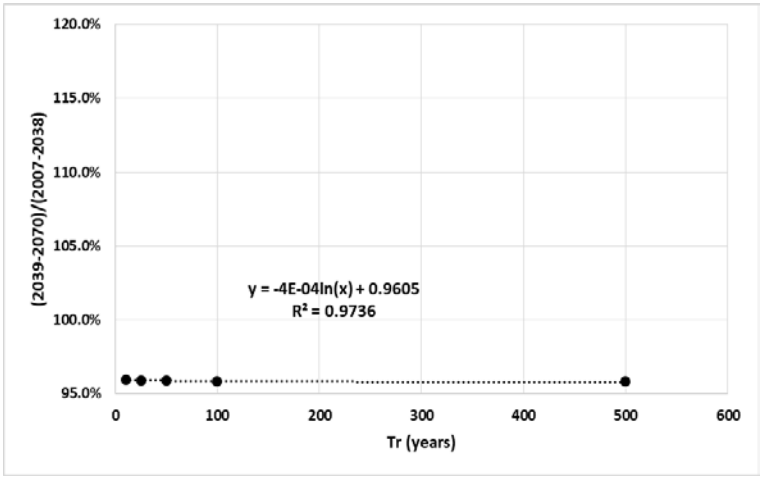

(a)

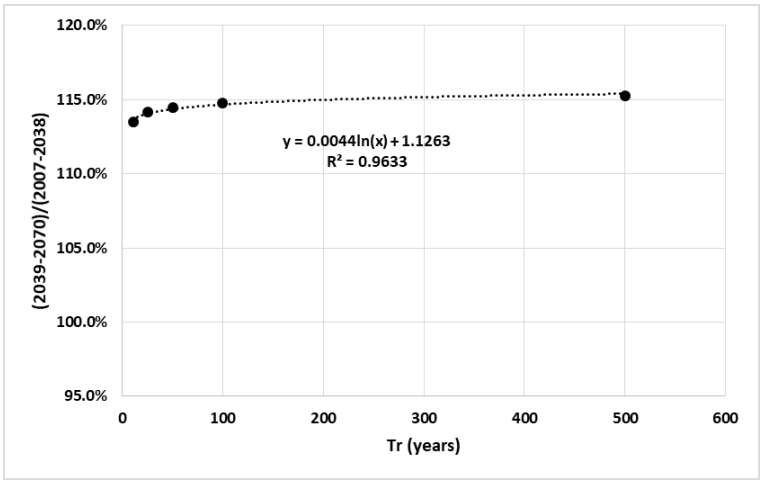

(b)

Fig. 4.11. Flow rate projection ratio (2nd Stage (2039–2070)/1st Stage (2007–2038)) trend line in terms of return periods. (a) Analog method (ANA)—BCC-CSM1-1; (b) ANA—MRI-CGCM3.

4.3.2. Hazard and risk maps.

After calculating the projected flow rate by entering for each return period (2nd Stage (2039–2070)/1st Stage (2007–2038)) the flow rate ratio in the trend line fitted for flood surface, economic damage and inhabitants potentially affected (Figure 4.5), new climate change estimations show similar results as for flow rate (Table 4.3).

Table 4.3. Projection ratio 2nd Stage (2039–2070)/1st Stage (2007–2038) for the flow rate, flood surface, inhabitants potentially affected and flood damage's economic value.

ANA—BCC-CSM1-1

Flow rate (%)	Instant Flow rate (m3/s)	Return Period (years)	Flood Surface (%)	Inhabitants (%)	Economic value (%)
-4.0	132.4	10	-2.9	-13.3	-4.5
-4.1	205.1	100	-3.1	-7.6	-7.3
-4.2	261.5	500	-3.2	-6.6	-8.2

ANA —MRI-CGCM3

Flow rate (%)	Instant Flow rate (m3/s)	Return Period (years)	Flood Surface (%)	Inhabitants (%)	Economic value (%)
13.5	156.7	10	9.6	44.8	17.4
14.8	245.6	100	11.0	27.3	29.7
15.3	314.7	500	11.4	24.2	33.7

As for flow rate, the MRI-CGCM3 climate model shows an increase in flood risk effects due to climate change, while BCC-CSM1-1 shows a decrease. Results are enlarged for economic value and inhabitants potentially affected, while flooded surface decreases.

A logarithmic trend line is the one that best fits, and represents how the atmosphere behaves (Figures 4.12, 4.13 and 4.14).

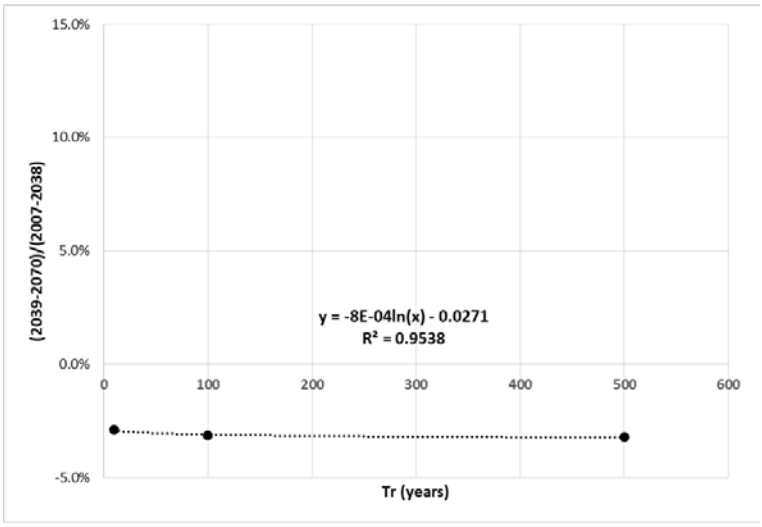

(a)

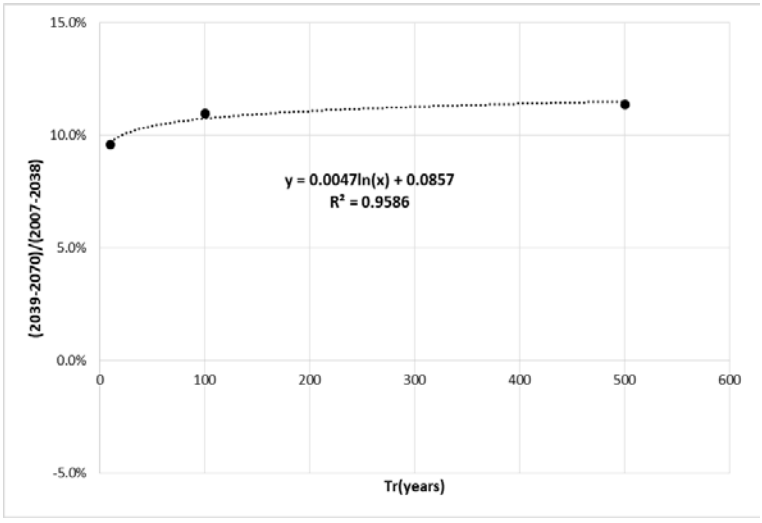

(b)

Fig. 4.12. Second Stage (2039–2070)/1st Stage (2007–2038) flood surface ratio trend line in terms of return periods. (a) AN—BCC-CSM1-1; (b) ANA—MRI-CGCM3.

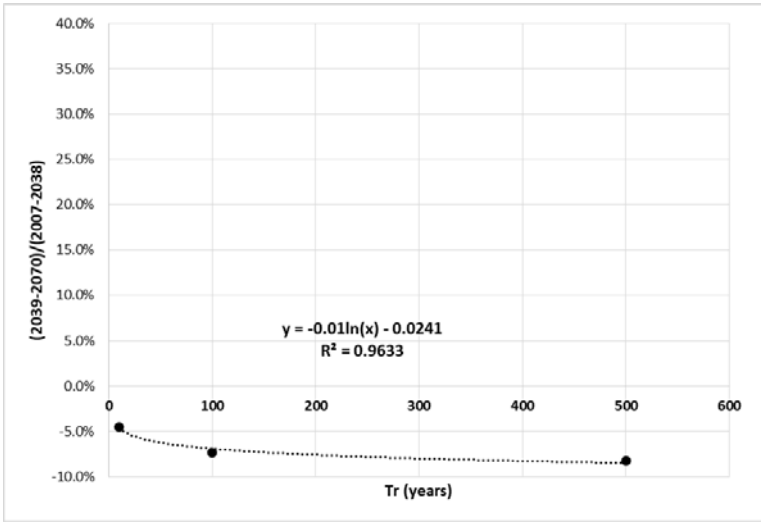

(**a**)

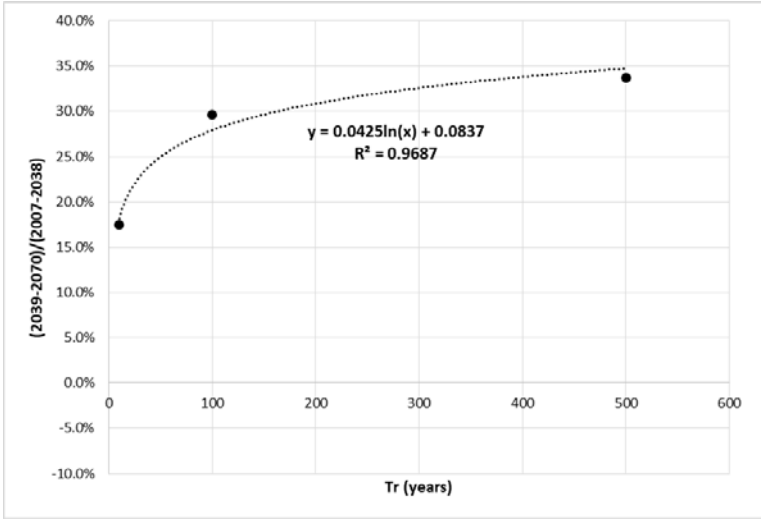

(**b**)

Fig. 4.13. Second Stage (2039–2070)/1st Stage (2007–2038) economic damage ratio trend line in terms of return periods. (a) ANA—BCC-CSM1-1; (b) ANA—MRI-CGCM3.

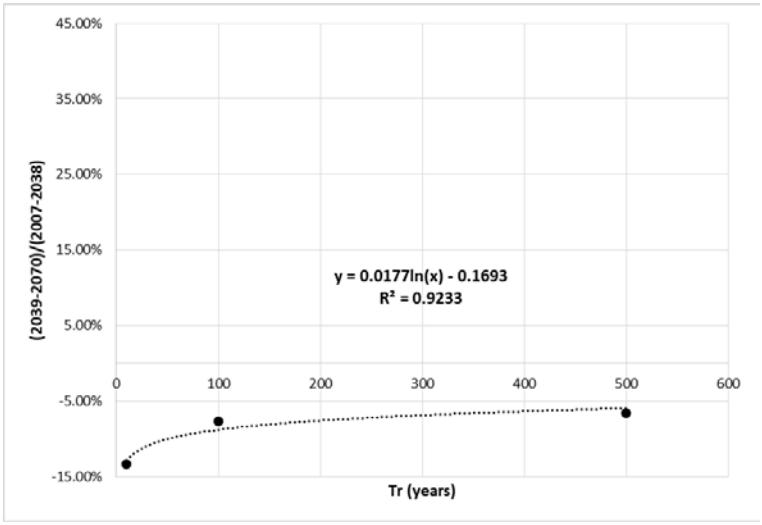

(a)

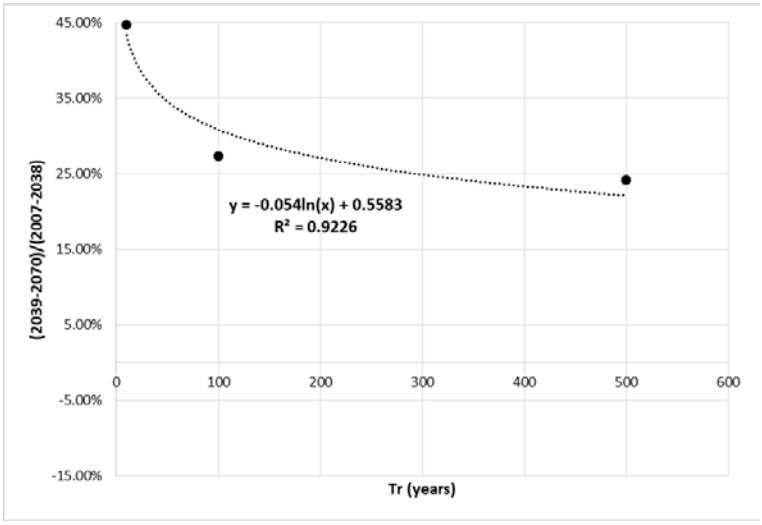

(b)

Fig. 4.14. Second Stage (2039–2070)/1st Stage (2007–2038) inhabitants potentially affected ratio trend line in terms of return periods. (a) ANA—BCC-CSM1-1; (b) ANA—MRI-CGCM3.

Flooded surface, inhabitants potentially affected and flood economic damage value can be calculated in absolute terms and are shown in Table 4.4 for ES091_HIJ_01_02_04_05_06.

Table 4.4. Absolute terms for the flow rate, flood surface, inhabitants potentially affected and flood damage's economic value for selected climate change projections[1].

ANA—BCC-CSM1-1

Flow rate (m3/s)	Return Period (yrs.)	Surface (km2)	Inhabitants	Economic value (€)
132.4	10	2.703	300	27887407
205.1	100	3.722	907	52640944
261.5	500	4.472	1386	83327840

ANA—MRI-CGCM3

Flow rate (m3/s)	Return Period (yrs.)	Surface (km2)	Inhabitants	Economic value (€)
156.7	10	3.049	501	34286399
245.6	100	4.263	1250	73649691
314.7	500	5.145	1843	121426897

[1] Obtained for overall ES091_HIJ_01_02_04_05_06 potential significant flood risk area, including the Spanish Public Water Domain (RDPH).

Chapter 5
Discussion

5.1. Overall discussion.

The previous analyses evidence a tendency to a change in the pattern of the snow-related phenomena in Spain, which will decrease its regulatory effect on rivers. Melted snow streams to rivers, increasing their flow significantly. Therefore, the change in melting patterns also leads to a change in flow patterns. As melting will move from spring to winter, maximum flows are also expected to significantly increase during winter.

Especially, in terms of future flood events, the change in the snow behaviour pattern gives rise to increasing the risk of flooding and their damaging effects, with an expected increase in the number of episodes with strong flow peaks. Future snowmelt time in the four regions analysed will coincide with the first half of the year, where precipitations are also expected to increase. Besides, an increase in the average precipitations is expected in the Pyrenees, Sierra Nevada and the Central System. In the Cantabrian Mountains, precipitations along the year may decrease, but the heavy snowfall episodes expected along with the shorter duration of snow on the peaks will also cause an increased risk of flooding.

All in all, the effect of climate change on the snow-related phenomena shows that the regulatory effect of the snow with respect to the incorporation of runoff into the riverbeds will be less significant in the future. This will require different management and probably force a greater need for reservoir capacity to achieve optimal regulation and maintain current supply guarantee conditions for the populations and agricultural lands. At the same time, extreme flood situations will continue to occur, requiring new flood risk management plans.

5.2. Limitations of the hydrological model.

The ASTER hydrological model has been calibrated and validated in the Pyrenees for a long period that ranges from 1950 to 2005 (Arenillas, Cobos, G., & Navarro, 2008), showing a good fitting for the already changing climate variables caused by climate change that were non-explicit, such as radiation. However, greater changes in radiation are expected in the next 50 years, so the model might show uncertainties associated with this variable. Radiation depends on multiple factors that are difficult to predict. Besides, other effects such as snow impurities affecting snow albedo may have a greater effect on melting than the radiation input itself (Pey, et al., 2020).

However, for the Pyrenees, where average $Mf_{,max}$ deals 4.60 mm/ºC/day in July and average $Mf_{,min}$ 1.35 mm/ºC/day in January (see Table 2.2), and considering a sinusoidal radiation distribution for a representative place of the Pyrenees, an advancement of the snowmelt from April to March represents a reduction of average $Mf_{,april}$ of 3.14 mm/ºC/day to 2.86 mm/ºC/day. A reduction from May to April means a reduction of 3.76 mm/ºC/day to 3.14 mm/ºC/day.

This means that for a given temperature, M_c is reduced approximately 9% (2.86/3.14) from April to March and a 16.4% from May to April (3.14/3.76) due to the radiation effect associated with temperature changes. On the other hand, an increase of 1.5ºC in the average temperature, from 5.8ªC to 7.3ªC for a given month means an approximate increase of 29% of the snowmelt Comparing both values, radiation plays a significant role to counter-act melting due to an increase in temperatures.

Other limitations of the model that may lead to uncertainties have already been stated in a previous section, such as infiltration due to future development of vegetation, which may not be easy to predict and may be influenced as well by other anthropic effects.

5.3. Variations in the pattern of snow-related phenomena in Spanish Mountains due to the climate change effect.

Nowadays the influence of snow on the contribution to water resources in Spain is highly variable in each of the different regions analysed.

For instance, and according to the work of Arenillas et al. (Arenillas, Cobos, G., & Navarro, 2008), who studied snow-related phenomena in Spain during the period from 1950 to 2007, in the Central System, the snow at its highest point (spring) represents a total of 10% of the rainfall received, but this value reduces to 5% for the entire hydrological year. In regions where snow behaviour is much more accentuated, such as Sierra Nevada or the Pyrenees, these values can rise to a maximum of 55% and 40% respectively, leaving values of 45% and 28% for the entire hydrological year respectively. It should be noted that higher elevation, as is the case of Sierra Nevada and the Pyrenees, implies longer snow permanence and greater regulatory effect.

The hypothesis of slower snowmelt in a warmer world due to contraction of the snowmelt season to a time of lower available energy (Musselman, Clark, Liu, Ikeda, & Rasmussen, 2017), must be combined with the response of the snowpack to the

magnitude and sign of changes in precipitation (López-Moreno, Pomeroy, Revuelto, & Vicente-Serrano, 2013).

5.3.1. Pyrenees.

In the Pyrenees, the water accumulated in the form of snow in the mountains for the climate change scenario undergoes an early meltdown of about 30 days compared to the current situation. This implies a lower regulatory effect from the point of view of water resources. The flow increases in the rivers during the winter season and at the beginning of spring, while the contribution of flows from the month of April is reduced. This scenario denotes a lower regulatory effect of circulating flows and therefore will force different management of the reservoirs to the current one, requiring greater regulation capacity to achieve supply conditions similar to the actual ones. A decrease on snow accumulation about 20% for every 1 °C, and a reduction on the duration of the snowpack about 20–30 days per °C was estimated for a small snow-dominated basin in the Spanish Pyrenees (López-Moreno, Pomeroy, Revuelto, & Vicente-Serrano, 2013).

5.3.2. Sierra Nevada.

In Sierra Nevada melting of the accumulated snow is advanced in around 30 days. This advance is directly reflected in flowing flows, which suffer a decrease in the months of greatest demand. Therefore, the future scenario shows that the regulatory effect of water resources associated with the snow-related phenomena will be reduced.

5.3.3. Central System.

In the Central System, climate change will lead to snowmelt increasing until reaching its maximum value in February, approximately 30 days earlier compared with the time it normally occurs today. This circumstance implies an increase in circulating flows between the months of January and March.

5.3.4. Cantabrian Mountains.

In the Cantabrian Mountains, a reduction of the regulatory effect of the accumulated snow in mountain areas is also detected, producing an earlier snowmelt of about 45 days and a much more accentuated low water level in rivers from April. These results agree with previous studies predicting that by the end of the twenty-first century, the peak flow of many North American and European rivers is expected to occur 30–40 days earlier as a result of earlier snowmelt (Stewart, Cayan, & Dettinger, 2004); (Arnell, 1999), but changes in precipitation caused by climate change can increase or reduce flow rates.

5.4. Flood risk increase due to the climate change effect.

It must be considered that snow accumulated is very sensitive to weather conditions, and a generalized increase in temperatures will cause a rapid and important melting and a higher probability of direct rainfall instead of snow accumulation that will provide significant water resources added to those already streaming. Thus, climate change

scenarios show a greater risk of flooding situations with more damaging effects. Particularly, the increase in temperatures and decrease in average accumulations, or the delay in the accumulation of snow, may generate extreme events in which all the precipitation occur in liquid form (water), instead of part of the same being retained in the form of snow in the highest parts of mountains. This phenomenon has already happened in December 2019 in the town of Reinosa (Lastrada, Cobos, & Torrijo, 2020), which suffered the worst flooding in memory (return period estimated about 300 years) causing great damage and affecting residents.

The suggested methodology for the case study of Reinosa allows to quantify the increase of flood risk in terms of flow rate, flooded surface, inhabitants potentially affected and economic damage for different return periods.

5.5. Climate models. Limitations.

It is important to mention that all the previous analyses are entirely based on a single climate change scenario, so even though the climate model used (ANA-MRI-CGCM3-rcp85) showed a good match with the present state in Spain, some uncertainty may arise. Previous works have shown a decrease in the magnitude of extreme floods for climate model projections in Spain (Garijo & Mediero, 2018). This is partly due to the use of global climate models from the Spanish Meteorological Agency (AEMET), which tend to provide lower extremes with a smaller variability (Garijo, Mediero, & Garrote, 2018).

Comparison between observed meteorological data and projections of climate scenarios, for a common time interval, has revealed a significant difference between the series. This means that the results must in any case be interpreted in relative terms, evaluating trends and not absolute values.

Results for both selected climate models show important differences between each other in absolute and relative terms, indicating that there is significant uncertainty in the projections, especially due to rainfall; and they suggest that for local impact studies, further analysis to regionalize outputs from global climate models still needs to be done. For the results to be reliable, climate models must adequately represent extreme phenomena, as most of them are suitable for evaluating water resource evolution.

There is a large uncertainty in climate projections that influences the estimation of future flood risk. The crucial action in the case of adaptation to floods is to carry out a detailed analysis to choose the best climate model and use results in relative terms between the short term (1st Stage) and long term (2nd Stage) of the projection period (Doroszkiewicz, Romanowicz, & Kiczko, 2019).

5.6. Seasonal and spatial variability of Snow Density in the Spanish Pyrenees.

The temporal and spatial variability of snow density (SDEN) were studied in this thesis in order to improve the ASTER hydrological model, using the biggest SDEN data bank for on-site manual samples and automatic measurements in the Spanish Pyrenees. More

than 375 manual samples and 21,000 automatic TNM data from the ERHIN program and Ebro Water Authority were used to define SDEN variability in the Spanish Pyrenees. Single and multiple linear regressions were conducted, relating SDEN with the time dependence and other drivers such as the seasonal accumulated precipitation, average temperatures, snow depth (SD) and elevation.

5.6.1. Comparison between automatic measurements (TNMs) and manual SDEN sampling.

The automatic measurements (TNMs) provided a better description of SDEN variability than the manual SDEN sampling, as the data volume was about 20 times larger.

For both the manual samples and the TNM data, the average SDEN values and the C.V. were very similar, not following a spatial pattern. This similarity was proven as well for the set of manual samples and the set of TNM measurements. Additionally, the C.V. for the winter snow was usually larger than that of the spring snow. The Izas TNM showed similar SDEN values compared with previous works, with 0.2 and 0.3 kg/L during the first months and increasing to 0.6 kg/L at the end of the season (López-Moreno, Quirós, Latron, & Fassnacht, 2010). However, it should be noted that similar values for the average and the C.V. are not representative of SDEN variability, either temporally or spatially.

5.6.2. Temporal variability of Snow Density.

Intra-annual time dependence was shown to be the predominant driver for almost all TNM sites. The densification rates ranged widely from 0.7×10^{-3} kg/L/day to 2×10^{-3} kg/L/day, without showing a spatial pattern, being 1.3×10^{-3} kg/L/day for the data from the set of TMNs. The densification rate for the set of manual samples was set to 1.2×10^{-3} kg/L/day, which is very similar to the automatic measurements. The densification rates were higher than those estimated for alpine regions in the former Soviet Union and the US, with average spring SDENs (kg/L) and snow densification rates (kg/L/day) of 0.25 kg/L and 0.79×10^{-3} kg/L/day, respectively, for the former Soviet Union and 0.31 kg/L and 1.07×10^{-3} kg/L/day, respectively, for the US. (Bormann, Westra, Evans, & McCabe, 2013).

5.6.3. Significance of climate drivers.

The seasonal accumulated precipitation presented a more dominant influence than daily precipitation, being the second most dominant SDEN driver for all sites except two. Historical behaviour showed a greater influence than daily behaviour. The third most important driver was the temperature. The 7-day average temperatures showed the best fitting to SDEN. Snow densification depends on punctual temperatures for the accumulation process, but during melting cycles, average temperatures may describe it better (Mizukami & Perica, 2008). SD was found to be less significant. For low SD, both low and high SDEN can be found, depending on an early season dominated by accumulation processes or a late season dominated by melting processes (Mizukami & Perica, 2008); (Jonas, 2009). For the early season, SDEN will depend on the proportion

of precipitation falling as rain and snow, so it is also possible to reach high SDEN values. However, the significance threshold of SDEN is distinctly reduced for high SD values. SDEN for the late-season snow shows higher values than the early-season snow for maximum SD as densification continues, even though the SD may keep similar values for a certain period.

The established significance order for the drivers matched with previous studies, where precipitation was the dominant climate variable at most sites, followed by the average temperature and melt-refreeze (MRF) events (Bormann, Westra, Evans, & McCabe, 2013).

5.6.4. Multiple Linear Regression models for snow density.

Multiple Linear Regression (MLR) models were created for the automatic TNM measurements and were compared with the manual samples. The predictors were added progressively from more to less dominant. Elevation was added as a predictor for the set of TMNs series, showing that the SD was enough to describe that component of SDEN variability. The adjusted R^2 ranged from 0.54 for the Bachimaña TNM to 0.83 for the Ordiceto TNM, and the set of TNMs showed an adjusted R^2 of 0.57.

The R^2 values are similar to those obtained in the central Spanish Pyrenees, although the scale of work was different (López-Moreno, et al., 2013), and to those for spring snow in Alpine regions of the former Soviet Union and the US ($R^2 = 0.68$) (Bormann, Westra, Evans, & McCabe, 2013). These R^2 were obtained using MLR models with five variables (Precipitation, interactive SD_{max} * Temp, Cooling Degree Day, Latitude and Elevation). In the Swiss Alps, according to three elevation range classes (≥2000 m, ≥1400 and <2000 m, <1400 m) and 12 seasonal classes (months), SDEN was fitted to the SD with the R^2 values ranging from 0.02 to a maximum of 0.58 (Jonas, 2009).

5.6.5. Improvement of automatic measurements (TNMs) network.

The results presented in Table 3.6 show that, in order to increase the available data and reduce uncertainties to enlarge the knowledge of SDEN in the Spanish Pyrenees, further revision and calibration should be carried out on TNMs 3 (Canal Roya), 5 (Lapazosa), 10 (Airoto) and 11 (Aixeus). The last two are essential to represent spatial variability due to the Mediterranean climate. Other TNMs, such as numbers 8 (Salenques), 14 (Sarrios-Formigal) and 15 (Besurta), should enlarge their data bank to be representative and contribute to similar studies. Good maintenance of the meteorological network is crucial for reducing outliers, gaps or false nulls and the undervaluation of precipitation.

Chapter 6
Conclusions and future research lines

6.1. Conclusions.

This thesis has studied the expected behaviour of the complex snow-related phenomena in Spain in the next 50 years according to a climate change scenario. The obtained results show a great variability for the studied mountain regions and have made it possible to quantify the variation in the behaviour of snow resources and how this will affect the circulating flows through the rivers. The main variables that control the snow-related phenomena were analysed: temperature, precipitation, snowfall, snow accumulation, snowmelt and flow produced. The most important aspects related to the snow-related phenomena were assessed, such as changes in the periods of snow, in the expected maximum and average values, duration of the bulk of the snow reserves and intensity and duration of the snowmelt process. All these changes are essential to establish their influence and contribution in flooding as well as for the optimal management of water resources, considering the regulatory effect that snow-related phenomena have in Spain (its effective contribution is delayed in time).

From a flooding risk point of view, climate change will lead to more flooding scenarios due to both a decrease of the snowfall that ranges in average from 6.5% to 15.7% and is not related to a decrease in the average precipitation, and very rapid meltdowns associated with increases in temperature that may be accompanied by liquid rainfall, revealing a future greater frequency of flooding and with higher intensity than nowadays.

However, these changes in the maximum flows result from a complex relation between changes in the snow-related phenomena and changes in precipitation. As a matter of fact, an increase in maximum snowmelt intensities of 2.1% in the Pyrenees and 7.4% in the Cantabrian Mountains, lead to a respective increase of 8.0 % and 2.0% for maximum flows, while a decrease in maximum snowmelt intensities that range from 15.7% in the Cantabrian Mountains to 12.0% in Sierra Nevada, lead to a maximum flow decrease of 7.1% for the first, but an increase of 58.9% for the latter.

More concerning are the implications of the climate change scenario in the regulatory effect of the water resources, with a decrease in average flow fluctuating from 2.4% in the Pyrenees to 7.3% in Cantabrian Mountains, only increasing in the Central System by 4.0%. Therefore, this work predicts results that may be very important to implement future water policies. Results show that in a future scenario the volume of water stored in the form of snow in the upper areas of the basins will generally be significantly reduced, about 42% in Central System and Sierra Nevada and about 28% in the Pyrenees and Sierra Nevada, while average snow melting will be initiated approximately 45 days earlier than presently for the Cantabrian Mountains and 30 days for the rest of the studied mountain regions. All these issues will cause premature incorporation of runoff from snow melting, reducing up the average snowmelt from 6.6% in the Pyrenees to 15.7% in Cantabrian Mountains, and leading to a greater flow circulating in winter months and a reduction of flows in spring and summer.

However, the greater demand for water resources will continue to occur in spring and summer, which will create a greater mismatch in terms of the availability of water resources and the demand for them. This future scenario is very worrying since it will require two essential modes of action to maintain the guarantee of supply based on sustainability criteria. In the first place, a demand adjustment will be required, i.e., a more sustainable use of water resources, consumption adjustment and reuse. Secondly, more efficient management of the existing regulation reservoirs will be needed in accordance with the new climate change scenario. If these two lines of action are not developed, a serious gap will be created between demand and available resources, jeopardizing the current balance.

Furthermore, this thesis has studied SDEN in the Spanish Pyrenees. The correlation coefficients were higher than the adjusted R^2 found for single linear regressions based on its time evolution, both for the manual samples and the automatic TNM data, with the adjusted R^2 ranging from 0.27 for Eriste to 0.73 for Ordiceto and 0.44 for the set of TNMs. This greater correlation means the existence of variability in SDEN can be explained by meteorological drivers, which are highly variable in time and space.

Finally, the climate change's effect on flood risk in basins with significant snow influence has been studied. The proposed methodology allows the assessment of the climate change effect on a given territory, in terms of hazard and flood risk. It considers both rainfall and temperature as input variables, and allows a fast evaluation and comparison of various climate models.

This evaluation enables one to define actions in terms of a cost–benefit analysis and prioritize the ones that should be included in flood risk management plans due to climate change, as these management plans must contain effective actions in the short, medium and long term and cannot ignore the effect of climate change.

In the specific case of Hijar River Basin, and Reinosa, MRI-CGCM3 model trend analysis shows that climate change will increase damage to society, both economic and personal, while BCC-CSM1-1 shows a small decrease. As the MRI-CGCM3 model fits better with annual maximum real daily flow rates than BCC-CSM1-1, it can be concluded that climate change will cause a significant increase of potential affected inhabitants and economic damage due to flood risk that will require mitigation actions.

This assumption might match with previous years' observations, especially given the high number of low probability events recorded in Spain. This is the specific case of the Hijar River that in 2019 registered two floods, the one on December 2019 being the largest ever registered in Reinosa Gauging Station and related with a low probability event (300 years return period). This conclusion is consistent with the Fifth Assessment Report (AR5) of the IPCC (2013-14), which points out that it is likely that the frequency or intensity of intense rainfall has increased in Europe.

6.2. Future research lines.

This work gives continuity to the work initiated in the 1980s with the ERHIN program (ERHIN programme, 2021) and by M. Arenillas and E. Martínez de Pisón, and constitutes the fourth doctoral thesis following a research line on the study of the snow phenomenon in the Department of Geotechnical Engineering of the Polytechnic University of Valencia, after those carried out by R. Martínez (Martínez, 1988), I. Cantarino (Cantarino I. , 1994) and G. Cobos (Cobos, 2004).

The high space-time variability associated with the snow phenomenon, confirmed in this study, shows the importance of persevering in a research line dedicated to the study of new data collection systems. This will allow the knowledge improvement of the snow phenomenon, as well as the optimization of the results of hydrological snow models such as ASTER.

In particular, the following three research lines are proposed.

Firstly, it is worth mentioning that, in the literature, different climate models associated with climate change scenarios lead to a high variability of results. Therefore, significant efforts must be devoted to determining the goodness of the chosen climate model.

To this end, the application of the present methodology to the study of the Maladeta glacier is considered to be of great interest in the near future. The large data bank that exists thanks to the ERHIN program together with the future evolution of this glacier, which can be extrapolated from the on-site data, could allow one to determine which climate model is the one that best adapts to this area of the Pyrenees.

Additionally, the presented methodology to study the climate change effect on the snow water resources could be worldwide applied, in any basin where these resources are significant.

As second research line, the assessment of the SDEN presented in this work could be applied in other mountainous areas or other regions with similar or different climates.

Second, the results contribute to enlarging the knowledge of SDEN in the Pyrenees and enable its description in a more accurate way. The SDEN regression models that are given in this work may allow us in the future to estimate SDEN, and consequently SWE, using an economical and extensive SD and meteorological network.

Additionally, these SDEN regression models can be implemented in hydrological snow models to describe more complex snow transport or forced-convection phenomena as long as wind velocities are increasingly available.

Finally, the impact of climate variability on SDEN could be studied based on the present approach to relate SDEN and the given climate drivers.

Finally, as third research line, this methodology could be applied in every potential significant flood risk area to be able to prioritize the actions to be included in flood risk management plans.

Chapter 7
Final conclusion

In the present study the effect of the climate change on the snow water resources in the Spanish mountains has been evaluated. Additionally, in order to achieve a better estimate of the snow water equivalent of these areas, a study of the spatial variability of snow density has been accomplished, relating it to the main available climate variables.

Firstly, a thorough review of the state of the art has been carried out, evaluating previous studies related with the variability of snow density and with the future evolution of water resources, with special emphasis on basins with a significant effect of snow, as from the point of view of the changes associated with the risk of flooding. This work has included the research of available data.

Secondly, once the possible contributions of the study have been raised, the objectives of this doctoral thesis have been set. Subsequently, a conceptual framework and methodology that took into account the available data has been developed.

Next, the results obtained have been analysed and the discussion of these has led to several conclusions on the evolution of snow water resources and the increase of flood risk that may be included in future water management plans.

As a final part of these thesis, several future research lines have been presented in order to reinforce some of the conclusions of the study and enhance the knowledge in this field. There is a large uncertainty in climate projections that influences the estimation of future flood risk. The crucial action in the case of adaptation to floods is to carry out a detailed analysis to choose the best climate model.

Therefore, the defined objectives have been achieved. Firstly, estimating for the main Spanish mountain areas the effect of the climate change effect on the future evolution of average and maximum precipitation, accumulated snow, snowmelt and flow. Secondly, finding the climate variables that best describe snow density, i.e. day, accumulated precipitation, 7-day average temperature and snow depth. Finally, presenting a methodology to evaluate the increase of flood risk due to climate change (flood surface, economic damage ratio and inhabitants potentially affected).

On the basis of all the above, the current investigation is hereby terminated.

References

AEMET. (2021, accessed on February). Retrieved from http://www.aemet.es/es/serviciosclimateos/cambio_climat

Akitaya, E. (1974). Studies on depth hoar. *Contrib. Inst. Low Temp. Sci.*, 26, 1-67.

Alonso, R., del Pozo, J., Buisán, S., & Álvarez, J. (2021). Analysis of the snow water equivalent at the AEMet-formigal field laboratory (Spanish Pyrenees) during the 2019/2020 winter season using a stepped-frequency continuous wave radar (SFCW). *Remote Sens.*, 13, 616.

Alonso-González, E., López-Moreno, J., Gascoin, S., García-Valdecasas Ojeda, M., Sanmiguel-Vallelado, A., Navarro-Serrano, F., . . . Essery, R. (2018). Daily gridded datasets of snow depth and snow water equivalent for the Iberian Peninsula from 1980 to 2014. *Earth Syst. Sci.*, 1-24.

Alonso-González, E., López-Moreno, J., Gascoin, S., García-Valdecasas Ojeda, M., Sanmiguel-Vallelado, A., Navarro-Serrano, F., . . . Essery, R. (2018). Daily gridded datasets of snow depth and snow water equivalent for the Iberian Peninsula from 1980 to 2014. *Earth Syst. Sci. Data*, 10, 303-315.

Anderson, E. (1968). Development and Testing of Snow Pack Energy Balance Equations. *Water Resour. Res*, 4, 19-37.

Anderson, E. (1973). *Snow Accumulation and Ablation Model.* Silver Spring, MA, USA: National Weather Service River Forecast System. US Department of Commerce, National Oceanic and Atmospheric Administration, National Weather Service.

Anderson, E. (1976). A Point Energy and Mass Balance Model of a Snow Cover. Silver Spring, MA, USA: US Department of Commerce, National Oceanic and Atmospheric Administration, National Weather Service, Office of Hydrology.

Anderson, E. (2006). Snow Accumulation and Ablation Model - SNOW 17. Newburyport, MA, USA: US Department of Commerce, National Oceanic and Atmospheric Administration, National Weather Service, National Weather Service River Forecast System.

Anderton, S., White, S., & Alvera, B. (2004). Evaluation of spatial variability in snow water equivalent for a high mountain catchment. *Hydrol. Process.*, 18, 435-453.

Arenillas, M., Cobos, G., & Navarro, J. (2008). *Datos sobre la nieve y los glaciares en las cordilleras españolas.* Madrid: Ministerio de Medio Ambiente.

Armstrong, R. (1980). An analysis of compressive strain in adjacent temperature-gradient and equi-temperature layers in a natural snow cover. *J. Glaciol.*, 26, 283-289.

Arnell, N. (1999). The effect of climate change on hydrological regimes in Europe: a continental perspective. *Glob. Environ. Change*, 9, 5-23.

Barry, R. (1992). Mountain climatology and past and potential future climate changes in mountain regions: a review. *Mountain Res. Devel.*, 12, 71-86.

Beniston, M. (1997). Variations of snow depth and duration in the Swiss Alps over the last 50 years: links to changes in large-scale climate forcing. *Clim. Change*, 36, 281-300.

Beniston, M., Keller, F., & Goyette, S. (2003). Snow pack in the Swiss Alps under changing climate conditions: an empirical approach for climate impact studies. *Theoret. Appl. Climatol.*, 74,19-31.

Bilello, M. (1984). *Regional and Seasonal Variations in Snow-Cover Density in the U.S.S.R.* Washington, DC, USA: CRREL Report RR84-22. US Army Corps of Engineers, Cold Regions Research & Engineering Laboratory.

Bormann, K., Westra, S., Evans, J., & McCabe, M. (2013). Spatial and temporal variability in seasonal snow density. *J. Hydrol.*, 484, 63-73.

Brown, R. (2000). Northern Hemisphere snow cover variability and change, 1915–1997. *J. Climate*, 13, 2339-2355.

Brun, E. (1989). Investigation on wet-snow metamorphism in respect of liquid-water content. *Ann. Glaciol.*, 13, 22-26.

Cantarino, I. (1994). *Cuantificación de la precipitación nival acumulada en la Cordillera Cantábrica. Aplicación a los regadios del páramo leonés.* Valencia: Ph. D. Thesis, Universitat Politècnica de València.

Cantarino, I. (1998). *Modelo *Aster. Fundamentos y Aplicación.* Madrid: Ministerio de Medio Ambiente.

Cobos, G. (2004). *Cuantificación de las reservas hídricas en forma de nieve y previsión en tiempo real de los caudales fluyentes de la fusión. aplicación al Pirineo español: cuenca alta del río Aragón.* Valencia: Ph. D. Thesis, Universitat Politècnica de València.

Cobos, G., & Collado, J. (2019, accessed on December). *ASTER. Modelo hidrológico de simulación y previsión aplicado a cuencas donde el fenómeno nival es relevante. Manual de usuario*. Retrieved from http://www.spesa.es/paginas/basededatos/ASTER_Manual_Usuario.pdf

Cobos, G., Francés, M., & Arenillas, M. (2010). Le programme ERHIN. Modélisation nivo-hydrologique pour la gestion de l'eau du Bassin De l'Ebre. The ERHIN programme. Hydrological-nival modelling for the management of water resources in the Ebro Basin. *La Houille Blanche*, 3, 58-64.

Colbeck, S. (1982). An overview of seasonal snow metamorphism. *Rev. Geophys. Space Phys*, 20, 45-61.

Collados-Lara, A., Pulido-Velázquez, D., Pardo-Igúzquiza, E., & Alonso-González, E. (2020). Estimation of the spatiotemporal dynamic of snow water equivalent at mountain range scale under data scarcity. *Sci. Total Environ.*, 41, 140485.

Corripio, J., & López-Moreno, J. (2017). Analysis and predictability of the hydrological response of mountain catchments to heavy rain on snow events: A case study in the Spanish pyrenees. *Hydrology*, 4, 20.

Díez-Herrero, A., & Garrote, J. (2020). Flood Risk Assessments: Aplications and Uncertainties. *Water 12 no. 8*, 2096. https://doi.org/10.3390/w12082096.

Dingman, L. (2002). *Physical Hydrology.* Upper Saddle River, NJ, USA: 2nd ed. Prentice Hall.

Dixon, D., & Boon, S. (2012). Comparison of the SnowHydro snow sampler with existing snow tube designs. *Hydrol. Process.*, 26, 2555-2562.

Doroszkiewicz, J., Romanowicz, R., & Kiczko, A. (2019). The Influence of Flow Projection Errors on Flood Hazard Estimates in Future Climate Conditions. *Water*, 11, 49.

Elder, K., Dozier, J., & Michaelsen, J. (1991). Snow accumulation and distribution in an Alpine watershed. *Water Resour. Res.*, 27, 1541-1552.

ERHIN programme. (2021, accessed on February). *https://www.miteco.gob.es/es/agua/temas/evaluacion-de-los-recursos-hidricos/ERHIN/*. Retrieved from Dirección General del Agua, Ministerio para la Transición Ecológica y el Reto Demográfico.

Essery, R. (2015). A factorial snowpack model (FSM 1.0). *Geosci. Model Dev.*, 8, 3867-3876.

European Commision Directive 2007/60/Ec. (2007). European Commission. Directive 2007/60/Ec of the European Parliament and of the Council of 23 October 2007 on the assessment and management of flood risks. Off.J.L 288/27.

European Environmental Agency. (2010). *Mapping the Impacts of Natural Hazards and Technological Accidents in Europe, EA Technical Report 13/2010.* Copenhagen, Denmark: http://www.eea.europa.eu/publications/mapping-the-impacts-of-natural.

European Flood Awareness (EFAS). (accessed on 2019). Retrieved from https://www.efas.eu/en/news/summary-efas-notifications-2019

Farnes, P., Goodison, B., Peterson, N., & Richards, R. (1982). Metrication of manual snow sampling equipment. *In Proceedings of the 50th Annual Meeting.* Reno, NV: Western Snow Conference.

Garijo, C., & Mediero, L. (2018). Influence of climate change on flood magnitude and seasonality in the Arga River catchment in Spain. *Acta Geophys.*, 66, 769-790.

Garijo, C., Mediero, L., & Garrote, L. (2018). Usefulness of AEMET generated climate projections for climate change impact studies on floods at national-scale (Spain). *Ingeniería del Agua*, 22, 153-166.

Gartska, W. (1964). Snow and Snow survey. In V. Chow, *Handbook of Applied Hydrology* (pp. Section 10, 10-12). New York, NY, USA: Ed. McGraw-Hill.

Gray, D., & Male, D. (2004). *Handbook of Snow, Principles, Processes, Management & Use.* Westchester County, NY, USA: Pergamon Press, Inc.

Henderson, G., & Leathers, D. (2010). European snow cover extent variability and associations with atmospheric forcings. *Int. J. Climatol.*, 30,1440-1451.

Intergovernmental Panel on Climate Change. (2019, accessed on December). Retrieved from https://archive.ipcc.ch/

Jaagus, J. (1997). The impact of climate change on the snow cover pattern in Estonia. *Clim. Change*, 36, 65-77.

Jiménez, A., Montañés, C., Mediero, L., Incio, L., & Garrote, J. (2018). El Mapa De Caudales Máximos De Las Cuencas Intercomunitarias. https://www.miteco.gob.es/es/agua/temas/gestion-de-los-riesgos-de-inundacion/snczi/Mapa-de-caudales-maximos/ . *Revista de Obras Públicas*, 3533, 7-32.

Jonas, T. (2009). Estimating the snow water equivalent from snow depth measurements in the Swiss Alps. *J. Hydrol.*, 378, 161-167.

Kershaw, G., & McCulloch, J. (2007). Midwinter snowpack variation across the Arctic treeline, Churchill, Manitoba, Canada. *Arct. Ant-arct. Alp. Res.*, 39, 9-15.

Kinar, N., & Pomeroy, J. (2009). Automated determination of snow water equivalent by acoustic reflectometry. *IEEE Trans. Geosci. Remote Sens.*, 47, 3161-3167.

Klein, G., Vitasse, Y., & Rixen, C. (2016). Shorter snow cover duration since 1970 in the Swiss Alps due to earlier snowmelt more than to later snow onset. *Clim. Change*, 139, 637-649.

Kodama, M., Nakai, K., Kawasaki, S., & Wada, M. (1979). An application of cosmic-ray neutron measurements to the determination of the snow-water equivalent. *J. Hydrol.*, 41,85-92.

Krasovskaia, I., & Gottschalk, L. (2002). River flow in a changing climate. *Hydrol. Sci. J.*, 47(4) 567-609.

Lantarón, J. (2007). *Modelo Físico de Acumulación y Fusión de la Nieve. Aplicación en Sierra Nevada (España).* Granada: Ph.D Thesis, University of Granada, Cordoba and Malaga.

Lastrada, E., Cobos, G., & Torrijo, F. (2020). Analysis of Climate Change's Effect on Flood Risk. Case Study of Reinosa in the Ebro River Basin. *Water*, 12(4), 1114.

López Moreno, J., & García-Ruiz, J. (2004). Influence of snow accumulation and snowmelt on streamflow in the central Spanish Pyrenees/Influence de l'accumulation et de la fonte de la neige sur les écoulements dans les Pyrénées centrales espagnoles. *Hydrol. Sci*, 49, 802.

López-Moreno, J., & Nogués-Bravo, D. (2006). Interpolating local snow depth data: An evaluation of methods. *Hydrol. Process.*, 20, 2217-2232.

López-Moreno, J., Fassnacht, S., Heath, J., Musselman, K., Revuelto, J., Latron, J., . . . Jonas, T. (2013). Small scale spatial variability of snow density and depth over complex alpine terrain: Implications for estimating snow water equivalent. *Adv. Water Resour.*, 55, 40-52.

López-Moreno, J., Leppänen, L., Luks, B., Holko, L., Picard, G., Sanmiguel-Vallelado, A., . . . Gillemot, K. (2020). Intercomparison of measurements of bulk snow density and water equivalent of snow cover with snow core samplers: Instrumental bias and variability induced by observers. *Hydrol. Process.*, 34, 3120-3133.

López-Moreno, J., Pomeroy, J., Revuelto, J., & Vicente-Serrano, S. (2013). Response of snow processes to climate change: spatial variability in a small basin in the Spanish Pyrenees. *Hydrol. Process.*, 27, 2637-2650.

López-Moreno, J., Quirós, B., Latron, J., & Fassnacht, S. (2010). Instalación y uso de un colchón de nieve para la monitorización del manto de nieve, cuenca experimental de Izas (Pirineo Central). *Geogr. Res. Lett.*, 36,73-82.

Mandal, S., & Sharma, M. (2020). Spatial changes in glaciers between 1965 and 2018 in Tirungkhad Watershed, Upper Sutlej Basin, Himachal Pradesh. *Earth Syst. Environ.*, 427-438.

Martínez, R. (1988). *Metodología para el estudio de la precipitación nival acumulada en la alta montaña española. Aplicación al Pirineo.* Valencia: Ph. D. Thesis, Universitat Politècnica de València.

Mellor, M. (1964). *Snow and Ice on the Earth's Surface.* Hanover, NH, USA: Cold Regions Research and Engineering Laboratory, Report II.

Meloysund, V., Leira, B., Hoiseth, K., & Liso, K. (2007). Predicting snow density using meteorological data. *Meteorol. Appl*, 14, 413-423.

MITECO. (accessed on 2019). *Plan de Gestión del Riesgo de Inundación.* Retrieved from https://www.miteco.gob.es/es/agua/temas/gestion-de-los-riesgos-de-inundacion/planes-gestion-riesgos-inundacion/

MITECO. (accessed on 2019). *Propuesta de mínimos para la realización de los mapas de riesgo de inundación. Directiva de inundaciones - 2º Ciclo*. Retrieved from https://www.miteco.gob.es/en/agua/temas/gestion-de-los-riesgos-de-inundacion/Metodologia%20mapas%20de%20riesgo%20Dir%20Inundaciones%20JULIO%202013_tcm38-98530.pdf

Mizukami, N., & Perica, S. (2008). Spatiotemporal characteristics of snowpack density in the mountainous regions of the western United States. *J. Hydrometeorol.*, 9, 1416-1426.

Moore, R., Hamilton, A., & Scibek, J. (2002). Winter streamflow variability, Yukon Territory, Canada. *Hydrol. Processes*, 16, 763-768.

Mora Alonso-Muñoyerro, J. (2015). *omportamiento hidrológico de cuencas de media montaña españolas: efectos de los procesos de acumulación / fusión de nieve en terrenos permeables sobre la infiltración y régimen de caudales Alto Tajo.* Madrid: Ph. D. Thesis. E.T.S.I. Caminos, Canales y Puertos (UPM).

Mora, J., Ferrer, C., Arenillas, M., & Cobos, G. (2004). Hydrological peculiarities of mountain basins. The case of the Spanish Pyrenees. *International Conference on water observation and informations system for decision support.* Macedonia.

Morán-Tejeda, E., Fassnacht, S., Lorenzo-Lacruz, J., López-Moreno, J., García, C., Alonso-González, E., & Collados-Lara, A. (2019). Hydro-Meteorological characterization of major floods in Spanish mountain rivers. *Water*, 11, 2641.

Morán-Tejeda, E., Lorenzo-Lacruz, J., López-Moreno, J., Rahman, K., & Beniston, M. (2014). Streamflow timing of mountain rivers in Spain: Recent changes and future projections. *J. Hydrol.*, 517, 1114-1127.

Morin, G., Fortin, J., Lardeau, J., Sochanska, W., & Paquette, S. (1981). *Modèle CEQUEAU: manuel d'utilisation. INRS-Eau.* Quebec, Canada: Rapport scientifique n1 93.

Musselman, K., Clark, M., Liu, C., Ikeda, K., & Rasmussen, R. (2017). Slower snowmelt in a warmer world. *Nature Clim. Change*, 7, 214-219.

Navarro-Serrano, F., & López-Moreno, J. (2007). . Spatio-temporal analysis of snowfall events in the Spanish Pyrenees and their relationship to atmospheric circulation. *Geogr. Res. Lett.*, 43, 233-254.

Nijssen, B., O'Donell, G.M., Hamlet, A. F., & Lettenmaier, D.P. (2001). Hydrologic sensitivity of global rivers to climate change. *Clim. Change*, 50, 143-175.

Nyaupane, N., Thakur, B., Kalra, A., & Ahmad, S. (2018). Evaluating Future Flood Scenarios Using CMIP5 Climate Projections. *Water*, 10, 1866.

Onuchin, A., & Burenina, T. (1996). Climatic and geographic patterns in snow density dynamics. *North Eurasia Arct. Alp. Res*, 28, 99-103.

Paquet, E., Laval, M., Basalaev, L., Belov, A., Eroshenko, E., Kartyshov, V., . . . Yanke, V. (2007). An application of cosmic-ray neutron measurements to the determination of the snow water equivalent. *Proceedings of the 30th International Cosmic Ray Conference.* Mérida: Universidad Nacional Autónoma de Mexico.

Pey, J., Revuelto, J., Moreno, N., Alonso-González, E., Bartolomé, M., Reyes, J., . . . López-Moreno, J. (2020). Snow Impurities in the Central Pyrenees: From Their Geochemical and Mineralogical Composition towards Their Impacts on Snow Albedo. *Atmosphere*, 11(9), 937.

PREEMPT. (accessed on 2019). *Policy-Relevant Assessment of Socio-Economic Effects of Droughts and Floods, To Establish a Damage-Water Depth Relationship*. Retrieved from http://www.feem-project.net/preempt/

Rohrer, M., Braun, L., & Lang, H. (1994). Long-term records of snow cover water equivalent in the Swiss Alps:. *Nord. Hydrol.*, 25, 53-64.

Sanmiguel_Vallelado, A., Morán-Tejeda, E., Alonso-González, E., & López-Moreno, J. (2017). Effect of snow on mountain river regimes: An example from the Pyrenees. *Earth Science*, 11, 515-530.

Serreze, M., Clark, M., Armstrong, R., McGinnis, D., & Pulwarty, R. (1999). Characteristics of the western United States snowpack telemetry (SNOTEL) data. *Water Resour. Res.*, 35, 2145-2160.

Sommerfeld, R., & LaChapelle, E. (1970). The classification of snow metamorphism. *J. Glaciol.*, 9, 3-17.

Soulsby, C., Helliwell, R., Ferrier, R., Jenkins, A., & Harriman, R. (1997). Seasonal snowpack influence on the hydrology of a sub-artic catchment in Scotland. *J. Hydrol*, 192, 17-32.

Stewart, I., Cayan, D., & Dettinger, M. (2004). Changes in Snowmelt Runoff Timing in Western North America under a `Business as Usual' Climate Change Scenario. *Climate Change*, 62, 217-232.

Sturm, M., & Holmgren, J. (1998). Differences in compaction behavior of three climate classes of snow. *Ann. Glaciol.*, 26, 125-130.

Szwed, M., Pinskwar, I., Kundzewicz, Z., Graczyk, D., & Mezghani, A. (2017). Changes of snow cover in Poland. *Acta Geophys.*, 65,6576.

Vincent, C., Kappenberger, G., Valla, G., Bauder, A., Funk, M., & Le Meur, E. (2004). Ice ablation as evidence of climate change in the Alps over the 20th century. *J. Goephys. Res.*, 109(D10), D10104.

World Meteorological Organization. (2018). *Guide to Instruments and Methods of Observation. Volume II: Measurement of Cryospheric Variables.* Geneva, Switzerland: World Meteorological Organization.

Ye, B., Yang, D., & Kaine, D. (2003). Changes in Lena River streamflow hydrology: human impacts versus natural variations. *Water Resour. Res.*, 39(7), 8-1 - 8-13.

Ye, K., & Lau, N. (2017). Influences of surface air temperature and atmospheric circulation on winter snow cover variability over Europe. *Int. J. Climatol.*, 37, 2606-2619.

Yuanyuan, L., Sayers, P., Yuanyuan, L., Galloway, G., Penning-Roswell, E., Fuxin, S., . . . Asian Development Bank. (accessed on 2020). *Flood Risk Management: A Strategic Approach*. Retrieved from https://unesdoc.unesco.org/ark:/48223/pf0000220870

Zemp, M., Frey, H., Gärtner-Roer, I., Nussbaumer, S., Hoelzle, M., Paul, F., . . . Vincent, C. (2015). Historically unprecedented global glacier decline in the early 21st century. *J. Glaciol.*, 61(228), 745-762.

Zhu, T., Lund, J., Jenkins, M., Marques, G., & Ritzema, R. (2007). Climate change, urbanization, and optimal long-term floodplain protection. *Water Resour. Res.*, 43, 122-127.

Appendix 1 – A Decrease in the Regulatory Effect of Snow-Related Phenomena in Spanish Mountain Areas Due to Climate Change

Lastrada, E.; Garzón-Roca, J.; Cobos, G.; Torrijo, F.J. A Decrease in the Regulatory Effect of Snow-Related Phenomena in Spanish Mountain Areas Due to Climate Change. Water 2021, 13, 1550. https://doi.org/10.3390/w13111550

water

MDPI

Article

A Decrease in the Regulatory Effect of Snow-Related Phenomena in Spanish Mountain Areas Due to Climate Change

Eduardo Lastrada [1,*], Julio Garzón-Roca [2], Guillermo Cobos [1] and Francisco Javier Torrijo [1,3]

[1] Department of Geological and Geotechnical Engineering, Universitat Politècnica de València, 46022 Valencia, Spain; gcobosc@trr.upv.es (G.C.); fratorec@trr.upv.es (F.J.T.)
[2] Independent Researcher, 46022 Valencia, Spain; ing.jgarzon@gmail.com
[3] Research Centre PEGASO, Universitat Politècnica de València, 46022 Valencia, Spain
* Correspondence: edlasmar@aaa.upv.es

Abstract: Climate change undoubtedly will affect snow events as temperature and precipitation are expected to change in the future. Spanish mountains are especially affected by that situation, since snow storage is there focussed on very specific periods of the hydrological year and plays a very important role in the management of water resources. In this study, an analysis of the behaviour of the complex snow-related phenomena in the four main mountain regions of Spain in the next 50 years is conducted. The ASTER hydrological model is applied using temperature and precipitation data as basic input, estimated under a climate change scenario. Results show different changes in the maximum and average expected flows, depending on the very different magnitude and sign of changes in precipitation. An increase of flooding episodes may occur as a result of a complex relation between changes in precipitation and an increase in maximum snowmelt intensities that range from 2.1% in the Pyrenees to 7.4% in the Cantabrian Mountains. However, common patterns are shown in a shorter duration of the snow bulk reserves, expected to occur 45 days earlier for the Cantabrian Mountains, and about 30 days for the rest of the studied mountain regions. Changes observed also lead to a concerning decrease in the regulatory effect of the snow-related phenomena in the Spanish rivers, with a decrease in the average snow accumulation that ranges from about 28% for the Pyrenees and Sierra Nevada to 42% for the Central System and the Cantabrian Mountains. A decrease in average flow is expected, fluctuating from 2.4% in the Pyrenees to 7.3% in Cantabrian Mountains, only increasing in the Central System by 4.0%, making all necessary to develop new adaptation measures to climate change.

Keywords: snowmelt; snow; water resources; ASTER; climate change

Citation: Lastrada, E.; Garzón-Roca, J.; Cobos, G.; Torrijo, F.J. A Decrease in the Regulatory Effect of Snow-Related Phenomena in Spanish Mountain Areas Due to Climate Change. *Water* **2021**, *13*, 1550. https://doi.org/10.3390/w13111550

Academic Editors: Rafael Pimentel, Juan Ignacio López Moreno, María-José Polo and Simon Gascoin

Received: 22 February 2021
Accepted: 28 May 2021
Published: 31 May 2021

1. Introduction

In the current era, where society demands sustainable development together with a respectful treatment of the environment, the availability of water resources is an essential issue both qualitatively and quantitatively. The quantification of water resources in the form of snow is therefore of high interest as it corresponds to a natural system for regulating the flow of water. Researches showed the connection between the timing and volume of snow accumulation and snowmelt in hydrological systems [1–3]. Snow melting creates a set of water resources which need to be controlled and quantified, establishing their flow contribution to the rivers. Forecasting both variables, snowmelt and flow contribution, is important for the ordinary management that each Basin Organization performs and acquires great relevance for managing extreme hydrological phenomena, i.e., droughts and flooding, especially when trying to envisage and mitigate the damage they may cause [4–8].

In Spain, the meteorological conditions of mountainous areas, as well as their geographical and geomorphological characteristics, cause the snow-related phenomena to be focussed on very specific periods of the hydrological year, mainly between December and May, while presenting great variability in time and location [9]. Accumulated precipitations

in the form of snow take place in these areas between November and April, while snowmelt is centred in spring, in the March–June period. This aspect implies an important regulatory effect of water resources [10], as the incorporation of the snowfalls into the fluvial channels are delayed during winter (at that time, snow is accumulated in the mountains).

Snowmelt in the highest parts of Spanish basins starts in spring and accelerates between the end of March and April, even continuing until July in the highest areas of the Pyrenees [9,10]. Normally this melted snow is gradually incorporated into the river networks and the reservoirs as runoff (ordinary regulation). Therefore, snow regulates the water resources of the country as it ensures a base flow in the rivers during the beginning of the summer period, which is characterized by low precipitation, high evapotranspiration and significant water demand. However, in certain specific weather conditions, such as a rapid increase in temperature combined with rains, significant melting of snow in short periods may occur, leading to high flows in river channels and causing flooding [4].

In the last decades various studies have been carried out to analyze the phenomenon of snow in Spain and its contribution to flooding [10–14].

In this paper, the expected behaviour of the snow-related phenomena in Spain in a future scenario considering the effect of climate change and their consequence in the regulatory effect role that snow has in Spanish rivers are assessed. The main variables that control the snow-related phenomena are studied: temperature, precipitation, snowfall, snow accumulation, snowmelt and flow produced. Four Spanish mountain regions are studied: the Pyrenees, Sierra Nevada, the Central System and the Cantabrian Mountains. The results of this work contribute to improve the knowledge about the effect of climate change in water resources in the form of snow in the main mountain regions of Spain, with few previous similar studies in the same region [15].

Changes in the snow patterns in mountains and ranges are undoubtedly one of the clearest indicators that climate change is taking place on our planet since snow is extremely sensitive to changes in global meteorological conditions [16–22]. Snow depends on the type of precipitation, i.e., in the form of snow or liquid, and water resources associated also depend on the duration of snow in mountains and the speed of snowmelt, which leads snow to disappearing as a stored water resource, being integrated into the river network. Both aspects are related among other factors to temperature [23]. An increment in temperature, as expected in climate change scenarios, will reduce precipitation in form of snow and considerably affect snowmelt by accelerating it.

In this work, variables that control the snow-related phenomena are obtained using the hydrological model ASTER [24–27], a model applied in several countries and implemented by Spanish water authorities as an accurate model in river basins with strong snow phenomena. Results obtained enable establishing both the actual state and the future scenario considering forecasts given by climate models approved by the IPCC [28].

In the near future, a more efficient consumption of water will be required to allow a sustainable life system over time. The management of water resources in a country like Spain, where those resources are scarce, will be more complex. The study on how the snow-related hydrological processes evolve in the main mountainous areas of Spain is therefore decisive to quantify its regulatory effect and establish future management plans.

2. Materials and Methods

2.1. Mountain Regions Studied

The Pyrenees, Sierra Nevada, the Central System and the Cantabrian Mountains were the Spanish mountain regions selected to be studied in this work. Those areas are defined by Spanish Institutions [29] as regions where the snow-related phenomena reach a special relevance. These four regions also match with areas occupied by ice during the last ice age.

The Pyrenees extends about 490 km between Spain and France and its highest altitude corresponds to the peak of Aneto with 3404 m. The set of headwaters of the main rivers of the Spanish Pyrenees were simulated, covering an area of 10,300 km^2 with an average elevation of around 1400 m.

Sierra Nevada extends about 80 km to the south of Spain and its highest altitude is the Mulhacen with 3479 m. In this region there are two delimited areas: the Guadalquivir river basin and the Mediterranean basin; the simulation covers an area of 1253 km^2 with an average elevation of around 1500 m.

The Central System extends about 600 km in the central area of the Iberian Peninsula, just north of the 40th parallel, and its highest altitude corresponds to the peak of Almanzor with 2592 m. This mountain range is in fact a succession of ranges separated by valleys or mountain passes. Gredos, Guadarrama and Ayllon are some of those ranges. In this region, the simulation covers an area of 7758 km^2 with an average elevation of around 1069 m. Unlike the two previous regions, the snow-related phenomena in the Central System have unequal importance that depends on each basin since their average levels vary between 850 m and 1500 m.

The Cantabrian Mountains extend about 480 km in the north of Spain, parallel to the Cantabrian Sea (Bay of Biscay) and their highest altitude is the Torre Cerredo with 2648 m; this range is the most western one in Europe. In this region, there are two main areas: the Duero river area and the Cantabrian Sea area. In total, the simulation covers an area of 14,099 km^2 with an average elevation of around 1169 m. Snow is especially important in the cloud fronts coming from the north since this mountain range is the first orographic obstacle found by these fronts in their movement from north to south. The fronts discharge significant precipitations in the form of snow, making the Cantabrian Mountains the largest snow-covered surface of Spain.

Table 1 lists the number of basins analysed in each region as well as some statistical values regarding their size along with the actual average values of temperature and precipitation (time period 2007–2018). The location of the regions in Spain and the set of basins studied in each region are displayed in Figure 1.

Table 1. Basins on each region analysed.

Mountain Range	No. Basins	Total Area [km^2]	Basin Area [km^2]			Avg. Temperature [°C]	Avg. Precipitation [mm]
			Min	Max	Avg		
Pyrenees	11	10,300	295	2186	936	5.8	1115
Sierra Nevada	2	1253	177	1076	627	8.5	558
Central System	11	7758	247	1848	775	9.9	1107
Cantabrian Mountains	30	14,099	154	1851	728	7.3	1220

2.2. Variables Analysed

The main variables that control the snow-related phenomena and their contribution in terms of water resources are temperature, precipitation, snowfall, snow accumulation, snowmelt and flow produced.

Temperature fluctuation over a year affects the precipitation in form of snow as well as melting period and speed. Temperature evolution is essential to define what will be the change in the importance of snow in each region and what will be the change in the way in which this resource becomes part of the flows in rivers (melting).

Precipitation may be in form of snow or water, with the threshold temperature between these two varying from +2 °C to −2 °C according to several atmospheric conditions. Thus, precipitation refers to the total precipitation while snowfall refers to the precipitation in form of snow. Precipitations evolution will affect the snow-related phenomena, as the more total precipitation the more snowfall, although temperature also influences the latter.

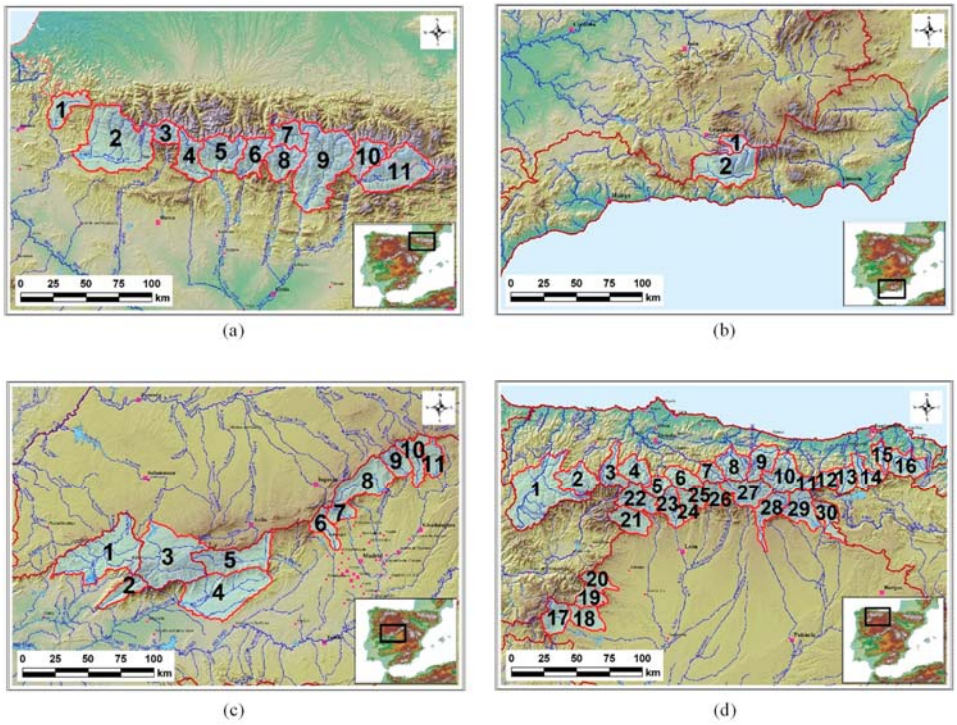

Figure 1. Location of the Spanish mountain regions studied and set of basins analysed on each region: (**a**) Pyrenees; (**b**) Sierra Nevada; (**c**) Central System; (**d**) Cantabrian Mountains.

The temperatures and the precipitations (both rainfall and snowfall) are the inputs required by the ASTER model to predict the snow accumulation, the snowmelt and the flow (model outputs).

Snow accumulation refers to the water resources accumulated in the basin in form of snow. These water resources will be incorporated into the river networks (flow) by snowmelt. Usually, snow starts to melt practically at the same time as the first snowfall begins, especially in the lower areas of the basin during the first months.

Later, with the increment of temperatures in spring, melting starts in the highest areas where snow was accumulated throughout the winter. This leads to a rapid increase in the contributions (flow) due to this phenomenon. Thus, the alteration in the temperature regime could cause melting in a basin to be advanced, making it coincide with raining periods and increasing the flows of liquid water in the rivers, raising the risk of flooding and affecting the current management of a basin.

2.3. ASTER Hydrological Model

ASTER is a continuous simulation distributed hydrological model that simulates the hydrological behaviour of a high mountain sub-basin and calculates the expected stream flow in a river and the equivalent volume of water stored at any time in the studied basin using precipitation and temperature as the main inputs variables. This model, used currently by Spanish water authorities [25,26] was specially developed for basins with steep reliefs, with very marked meteorological changes in time and space [30,31]. Some remarkable features of the ASTER model include the possibility of choosing different spatial and temporal series for the simulation, the fragmented treatment of precipitation and temperature variables and the specific and distributed analysis of the snow-related

phenomena. In this work a daily time resolution was used, matching the time series resolution provided by the climate models. The daily accumulated precipitation and the average daily temperature were the input variables of the model, from which the evolution of the snow-related phenomena and the daily flows were obtained.

ASTER model calculation algorithm follows the classical hydrological models based on quasi—Distributed continuous simulation deposits similar to the Canadian CEQUEAU model [32], with a variable temporal operating scale. The snowmelt routine is based on the studies carried out by Anderson [33] and applied in the US model NWSRFS of the National Weather Service [34–36]. Particularly, the model calculates snowmelt and snow accumulation making use of an energy balance equation [25,26].

For defining the snow accumulation, quantification of snowfall is conducted based on a given temperature named "rain/snow temperature" $T_{rain/snow}$ which is defined for each basin, a typical value being around 1.5 °C. For that value, half precipitation is considered to fall as snow and half as water. If precipitation temperature is greater than $T_{rain/snow}$ by 2 °C, all the precipitation is considered as liquid form. If precipitation temperature is lower than $T_{rain/snow}$ by 2 °C, all the precipitation is considered to fall as snow. A linear interpolation is made between the previous values.

Snowmelt is equal to the result of two components: snowmelt due to precipitation (M_p) and snowmelt without rainfall (M_c).

The snowmelt due to precipitation (M_p) is the snowmelt produced by the precipitation energy and it is calculated using Equation (1), assuming the snow surface temperature is equal to 0 °C [33]:

$$M_p = 0.0125 \cdot P \cdot f_p \cdot T_p \quad (1)$$

where P is the precipitation, in mm; T_p is the temperature of the precipitation, in °C; and f_p is a coefficient that estimates the fraction of precipitation in the form of rain, its value being set to 0.5 for $T_{rain/snow}$. Besides the precipitation energy, other secondary terms like radiation and condensation energy may be added to calculate snowmelt when precipitation occurs.

The snowmelt without rainfall (M_c) corresponds to the snowmelt on a dry day and is calculated using Equation (2), which is based on non-forced convection (note that this kind of estimations are commonly used in hydrological models along with other empirical relations depending on air temperature since estimating wind speed is difficult) [35]:

$$M_c = M_f \cdot (T_a - T_{mi}) \quad (2)$$

where T_a is the air temperature, in °C; T_{mi} is the snowmelt temperature in the basin, in °C; and M_f is the melt factor, in mm/°C, which varies seasonally and depends on several implicit factors, mainly on radiation (latitude, orientation, slope, albedo and vegetation cover), exposition and wind. This factor may be expressed by Equation (3) in terms of the maximum melt factor on 21 June ($M_{F,MAX}$) and the minimum melt factor on 21 December ($M_{F,MIN}$), both given in mm/°C/24 h [35,36]:

$$M_f = \frac{M_{F,MAX} + M_{F,MIN}}{2} + \sin\left(\frac{n \cdot 2\pi}{366}\right) \cdot \frac{M_{F,MAX} - M_{F,MIN}}{2} \quad (3)$$

where n is the number of days from 21 March. It should be noted that the value T_{mi} (snowmelt temperature) may be different from 0 °C. For instance, on calm and clear days, when solar radiation dominates the energy balance, melting can occur below 0 °C, while on clear nights, when the long wave radiation emitted is significant, there would be no melting until air temperature exceeds 0 °C. Therefore, T_{mi} needs to be calibrated in each case analysed.

By using the previous equations, the amount of water incorporated in the river networks can be obtained and added to the one directly produced by rain (precipitations in form of water) to estimate the flow expected on each period of the year.

2.4. Selection of the Climate Model

The input data required by the ASTER hydrological model are the temperatures and the precipitations (see Section 2.2), stemming from climate models.

In this work, temperature and precipitations time series provided by the Spanish Agency of Meteorology AEMET [29] are considered. In particular, among the 24 climate models made available by AEMET, ANA-MRI-CGCM3-rcp85 was selected for conducting the present study. This model provides regionalized climate projections from the CMIP5 (Coupled Model Intercomparison Project phase 5), according to the IPCC and framed within the greenhouse gas emission scenario (RCP 8.5), by using an analogic downscaling method (ANA).

The motivation for using the ANA-MRI-CGCM3-rcp85 model results is twofold: (i) previous experience [4]; and (ii) current validation (Figure 2). Previous experience refers to a previous work carried out by the authors [4], where the analyses showed that this climate model achieved a good fit with real annual-average daily-flow-rates. Besides, before using the model again for this study, the authors checked and demonstrated, for the particular case of the Arga river basin (see Figure 2), that the validity of the ANA-MRI-CGCM3-rcp85 model predictions still stands.

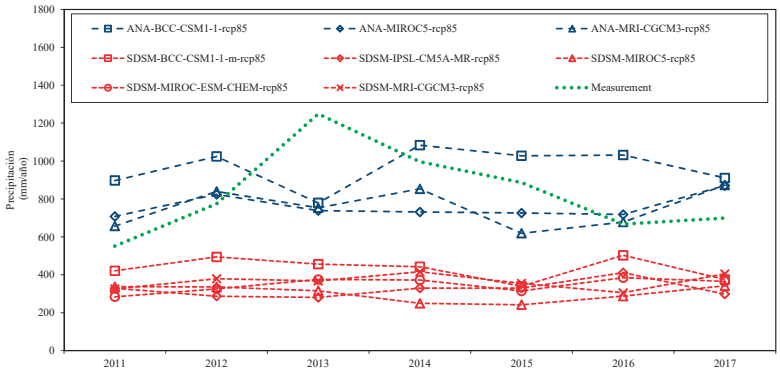

Figure 2. Estimated precipitation in the Arga river basin using several climate models provided by AEMET [28] for the time period 2011–2017 against the real observations measured by local authorities at that period.

Figure 2 shows the results of a thorough simulation study on the extreme rainfall predictions of several climate models (provided by AEMET), over the period 2011–2017 on the Arga river basin. In the figure, the results of the numerical study are compared with experimental data measured by the local authorities. According to Ebro Water Authority, Arga river basin is one of the best monitored basins in the region, being the experimental data reliable and thus suitable for validation purposes. From Figure 2, it can be concluded that ANA-MRI-CGCM3-rcp85 is the most accurate model and it is thus used as reference climate model for this work.

2.5. Calibration and Validation of the ASTER Model

For each hydrological basin studied in this work, the calibration of the ASTER hydrological model is done against the flow data measured at each of the rivers defining each of the hydrological basins studied, obtained from the recorded level-flow data in gauging stations (flow control points) for the reference time period, which in this case it extended from 1 October 2006 to 30 September 2010. The model is calibrated defining the hydrological parameters that make it possible to optimize the correlation coefficient and the Nash-Sutcliffe parameter (NSE) by statistically analysing the observed flow series and those estimated by the ASTER model. The resulting model is then validated by comparing the

flow model predictions from 1 October 2010 to 30 September 2018 with the corresponding available measured data.

Not only the flow, but also the snow accumulation predicted by the ASTER hydrological model in the four regions under analysis is confirmed with measured snow depth and snow density gathered from campaigns carried out three times per year at the beacon network during the last 30 years (EHRIN program) [29].

Table 2 shows a summary of the model parameters resulting from the calibration process. The calibration and validation carried out in a previous work for a longer period (1950–2005) in all the basins of the Pyrenees [9], showed a good consistency of the model to the variability that might be associated with climate change. However, several uncertainties still remain associated with changing climate conditions, such as infiltration due to evolution of vegetation, which may not be easy to predict and may be influenced as well by other anthropic effects non-related with climate change. As snowmelt is calculated based on temperature, other uncertainties associated with changes in incoming radiation or other parameters will result in temperature changes that will be taken into account by the model. As a distributed model, spatial interpolation and temperature and precipitation elevation gradients enable to transform grid data from climate models over complex terrain.

Table 2. Calibration parameters.

Parameter	Value	Pyrenees	Sierra Nevada	Central System	Cantabrian Mountains
$M_{F,MAX}$ [mm/°C/24 h]	Minimum	2.00	3.00	1.00	0.74
	Maximum	7.30	6.00	10.00	5.00
	Average	4.60	4.50	4.90	3.15
$M_{F,MIN}$ [mm/°C/24 h]	Minimum	0.10	1.00	0.10	0.10
	Maximum	5.00	2.00	5.00	3.00
	Average	1.35	1.50	1.38	1.60
Snowmelt temperature T_{mi} [°C]	Minimum	−0.25	1.00	0.00	0.10
	Maximum	1.60	2.00	3.00	3.00
	Average	0.65	1.50	1.12	1.17
Rain/snow temperature $T_{rain/snow}$ [°C]	Minimum	0.00	0.00	0.00	−1.70
	Maximum	1.48	2.50	3.10	4.00
	Average	0.88	1.25	0.96	0.67
Altimetry temperature gradient [°C/1000 m]	Minimum	−6.10	−6.50	−8.00	−6.00
	Maximum	−3.00	−6.30	−4.00	−1.77
	Average	−4.70	−6.40	−5.98	−4.37

3. Results

3.1. Results of the Validation of the ASTER Model

Table 3 shows the results of the validation of the ASTER model from 1 October 2010 to 30 September 2018, for several basins, representing the four studied mountain regions and for two different periods (the complete period and the snowmelt period). The average observed flow and the average flow that is calculated by the ASTER model are presented along with the coefficient of determination (R^2) and the Nash-Sutcliffe parameter (NSE), suggesting good predictive skills for the ASTER hydrological model.

Table 3. Validation results of the ASTER model from 1 October 2010 to 30 September 2018 for the complete period (1 January to 1 December) and for the snowmelt period (1 March to 31 May).

		Complete Period (1 January to 31 December)				Snowmelt Period (1 March to 31 May)			
Regions	**Basins**	**Observed Flow (m^3/s)**	**Calculated Flow (m^3/s)**	**R^2**	**NSE**	**Observed Flow (m^3/s)**	**Calculated Flow (m^3/s)**	**R^2**	**NSE**
Pyrenees	No.2	44.6	42.4	0.93	0.85	75.8	71.4	0.90	0.78
	No.11	12.2	11.8	0.89	0.78	24.2	24.0	0.87	0.78
	No.5	27.4	25.2	0.9	0.8	44.0	45.0	0.85	0.82
Sierra Nevada	No.1	2.2	2.2	0.85	0.7	4.7	4.5	0.82	0.68
Central System	No.1	21.6	19.2	0.9	0.81	39.4	35.3	0.91	0.83
	No.2	9.6	10.2	0.92	0.8	19.4	16.0	0.91	0.85
	No.9	4.5	4.8	0.9	0.82	9.9	8.7	0.93	0.85
Cantabrian Mountains	No.18	12.9	10.8	0.83	0.66	19.6	11.4	0.81	0.51
	No.16	22.08	21.6	0.89	0.8	26.4	23.8	0.90	0.79
	No.23	8.6	8.9	0.82	0.65	16.6	15.1	0.77	0.56

3.2. Results of the Projections for the Selected Climate Model

Using the values reported in Table 2 and the temperature and precipitations given by the ANA-MRI-CGCM3-rcp85 climate model, the ASTER hydrological model was used for conducting a future projection of the snow-related phenomena in the period 2041–2070.

Table 4 shows the resulting values of the temperature, precipitation, snowfall, snow accumulation, snowmelt and flow in the four regions analysed. For each parameter, the maximum and average values are listed, both in terms of the present-day scenario (from 2006 to 2018) and the future scenario, along with its relative change (Rel. change) as a percentage following Equation (4):

$$relative\ change = \frac{V_{fut} - V_{act}}{V_{act}} \cdot 100 \quad (4)$$

where V_{act} is the actual value of a parameter and V_{fut} is the future estimated value.

Table 4. Snow-related phenomena evolution.

Parameter	**Value**	**Measure**	**Pyrenees**	**Sierra Nevada**	**Central System**	**Cantabrian Mountains**
Temperature [°C]	Maximum value	Actual	23.20	23.81	28.47	18.87
		Future	24.50	23.07	28.05	21.25
		Rel. change	5.79%	−3.11%	−1.48%	12.61%
	Average value	Actual	5.80	8.48	9.87	7.29
		Future	7.30	9.82	11.42	8.63
		Rel. change	25.86%	15.80%	15.70%	18.38%
Precipitation [mm]	Maximum value	Actual	32.50	46.46	45.25	31.26
		Future	29.19	48.29	41.83	24.74
		Rel. change	−10.11%	3.93%	−7.55%	−20.86%
	Average value	Actual	3.10	1.53	3.03	3.34
		Future	3.20	1.61	3.18	3.26
		Rel. change	3.23%	5.23%	4.95%	−2.40%
Snowfall [mm]	Maximum value	Actual	27.40	23.28	20.48	15.82
		Future	27.03	24.33	19.91	20.55
		Rel. change	−1.45%	4.50%	−2.78%	29.91%
	Average value	Actual	1.30	0.46	0.46	0.83
		Future	1.20	0.43	0.40	0.70
		Rel. change	−7.69%	−6.52%	−13.04%	−15.66%

Table 4. *Cont.*

Parameter	Value	Measure	Pyrenees	Sierra Nevada	Central System	Cantabrian Mountains
Snow accumulation [hm^3]	Maximum value	Actual	4037.70	216.72	774.96	2072.12
		Future	3580.92	187.13	423.11	1476.73
		Rel. change	−11.31%	−13.67%	−45.40%	−28.73%
	Average value	Actual	858.6	49.38	77.94	333.02
		Future	621.00	35.10	45.40	190.10
		Rel. change	−27.62%	−28.95%	−41.74%	−42.91%
Snowmelt [hm^3]	Maximum value	Actual	190.86	13.61	94.6	381.24
		Future	194.91	9.52	101.64.9	280.25
		Rel. change	2.12%	−30.05%	7.44%	−26.49%
	Average value	Actual	12.64	0.56	3.53	11.63
		Future	11.80	0.50	3.05	9.80
		Rel. change	−6.6%	−12.0%	−13.6%	−15.7%
Flow [m^3/s]	Maximum value	Actual	845.60	76.04	1952.31	1783.68
		Future	918.98	120.83	1990.74	1656.25
		Rel. change	7.98%	58.90%	1.97%	−7.14%
	Average value	Actual	205.0	9.90	148.5	342.0
		Future	200.0	9.50	154.3	317.0
		Rel. change	−2.44%	−4.04%	3.88%	−7.31%

Maximum values represent the highest daily values found in the present-day scenario (from 2006 to 2018). Those maximum values cannot be directly compared with the ones corresponding to the future scenarios: the difference in the length of both periods may lead the maxima in the future scenario to representing much more rare events (once in 30 years) than those during the present-day period (once in 13 years). Consequently, a homogenization procedure was conducted for the future scenario results consisting of considering only the last 13 years of the climate projection (from 2058 to 2070) for computing the maximum values (highest daily values found in that period). Average values were not affected by that procedure and were computed for the whole 30-year period (from 2041 to 2070).

3.2.1. Pyrenees

Temperatures in the Pyrenees show a great increase in annual average values, with a moderate increase in the maximum value. Precipitations are expected to show a slight increase in terms of average values but a decrease in the maximum values. Both average and maximum snowfall values decrease due to the increment in average temperatures and the decrease of maximum precipitations.

Figure 3 shows average values for precipitation, accumulated snow, snowmelt and flow in the Pyrenees. Figure 3a confirms the slight increase in precipitations and it also reveals a change in the precipitation pattern, decreasing in summer-autumn and increasing in winter and spring. Figure 3b shows that the average accumulated snow decreases throughout the year. Even though the average snowmelt decreases for the whole year, the increase in temperatures results in an increase in snow meltdowns from January to April as displayed in Figure 3c. This also means a change in the snowmelt pattern, which will be forwarded in time and will take place more than a month before to the present-day scenario. Average flow decreases along the year too, but the increase in precipitations and snowmelt during the mentioned period leads to an increase in the flow stream to rivers during the first months of the year (Figure 3d). Advance in snowmelt and the decrease in precipitations in summer also result in decreasing the average flow between the months of June and October.

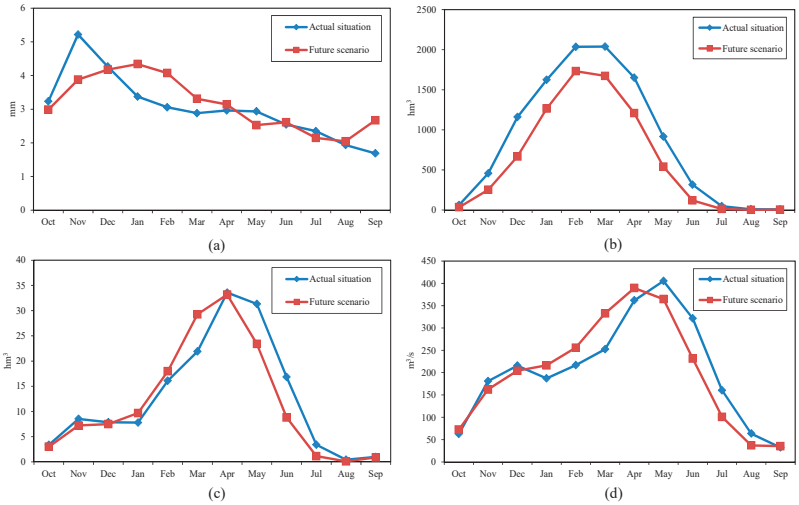

Figure 3. Average values for the snow-related phenomena evolution for a standard year in the Pyrenees. Actual situation (blue) and future scenario (red) simulated: (**a**) average precipitation; (**b**) average accumulated snow; (**c**) average snowmelt; (**d**) average flow.

Figure 4 shows the evolution of the previous variables in terms of maximum values. Figure 4a displays the increase in maximum precipitations during winter, matching the increase in average values indicated above, especially from December to February, a period where currently maximum precipitation values are low. The maximum accumulated snow shows a slight decrease with respect to the actual values between the months of February and May (Figure 4b). This also leads to having strong maximum snowmelt values in the same period (Figure 4c), confirming the change in the melting pattern and giving rise to an increase in the maximum flow values. As Figure 4d shows, maximum flow values experience a clear increase during winter and early spring.

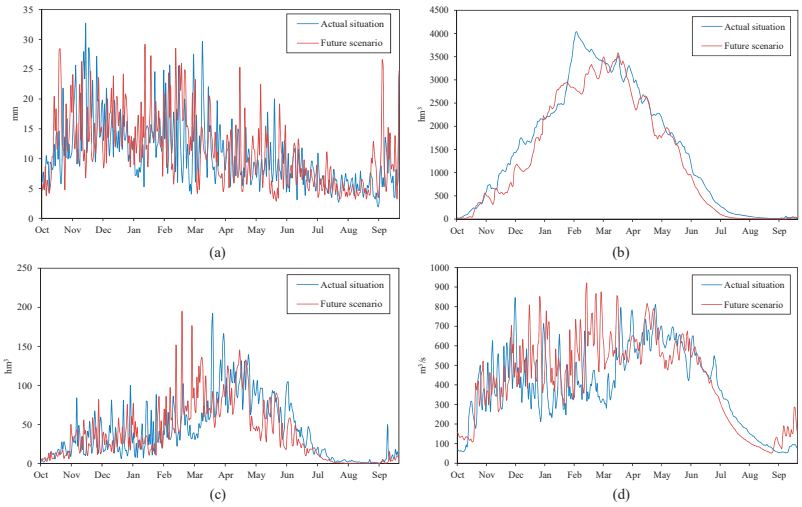

Figure 4. Snow-related phenomena evolution for a standard year in the Pyrenees. Actual situation (blue) and future scenario (red) simulated: (**a**) maximum precipitation; (**b**) maximum accumulated snow; (**c**) maximum snowmelt; (**d**) maximum flow.

3.2.2. Sierra Nevada

Temperatures in Sierra Nevada show a great increase in annual average values, while a slight decrease is observed in the maximum values. Precipitations increase, the increment being moderate for both the average and the maximum values. Maximum snowfall slightly increases in line with the total precipitation, although the average snowfall decreases due to the increment in average temperatures.

Figure 5 shows average values for precipitation, accumulated snow, snowmelt and flow in Sierra Nevada. Figure 5a displays how precipitations are concentrated in autumn in the present-day scenario, while in the future scenario precipitations will occur mainly in winter and early spring. This will cause a decrease in the accumulated precipitations in summer and autumn and reveals a change in the precipitation pattern. Average accumulated snow (Figure 5b) decreases throughout the year. Snowmelt average value decreases for the whole year, but Figure 5c shows a clear increase in average snowmelt from January to April, also leading to an advance in the snowmelt pattern (in the actual time, snowmelt mainly occurs in spring) due to the increase in temperatures similar to what was observed in the Pyrenees. A decrease in average annual flow is expected but also showing a pattern change: flow will decrease from June to January and increase in late winter and spring (Figure 5d).

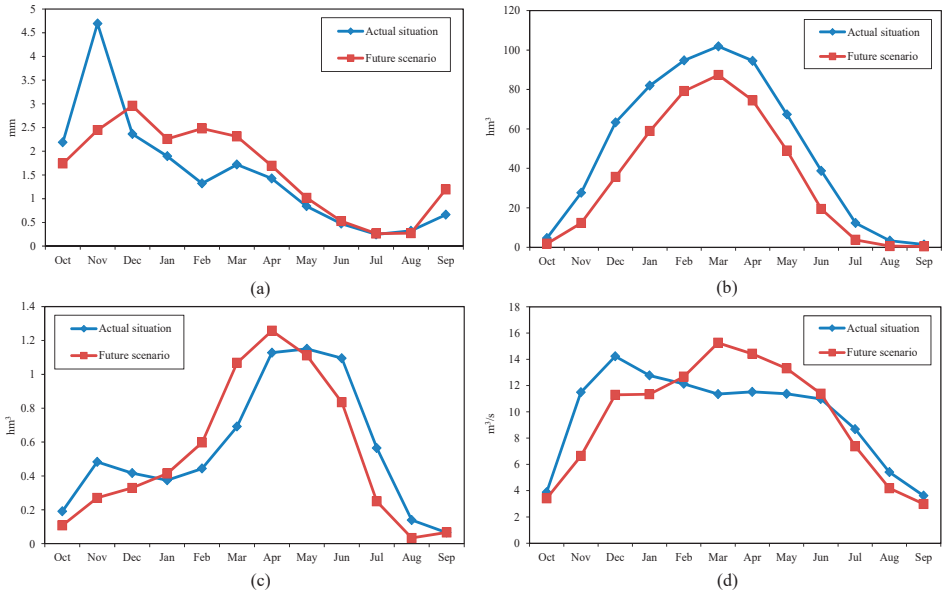

Figure 5. Average values for the snow-related phenomena evolution for a standard year in Sierra Nevada. Actual situation (blue) and future scenario (red) simulated: (**a**) average precipitation; (**b**) average accumulated snow; (**c**) average snowmelt; (**d**) average flow.

Figure 6 shows the evolution of the previous variables in terms of maximum values. Figure 6a confirms the increase of precipitations along the year with some of the highest maximum values expected in winter. Maximum accumulated snow is expected to decrease in the future scenario (Figure 6b) while the maximum snowmelt values will increase in the middle of the winter period (Figure 6c). This confirms the advance in the snowmelt pattern. As Figure 6d displays, the maximum flow will considerably increase along the year, and especially during the months of March to May, as a consequence of the forwarding of the snowmelt, thus confirming the tendency observed for average values.

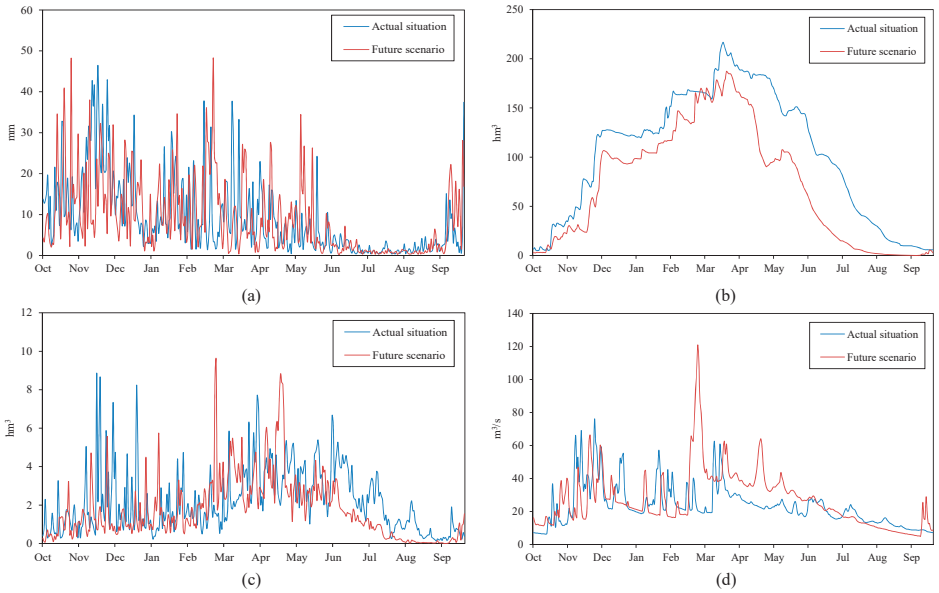

Figure 6. Snow-related phenomena evolution for a standard year in Sierra Nevada. Actual situation (blue) and future scenario (red) simulated: (**a**) maximum precipitation; (**b**) maximum accumulated snow; (**c**) maximum snowmelt; (**d**) maximum flow.

3.2.3. Central System

Temperatures in the Central System show a great increase in average values and a slight decrease in maximum values. Similarly, a moderate increase in average precipitations is expected while maximum values will show a decrease. Snowfall decreases both in terms of maximum and average values due to the increment in average temperatures.

Figure 7 shows average values for precipitation, accumulated snow, snowmelt and flow in the Central System. Figure 7a reveals a change in the precipitation pattern with precipitations decreasing in autumn and increasing along the months of January to April. Consequently, snow accumulations and flow rates will experience significant changes in both magnitude and temporal location with respect to the actual values. Figure 7b shows that the average accumulated snow decreases throughout the year, while Figure 7c displays an increase in snowmelt from January to March due to the increase in temperatures. Average annual flow experiences a slight increase, especially in months between January and April caused by the increase in snowmelt (Figure 7d).

Figure 8 shows the evolution of the previous variables in terms of maximum values. According to Figure 8a, maximum precipitation values in the future scenario will be higher in winter. Figure 8b shows that maximum snow accumulation will decrease throughout the whole year. Maximum snow accumulations will reach their peak in winter and will start decreasing from March, evidencing a change in the melting pattern which is also confirmed in Figure 8c. In the present-day scenario, the maximum snowmelt occurs in spring while in the future scenario is expected to take place in winter and decrease in the months of April and May. Therefore, melting will be forwarded and accelerated with respect to the actual situation. A moderate increase in the maximum flow value is detected and as Figure 8d shows in the Central System winter will favour the increase of flow due to the early melting expected to occur in those months. The advancement in the meltdown pattern together with the increase in total precipitations in the first half of the year will result in increasing

the maximum flow in this period. The maximum flow is expected to decrease in autumn as a consequence of the decrease in precipitations and the increase in temperatures.

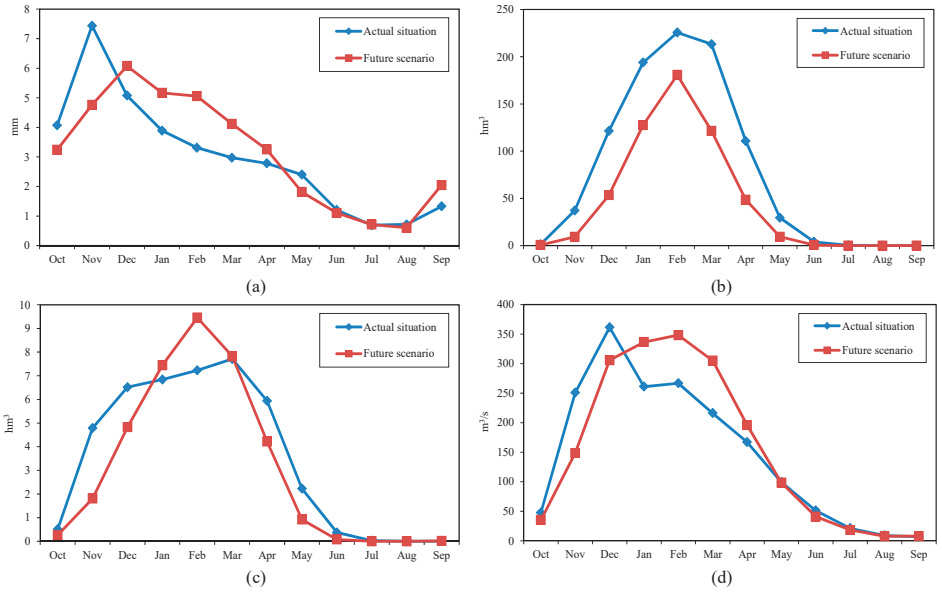

Figure 7. Average values for the snow-related phenomena evolution for a standard year in the Central System. Actual situation (blue) and future scenario (red) simulated: (**a**) average precipitation; (**b**) average accumulated snow; (**c**) average snowmelt; (**d**) average flow.

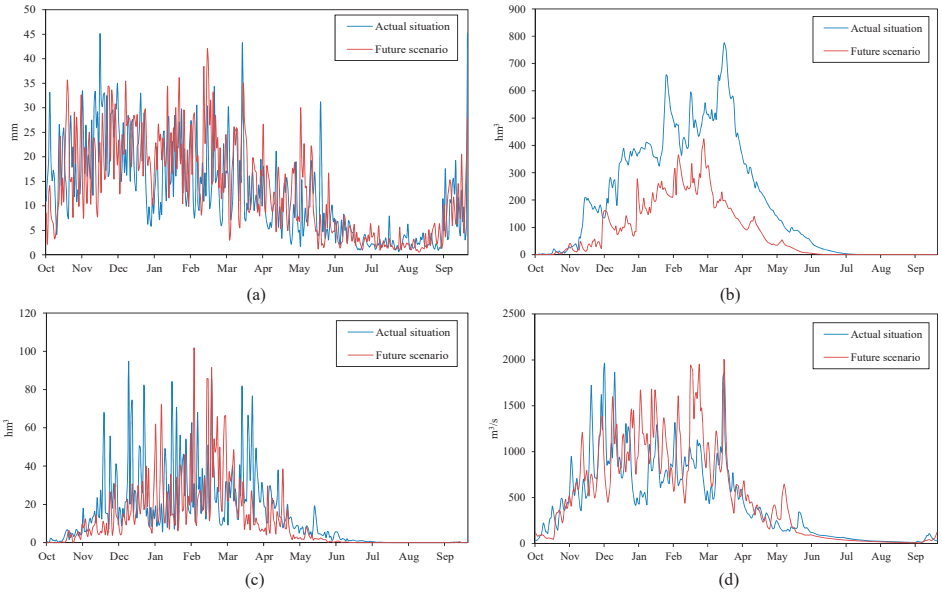

Figure 8. Snow-related phenomena evolution for a standard year in the Central System. Actual situation (blue) and future scenario (red) simulated: (**a**) maximum precipitation; (**b**) maximum accumulated snow; (**c**) maximum snowmelt; (**d**) maximum flow.

3.2.4. Cantabrian Mountains

Temperatures in the Cantabrian Mountains show an increase in both annual average and maximum values. Precipitations show a slight decrease in average values and a great decrease in maximum values. Average snowfall decreases due to the increment in average temperatures and the decrease in average precipitations, but maximum snowfall increases, which indicates that important heavy snowfalls are expected to occur in the future scenario.

Figure 9 shows average values for precipitation, accumulated snow, snowmelt and flow in the Central System. Figure 9a displays a change in the precipitation pattern similar to the ones observed in the previous regions studied, with precipitations decreasing in autumn and increasing in winter. Figure 9b confirms that the increase in temperatures and the decrease in average snowfall results in a significant decrease in the accumulated snow throughout the year. A change in the melting pattern is also observed in Figure 9c, as the highest average snowmelt values move from spring (present-day situation) to winter (future situation). Therefore, melting will be forwarded and accelerated with respect to the actual situation. A shorter duration of the snow mantle is also evidenced (difference length of the "plateaus" observed in Figure 9c). Figure 9d shows a clear change in the average flow pattern and how flow increases during the first months of the year as a result of snowmelt, despite the slight decrease in precipitations.

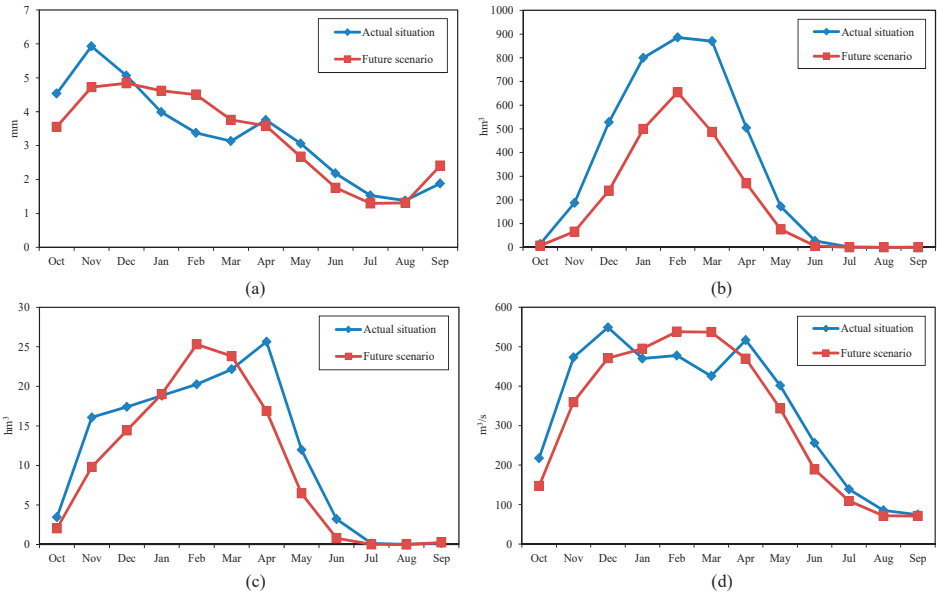

Figure 9. Average values for the snow-related phenomena evolution for a standard year in the Cantabrian Mountains. Actual situation (blue) and future scenario (red) simulated: (**a**) average precipitation; (**b**) average accumulated snow; (**c**) average snowmelt; (**d**) average flow.

Figure 10 shows the evolution of the previous variables in terms of maximum values. Figure 10a confirms the decrease in maximum precipitation. Figure 10b shows that the maximum accumulated snow also decreases throughout the whole year. The large increase in the maximum snowfall but the decrease in accumulated snow, points to a change in the snow pattern in which heavy snowfall will be favoured but their permanence on the peaks will be shorter due to the significant increase in temperatures. According to Figure 10c, the maximum snowmelt is expected to increase between January and April and decrease along the months of April and May. That confirms the change in the melting pattern observed with average values. As both the maximum snowmelt and maximum

precipitation decrease, the maximum flow also decreases. Figure 10d shows how the flow will increase during the first months of the year as a result of snowmelt, despite the slight decrease in precipitations, which evidences that the maximum flow will be influenced by snowmelt in a greater proportion than in the present time.

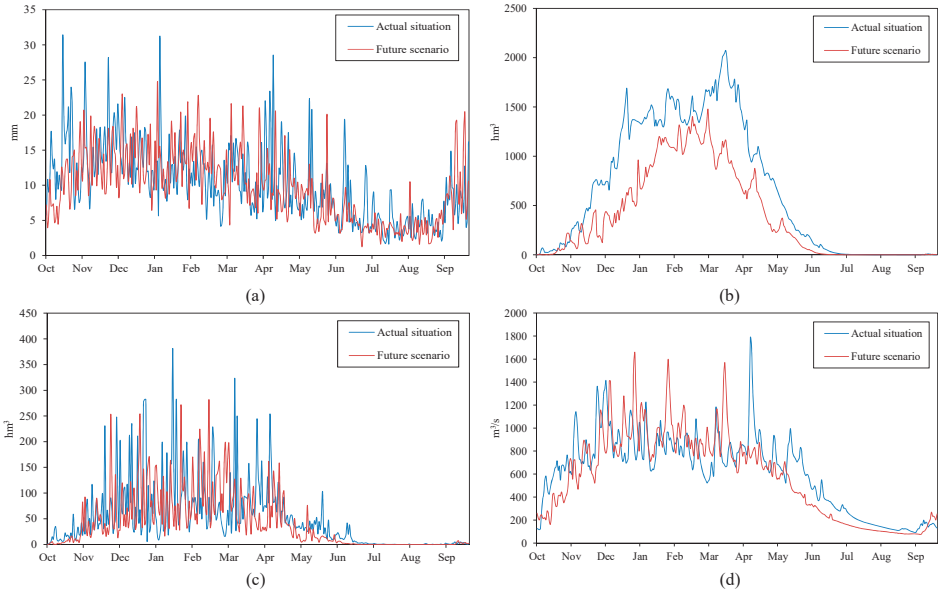

Figure 10. Snow-related phenomena evolution for a standard year in the Cantabrian Mountains. Actual situation (blue) and future scenario (red) simulated: (**a**) maximum precipitation; (**b**) maximum accumulated snow; (**c**) maximum snowmelt; (**d**) maximum flow.

4. Discussion

4.1. Radiation Influence

ASTER hydrological model has been calibrated and validated in the Pyrenees for a long period that ranges from 1950 to 2005 [9], showing a good fitting for the already changing climate variables caused by climate change that were non-explicit, such as radiation. However, greater changes in radiation are expected in the next 50 years, so the model might show uncertainties associated with this variable. Radiation depends on multiple factors that are difficult to predict. Besides, other effects such as snow impurities affecting snow albedo may have a greater effect on melting than the radiation input itself [37].

Nevertheless, melting related with radiation is not very significant in Spanish mountains, as both average and maximum snowmelt take place during medium radiation months. This is different to what occurs in other latitudes or places with higher elevations, where snow water equivalent storage is still important during high radiation periods.

Other limitations of the model that may lead to uncertainties have already been stated in a previous section, such as infiltration due to future development of vegetation, which may not be easy to predict and may be influenced as well by other anthropic effects.

4.2. Decrease in the Regulatory Effect and Increase of Extreme Events

The previous analyses evidence a tendency to a change in the pattern of the snow-related phenomena in Spain, which will decrease its regulatory effect on rivers. Nowadays the influence of snow on the contribution to water resources in Spain is highly variable in each of the different regions analysed. For instance, and according to the work of Arenillas et al. [9] who studied snow-related phenomena in Spain during the period from

1950 to 2007, in the Central System, the snow at its highest point (spring) represents a total of 10% of the rainfall received but this value reduces to 5% for the entire hydrological year. In regions where snow behaviour is much more accentuated, such as Sierra Nevada or the Pyrenees, these values can rise to a maximum of 55% and 40% respectively, leaving values of 45% and 28% for the entire hydrological year respectively. It should be noted that higher elevation, as is the case of Sierra Nevada and the Pyrenees, implies longer snow permanence and greater regulatory effect.

Melted snow streams to rivers, increasing their flow significantly. Therefore, the change in melting patterns also leads to a change in flow patterns. As melting will move from spring to winter, maximum flows are also expected to significantly increase during winter. The hypothesis of slower snowmelt in a warmer world due to contraction of the snowmelt season to a time of lower available energy [38], must be combined with the response of the snowpack to the magnitude and sign of changes in precipitation [39].

In the Pyrenees, the water accumulated in the form of snow in the mountains for the climate change scenario undergoes an early meltdown of about 30 days compared to the current situation. This implies a lower regulatory effect from the point of view of water resources. The flow increases in the rivers during the winter season and at the beginning of spring, while the contribution of flows from the month of April is reduced. This scenario denotes a lower regulatory effect of circulating flows and therefore will force different management of the reservoirs to the current one, requiring greater regulation capacity to achieve supply conditions similar to the actual ones. A decrease on snow accumulation about 20% for every 1 °C, and a reduction on the duration of the snowpack about 20–30 days per °C was estimated for a small snow-dominated basin in the Spanish Pyrenees [39].

In Sierra Nevada melting of the accumulated snow is advanced in around 30 days. This advance is directly reflected in flowing flows, which suffer a decrease in the months of greatest demand. Therefore, the future scenario shows that the regulatory effect of water resources associated with the snow-related phenomena will be reduced. In the Central System, climate change will lead to snowmelt increasing until reaching its maximum value in February, approximately 30 days earlier compared with the time it normally occurs today. This circumstance implies an increase in circulating flows between the months of January and March. In the Cantabrian Mountains, a reduction of the regulatory effect of the accumulated snow in mountain areas is also detected, producing an earlier snowmelt of about 45 days and a much more accentuated low water level in rivers from April. These results agree with previous studies predicting that by the end of the twenty-first century, the peak flow of many North American and European rivers is expected to occur 30–40 days earlier as a result of earlier snowmelt [40,41], but changes in precipitation caused by climate change can increase or reduce flow rates.

All in all, the effect of climate change on the snow-related phenomena shows that the regulatory effect of the snow with respect to the incorporation of runoff into the riverbeds will be less significant in the future. This will require different management and probably force a greater need for reservoir capacity to achieve optimal regulation and maintain current supply guarantee conditions for the populations and agricultural lands. At the same time, extreme flood situations will continue to occur, requiring new flood risk management plans.

Especially, in terms of future flood events, the change in the snow behaviour pattern gives rise to increasing the risk of flooding and their damaging effects, with an expected increase in the number of episodes with strong flow peaks. Future snowmelt time in the four regions analysed will coincide with the first half of the year, where precipitations are also expected to increase. Besides, an increase in the average precipitations is expected in the Pyrenees, Sierra Nevada and the Central System. In the Cantabrian Mountains, precipitations along the year may decrease, but the heavy snowfall episodes expected along with the shorter duration of snow on the peaks will also cause an increased risk of flooding.

It is important to mention that all the previous analyses are entirely based on a single climate change scenario, so even though the climate model used (ANA-MRI-CGCM3-rcp85) showed a good match with the present state in Spain, some uncertainty may arise. Previous works have shown a decrease in the magnitude of extreme floods for climate model projections in Spain [36]. This is partly due to the use of global climate models from the Spanish Meteorological Agency (AEMET), which tend to provide lower extremes with a smaller variability [42]. However, it must be considered that snow accumulated is very sensitive to weather conditions, and a generalized increase in temperatures will cause a rapid and important melting and a higher probability of direct rainfall instead of snow accumulation that will provide significant water resources added to those already streaming. Thus, climate change scenarios show a greater risk of flooding situations with more damaging effects. Particularly, the increase in temperatures and decrease in average accumulations, or the delay in the accumulation of snow, may generate extreme events in which all the precipitation occur in liquid form (water), instead of part of the same being retained in the form of snow in the highest parts of mountains. This phenomenon has already happened in December 2019 in the town of Reinosa [4], which suffered the worst flooding in memory (return period estimated about 300 years) causing great damage and affecting residents.

5. Conclusions

This paper has studied the expected behaviour of the complex snow-related phenomena in Spain in the next 50 years according to a climate change scenario. The results obtained show a great variability for the studied mountain regions and have made it possible to quantify the variation in the behaviour of snow resources and how this will affect the circulating flows through the rivers. The main variables that control the snow-related phenomena were analysed: temperature, precipitation, snowfall, snow accumulation, snowmelt and flow produced. The most important aspects related to the snow-related phenomena were assessed, such as changes in the periods of snow, in the expected maximum and average values, duration of the bulk of the snow reserves and intensity and duration of the snowmelt process. All these changes are essential to establish their influence and contribution in flooding as well as for the optimal management of water resources, considering the regulatory effect that snow-related phenomena have in Spain (its effective contribution is delayed in time).

From a flooding risk point of view, climate change will lead to more flooding scenarios due to both a decrease of the snowfall that ranges in average from 6.5% to 15.7% and is not related to a decrease in the average precipitation, and very rapid meltdowns associated with increases in temperature that may be accompanied by liquid rainfall, revealing a future greater frequency of flooding and with higher intensity than nowadays. However, these changes in the maximum flows result from a complex relation between changes in the snow-related phenomena and changes in precipitation. As a matter of fact, an increase in maximum snowmelt intensities of 2.1% in the Pyrenees and 7.4% in the Cantabrian Mountains, lead to a respective increase of 8.0 % and 2.0% for maximum flows, while a decrease in maximum snowmelt intensities that range from 15.7% in the Cantabrian Mountains to 12.0% in Sierra Nevada, lead to a maximum flow decrease of 7.1% for the first, but an increase of 58.9% for the latter.

More concerning are the implications of the climate change scenario in the regulatory effect of the water resources, with a decrease in average flow fluctuating from 2.4% in the Pyrenees to 7.3% in Cantabrian Mountains, only increasing in the Central System by 4.0%. Therefore, this work predicts results that may be very important to implement future water policies. Results show that in a future scenario the volume of water stored in the form of snow in the upper areas of the basins will generally be significantly reduced, about 42% in Central System and Sierra Nevada and about 28% in the Pyrenees and Sierra Nevada, while average snow melting will be initiated approximately 45 days earlier than presently for the Cantabrian Mountains and 30 days for the rest of the studied mountain regions. All

these issues will cause premature incorporation of runoff from snow melting, reducing up the average snowmelt from 6.6% in the Pyrenees to 15.7% in Cantabrian Mountains, and leading to a greater flow circulating in winter months and a reduction of flows in spring and summer.

However, the greater demand for water resources will continue to occur in spring and summer, which will create a greater mismatch in terms of the availability of water resources and the demand for them. This future scenario is very worrying since it will require two essential modes of action to maintain the guarantee of supply based on sustainability criteria. In the first place, a demand adjustment will be required, i.e., a more sustainable use of water resources, consumption adjustment and reuse. Secondly, more efficient management of the existing regulation reservoirs will be needed in accordance with the new climate change scenario. If these two lines of action are not developed, a serious gap will be created between demand and available resources, jeopardizing the current balance.

However, the previous analyses are entirely based on the results of a simplified distributed hydrological model, on a single climate change scenario and for a single climate model, thus some uncertainty may arise. Further investigation is therefore needed to confirm the conclusions of this work.

Author Contributions: Conceptualization, E.L., J.G.-R. and G.C.; methodology, E.L. and G.C.; project administration, G.C.; software, E.L.; validation, G.C.; formal analysis, E.L.; writing—original draft preparation, J.G.-R.; writing—review and editing, J.G.-R., E.L. and G.C.; visualization, F.J.T.; supervision, F.J.T. All authors have read and agreed to the published version of the manuscript.

Funding: This research received no external funding.

Institutional Review Board Statement: Not applicable.

Informed Consent Statement: Not applicable.

Data Availability Statement: The data presented in this study are available on request from the corresponding author. The data are not publicly available due to privacy reasons.

Acknowledgments: The authors acknowledge F. J. Sanchez, M. Aparicio and F. Pastor (Spanish Ministry for Ecological Transition and the Demographic Challenge), Tragsatec and ASTER model developer J. A. Collado (SPESA Ingenieria). The authors fully acknowledge the financial support provided by the Department of Geological and Geotechnical Engineering of the UPV.

Conflicts of Interest: The authors declare no conflict of interest.

References

1. Barry, R.G. Mountain climatology and past and potential future climate changes in mountain regions: A review. *Mountain Res. Devel.* **1992**, *12*, 71–86. [CrossRef]
2. Beniston, M. Variations of snow depth and duration in the Swiss Alps over the last 50 years: Links to changes in large-scale climate forcing. *Clim. Chang.* **1997**, *36*, 281–300. [CrossRef]
3. Nijssen, B.; O'Donell, G.M.; Hamlet, A.F.; Lettenmaier, D.P. Hydrologic sensitivity of global rivers to climate change. *Clim. Chang.* **2001**, *50*, 143–175. [CrossRef]
4. Lastrada, E.; Cobos, G.; Torrijo, F.J. Analysis of Climate Change's Effect on Flood Risk. Case Study of Reinosa in the Ebro River Basin. *Water* **2020**, *12*, 1114. [CrossRef]
5. Soulsby, C.; Helliwell, R.C.; Ferrier, R.C.; Jenkins, A.; Harriman, R. Seasonal snowpack influence on the hydrology of a sub-artic catchment in Scotland. *J. Hydrol.* **1997**, *192*, 17–32. [CrossRef]
6. Moore, R.D.; Hamilton, A.S.; Scibek, J. Winter streamflow variability, Yukon Territory, Canada. *Hydrol. Processes* **2002**, *16*, 763–768. [CrossRef]
7. Krasovskaia, I.; Gottschalk, L. River flow in a changing climate. *Hydrol. Sci. J.* **2002**, *47*, 597–609. [CrossRef]
8. Ye, B.; Yang, D.; Kaine, D.L. Changes in Lena River streamflow hydrology: Human impacts versus natural variations. *Water Resour. Res.* **2003**, *39*, 8-1–8-13. [CrossRef]
9. Arenillas, M.; Cobos, G.; Navarro, J. *Datos Sobre la Nieve y los Glaciares en las Cordilleras Españolas*; Ministerio de Medio Ambiente y Medio Rural y Marino: Madrid, Spain, 2008.
10. López-Moreno, J.I.; García-Ruiz, J.M. Influence of snow accumulation and snowmelt on streamflow in the central Spanish Pyrenees/Influence de l'accumulation et de la fonte de la neige sur les écoulements dans les Pyrénées centrales espagnoles. *Hydrolog. Sci. J.* **2004**, *49*, 1039–1050. [CrossRef]

11. Morán-Tejeda, E.; Fassnacht, S.R.; Lorenzo-Lacruz, J.; López-Moreno, J.I.; García, C.; Alonso-González, E.; Collados-Lara, A.-J. Hydro-Meteorological Characterization of Major Floods in Spanish Mountain Rivers. *Water* **2019**, *11*, 2641. [CrossRef]
12. Corripio, J.; López-Moreno, J. Analysis and Predictability of the Hydrological Response of Mountain. Catchments to Heavy Rain on Snow Events: A Case Study in the Spanish Pyrenees. *Hydrology* **2017**, *4*, 20. [CrossRef]
13. Sanmiguel-Vallelado, A.; Morán-Tejeda, E.; Alonso-González, E.; López-Moreno, J.I. E_ect of snow on mountain river regimes: An example from the Pyrenees. *Front. Earth Sci.* **2017**, *11*, 515–530. [CrossRef]
14. Alonso-González, E.; López-Moreno, J.I.; Gascoin, S.; García-Valdecasas Ojeda, M.; Sanmiguel-Vallelado, A.; Navarro-Serrano, F.; Revuelto, J.; Ceballos, A.; Esteban-Parra, M.J.; Essery, R.; et al. Daily gridded datasets of snow depth and snow water equivalent for the Iberian Peninsula from 1980 to 2014. *Earth Syst. Sci. Data Discuss* **2018**, *10*, 303–315.
15. Morán-Tejeda, E.; Lorenzo-Lacruz, J.; López-Moreno, J.I.; Rahman, K.; Beniston, M. Streamflow timing of mountain rivers in Spain: Recent changes and future projections. *J. Hydrol.* **2014**, *517*, 1114–1127. [CrossRef]
16. Jaagus, J. The impact of climate change on the snow cover pattern in Estonia. *Clim. Chang.* **1997**, *36*, 65–77. [CrossRef]
17. Henderson, G.R.; Leathers, D.J. European snow cover extent variability and associations with atmospheric forcings. *Int. J. Climatol.* **2010**, *30*, 1440–1451. [CrossRef]
18. Szwed, M.; Pińskwar, I.; Kundzewicz, Z.W.; Graczyk, D.; Mezghani, A. Changes of snow cover in Poland. *Acta Geophys.* **2017**, *65*, 65–76. [CrossRef]
19. Klein, G.; Vitasse, Y.; Rixen, C. Shorter snow cover duration since 1970 in the Swiss Alps due to earlier snowmelt more than to later snow onset. *Clim. Chang.* **2016**, *139*, 637–649. [CrossRef]
20. Beniston, M.; Keller, F.; Goyette, S. Snow pack in the Swiss Alps under changing climate conditions: An empirical approach for climate impact studies. *Theoret. Appl. Climatol.* **2003**, *74*, 19–31. [CrossRef]
21. Vincent, C.; Kappenberger, G.; Valla, F.; Bauder, A.; Funk, M.; Le Meur, E. Ice ablation as evidence of climate change in the Alps over the 20th century. *J. Geophys. Res.* **2004**, *109*, D10104. [CrossRef]
22. Zemp, M.; Frey, H.; Gärtner-Roer, I.; Nussbaumer, S.U.; Hoelzle, M.; Paul, F.; Haeberli, W.; Denzinger, F.; Ahlstrom, A.P.; Anderson, B.; et al. Historically unprecedented global glacier decline in the early 21st century. *J. Glaciol.* **2015**, *61*, 745–762. [CrossRef]
23. Ye, K.; Lau, N.C. Influences of surface air temperature and atmospheric circulation on winter snow cover variability over Europe. *Int. J. Climatol.* **2017**, *37*, 2606–2619. [CrossRef]
24. Cantarino, I. *Modelo *Aster. Fundamentos y Aplicación*; Ministerio de Medio Ambiente: Madrid, Spain, 1998.
25. Cobos, G.; Collado, J.A. ASTER. Modelo Hidrológico de Simulación y Previsión Aplicado a Cuencas Donde el Fenómeno Nival es Relevante. *Manual de Usuario.* Available online: http://www.spesa.es/paginas/basededatos/ASTER_Manual_Usuario.pdf (accessed on 27 December 2019).
26. Cobos, G. Cuantificación de las Reservas Hídricas en Forma de Nieve y Previsión en Tiempo Real de los Caudales Fluyentes de la Fusión. Aplicación al Pirineo Español: Cuenca Alta del río Aragón. Ph.D. Thesis, Universitat Politècnica de València, Valencia, Spain, 2004.
27. Cobos, G.; Frances, M.; Arenillas, M. The ERHIN Programme. Hydrological-Nival Modelling for the Management of Water Resources in the Ebro Basin. *Houille Blanche* **2010**, *3*, 58–64. [CrossRef]
28. AEMET, Agencia Estatal de Meterología. Available online: http://www.aemet.es/es/serviciosclimateos/cambio_climat (accessed on 8 February 2021).
29. EHRIN (Evaluación de los Recursos Hídricos Procedentes de la Innivación). Dirección General del Agua. *Ministerio para la Transición Ecológica y el Reto Demográfico.* Available online: https://www.miteco.gob.es/es/agua/temas/evaluacion-de-los-recursos-hidricos/ERHIN/ (accessed on 8 February 2021).
30. Mora, J.; Ferrer, C.; Arenillas, M.; Cobos, C. Hydrological peculiarities of mountain basins. The case of the Spanish Pyrenees. In Proceedings of the International Conference on water observation and information system for decision support, Ohrid, Macedonia, 24—25 May 2004.
31. Morin, G.; Fortin, J.P.; Lardeau, J.P.; Sochanska, W.; Paquette, S. *Modèle CEQUEAU: Manuel D'utilisation*; INRS-Eau, Rapport Scientifique n1 93; INRS-Eau: Quebec City, QC, Canada, 1981.
32. Anderson, E.A. Development and Testing of Snow Pack Energy Balance Equations. *Water Resour. Res.* **1968**, *4*, 19–37. [CrossRef]
33. Anderson, E.A. *National Weather Service River Forecast System. Snow Accumulation and Ablation Model*; US Department of Commerce, National Oceanic and Atmospheric Administration, National Weather Service: Silver Spring, MA, USA, 1973.
34. Anderson, E.A. *A Point Energy and Mass Balance Model of a Snow Cover*; US Department of Commerce, National Oceanic and Atmospheric Administration, National Weather Service, Office of Hydrology: Silver Spring, MA, USA, 1976.
35. Anderson, E.A. *Snow Accumulation and Ablation Model—SNOW 17*; US Department of Commerce, National Oceanic and Atmospheric Administration, National Weather Service, National Weather Service River Forecast System: Newburyport, MA, USA, 2006; p. 61.
36. Garijo, C.; Mediero, L. Influence of climate change on flood magnitude and seasonality in the Arga River catchment in Spain. *Acta Geophys.* **2018**, *66*, 769–790. [CrossRef]
37. Pey, J.; Revuelto, J.; Moreno, N.; Alonso-González, E.; Bartolomé, M.; Reyes, J.; Gascoin, S.; López-Moreno, J.I. Snow Impurities in the Central Pyrenees: From Their Geochemical and Mineralogical Composition towards Their Impacts on Snow Albedo. *Atmosphere* **2020**, *11*, 937. [CrossRef]

38. Musselman, K.; Clark, M.; Liu, C.; Ikeda, K.; Rasmussen, R. Slower snowmelt in a warmer world. *Nat. Clim Chang.* **2017**, *7*, 214–219. [CrossRef]
39. López-Moreno, J.; Pomeroy, J.; Revuelto, J.; Vicente-Serrano, S. Response of snow processes to climate change: Spatial variability in a small basin in the Spanish Pyrenees. *Hydrol. Process.* **2013**, *27*, 2637–2650. [CrossRef]
40. Stewart, I.T.; Cayan, D.R.; Dettinger, M.D. Changes in Snowmelt Runoff Timing in Western North America under a 'Business as Usual' Climate Change Scenario. *Clim. Chang.* **2004**, *62*, 217–232. [CrossRef]
41. Arnell, N.W. The effect of climate change on hydrological regimes in Europe: A continental perspective. *Glob. Environ. Chang.* **1999**, *9*, 5–23. [CrossRef]
42. Garijo, C.; Mediero, L.; Garrote, L. Usefulness of AEMET generated climate projections for climate change impact studies on floods at national-scale (Spain). *Ingeniería Agua* **2018**, *22*, 153–166. [CrossRef]

Appendix 2 – Seasonal Variability of Snow Density in the Spanish Pyrenees

Lastrada, E.; Cobos, G.; Garzón-Roca, J.; Torrijo, F.J. Seasonal Variability of Snow Density in the Spanish Pyrenees. Water 2021, 13, 1598. https://doi.org/10.3390/w13111598

water

MDPI

Article

Seasonal Variability of Snow Density in the Spanish Pyrenees

Eduardo Lastrada [1,*], Guillermo Cobos [1], Julio Garzón-Roca [2] and F. Javier Torrijo [1,3]

[1] Department of Geological and Geotechnical Engineering, Universitat Politècnica de València, 46014 Valencia, Spain; gcobosc@trr.upv.es (G.C.); fratorec@trr.upv.es (F.J.T.)
[2] Independent Researcher, 46014 Valencia, Spain; ing.jgarzon@gmail.com
[3] Research Centre PEGASO, Universitat Politècnica de València, 46014 Valencia, Spain
* Correspondence: edlasmar@aaa.upv.es

Abstract: Spanish latitudes and meteorological conditions cause the snow phenomena to mainly take place in mountainous areas, playing a key role in water resource management, with the Pyrenees as one of the most important and best monitored areas. Based on the most significant dataset of snow density (SDEN) in the Spanish Pyrenees for on-site manual samples and automatic measurements, in this study, single and multiple linear regression models are evaluated that relate SDEN with intra-annual time dependence and other drivers such as the seasonal accumulated precipitation, 7-day average temperatures, snow depth (SD) and elevation. The seasonal accumulated precipitation presented a more dominant influence than daily precipitation, usually being the second most dominant SDEN driver, followed by temperature. Average temperatures showed the best fitting to SDEN. The results showed similar densification rates ranging widely from 0.7×10^3 kg/L/day to 2×10^3 kg/L/day without showing a spatial pattern. The densification rate for the set of manual samples was set to 1.2 kg/L/day, very similar to the set of automatic measurements (1.3 kg/L/day). The results increase knowledge on SDEN in the Pyrenees. The SDEN regression models that are given in this work may allow us, in the future, to estimate SDEN, and consequently Snow Water Equivalent (SWE), using an economical and extensive SD and meteorological network, although the high spatial variability that has been found must be regarded. Estimating a relationship between SDEN and several climate drivers enables us to take into account the impact of climate variability on SDEN.

Keywords: snow density; Spanish Pyrenees; ERHIN program; water equivalent; climate variability

Citation: Lastrada, E.; Cobos, G.; Garzón-Roca, J.; Torrijo, F.J. Seasonal Variability of Snow Density in the Spanish Pyrenees. *Water* **2021**, *13*, 1598. https://doi.org/10.3390/w13111598

Academic Editor: Maria Mimikou

Received: 1 April 2021
Accepted: 3 June 2021
Published: 7 June 2021

1. Introduction

Snow in Spain plays a key role in water resource management and occurs essentially in mountainous areas due to Spanish latitudes and meteorological conditions [1–5]. One of the most important Spanish mountain regions is the Pyrenees, which extends about 490 km between Spain and France, connecting the Atlantic Ocean at its eastern limit with the Mediterranean Sea at its western limit (both of which influence the climate of the Pyrenees), and with Aneto Peak as its highest point (3404 m altitude). From the different parameters defining snow-related phenomena, snow density (SDEN) relates snow depths (SDs) with the snow water equivalent (SWE). Since SD measurements are much more frequent than the available SWE data, better knowledge and parameterization of SDEN will enable the achievement of a more accurate estimation of the SWE based on SD measurements. Moreover, as wind data become more available, hydrological models can determine a more accurate estimation of forced-convection snowmelt and snow transport, for which SDEN is needed. However, SDEN is a complex parameter that can vary temporally, spatially and even within the snowpack profile in the vertical direction.

The density of freshly fallen snow depends on three main climatic conditions: temperature, wind and humidity. Typical proposed density values for recently fallen snow are found between 0.07 and 0.15 kg/L, with 0.1 kg/L being the most common value [6–8].

The density of the new snow can also be estimated linearly, based on air temperature between −15 °C and 0 °C [9,10]. However, as SDEN depends on the liquid and snow form proportions, a higher SDEN can be given for fresh snow.

The aggregation of the ice grains begins as soon as snow touches the surface, increasing the snow cover density [11]. This process is known as sintering and plays an important role in snow densification. There are two distinct types of snow metamorphism: constructive metamorphism (recrystallization by vapor diffusion) and destructive metamorphism (equilibrium growth) [12]. A temperature gradient of about 10 °C/m is considered a threshold for the initiation of constructive metamorphism [13,14]. Liquid water causes destructive metamorphism to take place at a faster rate. Moreover, daily melting cycles associated with solar radiation and atmospheric temperature cause snow crystal metamorphism. This leads to a gradual loss of voids and an irreversible increase in the density of the snow layer over time [15]. At the same time, SDEN affects shortwave radiation penetration in snow. About 80% of this energy is absorbed in the first 5 to 15 cm of the snowpack [12]. The range depends on SDEN [16]. Compaction due to gravity should also be considered for SDs above 1 m [17]. In the Spanish Pyrenees, as the SD is deep for high elevations, this effect may not be negligible. In addition, precipitation over the snowpack will also increase SDEN [18]. These cycles can repeat until the whole snow layer is melted and frozen, turning into ice with an average density of 0.917 kg/L. However, defining an accurate proportion for each of these processes in the densification rate is not easy.

Different techniques were used to measure or estimate SDEN worldwide [19–23]. Common techniques include conventional on-site manual sampling, the non-destructive snow water equivalent (SWE) determination based on cosmic-ray neutron attenuation (CRN) [24,25], acoustic signal delays [26] and stepped-frequency continuous-wave radar, recently used at the AEMET Formigal-Sarrios test site (Spanish Pyrenees) and implemented in a coherent software-defined radio in the range from 150 MHz to 6 GHz [27]. The use of SWE products derived from satellite microwave radiometer-based measurements, combined with SD measurements, is another alternative technique, but the low spatial resolution of these products may not be suitable for mountainous and complex small catchments [28,29]. Snow pillows are also used for the non-destructive monitoring of SDEN, but they have a complex installation process, maintenance and have uncertainties associated with low SD and irregular snowmelt drainage [30].

Several studies [20,31–34] estimated linear density-time functions or densification rates, providing links to the physical processes. However, density models still need to cope with a high SDEN variability at low SD values, as it can range from low-density new snow to high-density slush. Regarding SDEN's relationship with time, it shows a gradual increase throughout the winter season. Across the western United States, SDEN was found to be location-dependent during early and midwinter, although the snowpack densification daily rate was nearly fixed regardless of the location. Considerable intra-annual variability in SDEN was also reported, with densification trends generally linear, but significantly less year-to-year variation [33]. The low intra-annual variability of SDEN was also observed in southern Canada [35]. In the Swiss Alps, SDEN was found to depend on the season, SD, elevation and location. Elevation had only a minor direct effect [36], as higher SDs at higher sites imply higher SDEN due to compaction in winter, while melting cycles at lower elevations and in the late winter season induce a compensating effect [21,33,36]. For the alpine regions in the former Soviet Union and the US, precipitation was the dominant climate variable, followed by average temperature [37].

In the Iberian Peninsula, snow observations and a validated daily gridded snowpack dataset were simulated from downscaled reanalysis [38], calculating SDEN for each time step with different maximum thresholds: 0.3 kg/L for cold (non-isothermal) and 0.5 kg/L for melting (isothermal) snow conditions [39]. In the central Pyrenees, statistically significant correlations between the SD and other topographic variables with SDEN were found, but they showed a great variability among sites and surveys. The absolute error in the SWE

estimated from the computed SDEN was less than 15% and was similar to that obtained by relating SDEN directly to SD [40].

The Spanish Pyrenees hold more than one hundred snow poles and up to thirteen automatic snow monitoring devices, or telenivometers (TNMs), operating since 2008. This instrumentation allows for the study of the seasonal variability of snowfall events [41]. Additionally, the Spanish and Ebro Water Authority have been carrying out on-site SDEN measurements since the early 1990s through the ERHIN program ("Estudio de Recursos Hídricos procedentes de la INnivación"—Study of Snow Water Resources) [42]. TNM data show significant variability in annual SD. Western regions (Atlantic Ocean weather) give the most annual accumulation in the winter months, while eastern regions (Mediterranean weather types) show more homogenous accumulation over winter, spring and late autumn. It is interesting to note that western TNMs also show behaviours similar to that observed for the western coast of the US, which is characterized by plenty of precipitation and relatively high air temperatures, both possible contributors to early season high SDEN [43].

The novelty of this paper remains in the definition of SDEN variability in the Spanish Pyrenees, using the vast amount of data from the ERHIN program obtained from manual sampling and non-destructive automatic measurements. A series of relationships are established with other parameters, and its temporal and spatial variability is characterized. Few comparable works in the world have used such a wide database (SNOTEL or WSL Institute for Snow and Avalanche Research SLF), and there are no similar precedents in the study area. To achieve this goal, a series of single and multiple linear regressions are conducted, relating SDEN with the time evolution variability, seasonal accumulated precipitation, SD, elevation and average temperatures.

2. Materials and Methods

The ERHIN program [44] started in 1986, studying snow phenomena in river basins in the mountainous regions of the Pyrenees, Sierra Nevada, the Central System and the Cantabrian Mountains. In this framework, on-site manual SDEN measurements were carried out and a dense network of snow poles and TNMs (SWE and SD non-destructive measurements) were installed. The Pyrenees is the densest region monitored, with 13 TNMs and more than 100 snow poles (Figure 1). The TNMs cover a range about 200 km long in the Pyrenees and are numbered from west to east.

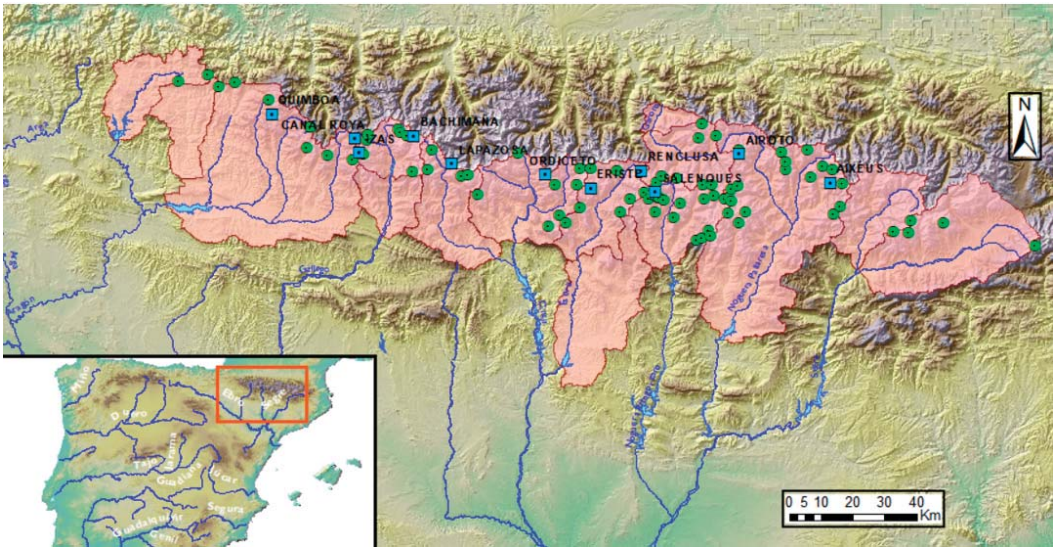

Figure 1. Snow poles (green) and telenivometers (TNM) (blue) network from the ERHIN program [44] in the Pyrenees.

2.1. On-Site Manual Sampling and Measurements

Since 1987, on-site manual SDEN measurements have been carried out at certain snow poles. At the same time, SD measurements were taken for the whole snow pole network. Sampling elevations range from 1440 m to 2615 m and cover up to three seasonal campaigns between December and May.

Figure 2 shows a 0.8 m stackable sampling tube of constant 53.8 mm diameter inside a section (22.72 cm^2) and 2.5 mm thick, with up to 4 m of maximum penetration depth. This SWE tube was handmade in 1986 at the Technical University of Valencia. Knowing the weight and dimensions of the core, and therefore its volume, by directly weighing it on a precision weighing scale, the net weight of the snow core is obtained, and the density is calculated.

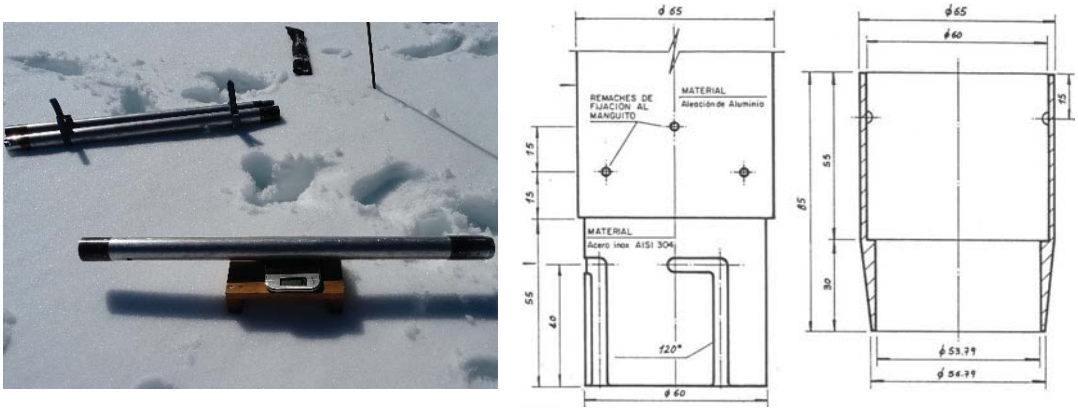

(**a**) (**b**)

Figure 2. On-site manual sampling. (**a**) Snow tubes. (**b**) Nozzle dimensions.

Table 1 shows the on-site manual sampling and elevation for sites in the same locations as 11 TNM sites. The number of samples is also included. The complete list of 35 snow pole sites and the number of samples are given as supplementary data. Figure 3 shows the elevation distribution for all of the samples taken, ranging from 1810 m to 2615 m for snow pole sites.

Table 1. On-site manual sampling sites. Snow poles are in the same locations as the TNM sites.

Name	X COORDINATE ETRS89H30	Y COORDINATE ETRS89H30	Elevation (m)	No. Samples	Sampling Period (Years)
1. Quimboa	682,767	4,748,419	1810	13	1998–2019
2. Izas	710,308	4,736,177	2080	9	2007–2012
3. Canal Roya	708,779	4,740,716	1860	17	1987–2019
4. Bachimaña	727,394	4,741,571	2220	61	1987–2019
5. Lapazosa	739,424	4,732,777	2115	11	2009–2019
6. Ordiceto	768,642	4,729,429	2380	65	1987–2015
7. Renclusa	799,030	4,730,578	2180	32	1987–2017
8. Salenques	803,363	4,723,843	2600	13	2008–2014
9. Eriste	783,155	4,725,107	2350	7	2009–2014
10. Airoto	829,803	4,735,946	2380	60	1987–2019
11. Aixéus	858,381	4,726,892	2400	66	1987–2019
Total samples				354	

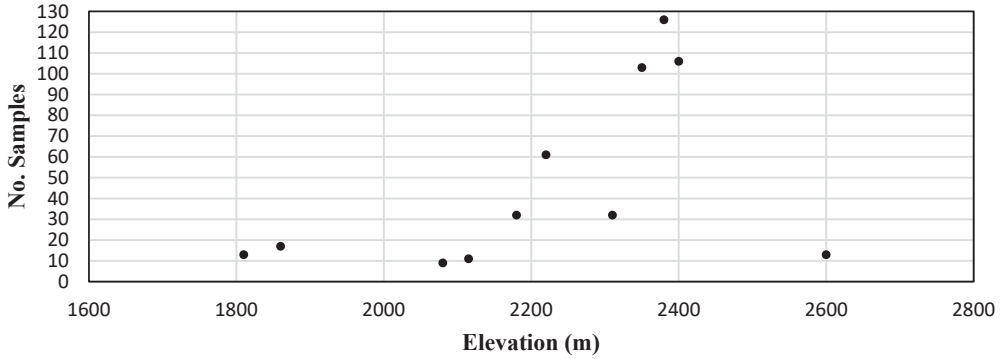

Figure 3. Number of snow density (SDEN) manual samples and elevation distribution.

2.2. On-Site Non-Destructive Measurements

First Cosmic-Ray Neutron (CRN) attenuation telenivometers (TNMs) were installed in 2008 along the Spanish Pyrenees (Figure 4), and two more were recently installed in 2015 and 2018. TNMs allow the obtaining of SWE high time resolution data (15 min) and SD vertical data (1 cm resolution). From those values, SDEN can be estimated according to Equation (1):

$$SDEN = \frac{SWE}{SD} \quad (1)$$

Figure 4. TNM and on-site manual sampling for the snow pole sampler.

Table 2 shows the name, situation, elevation, number of daily samples and sampling period for each TNM, which were located above 1800 m elevation and with 2600 m as the maximum elevation. It should be noted that SDEN calculated according to Equation (1) is not sensitive to a higher time resolution. Figure 1 shows the situation of the TNMs in the Pyrenees, (named from west to east), while Figure 5 shows the elevation distribution for the automatic TNM measurements. It is interesting to mention that the Eriste TNM is located at approximately the same distance from the Atlantic Ocean and the Mediterranean Sea.

Table 2. On-site non-destructive measurements. TNM sites.

Name	X COORDINATE ETRS89H30	Y COORDINATE ETRS89H30	Elevation (m)	No. Data	Data Period (Years)
1. Quimboa	682,648	4,748,214	1810	1465	2008–2021
2. Izas	710,243	4,735,937	2080	2107	2008–2021
3. Canal Roya	708,660	4,740,541	1971	1661	2008–2021
4. Bachimaña	727,282	4,741,345	2220	2086	2008–2021
5. Lapazosa	739,388	4,732,579	2140	1676	2008–2021
6. Ordiceto	768,527	4,729,209	2380	2043	2008–2021
7. Renclusa	798,925	4,730,377	2175	1737	2008–2020
8. Salenques	803,294	4,723,655	2600	263	2008–2010
9. Eriste	783,048	4,724,896	2350	2049	2009–2021
10. Airoto	829,707	4,735,723	2380	2004	2008–2021
11. Aixeus	858,269	4,726,759	2400	2010	2008–2021
14. Sarrios-Formigal	713,384	4,737,624	1800	643	2015–2021
15. Besurta	799,420	4,731,387	1930	317	2018–2021
Total samples				21,257	

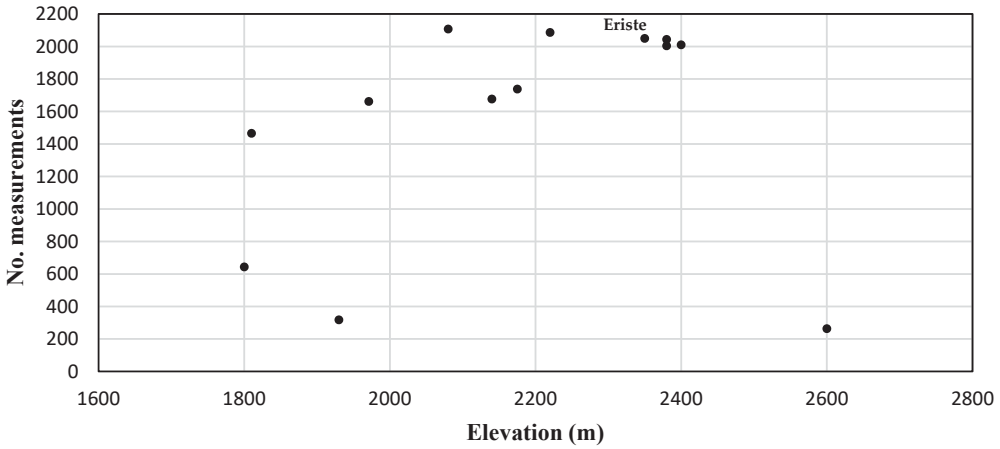

Figure 5. Number of SDEN automatic TNM measurements and elevation distribution.

Although the TNMs have been operating for a shorter period than the period covered by manual samples, daily data were registered, with more than 20,000 samples and officially provided by the Ebro Water Authority (http://www.saihebro.com/saihebro/index.php?url=/datos/usos/mapa:TNG/tipoestacion:TN accessed on 4 June 2021). Additionally, the maximum, average and minimum daily temperatures were available.

2.3. Other Data and Sources of Error

Supplementary Materials are provided for both on-site manual sampling and on-site non-destructive (TNM) daily measurements.

The daily data for precipitation from the closest meteorological stations within the same period as the TNM measurements are also given in the Supplementary Material.

The sources of error and uncertainties associated with snow sampling include the loss of part of the sample due to snowpack collapse when the sampler encounters hard layers. When the sampler is extracted from the snowpack for weighing, snow can also be lost [45] or stuck to the outside of the sampler. These errors may be increased by a snowpack with ice layers that give the false perception of reaching the ground, basal ice and layers of depth

hoar and non-cohesive crystals. New snow or wet snow can also increase sampling errors, especially if the observer is collecting core samples to be weighed later rather than using a spring balance and tube cradle. The experience of the observer plays an important role in reducing potential errors due to human failure. Depending on the temperature, new and wet snow will tend to stick in the tube, and this will result in an underestimation of the SWE, which could exceed 10%. Smaller diameter cutters (down to 20 cm^2) were more prone to plugging as they encountered ice lenses, and they were more likely to induce the collapse of non-cohesive layers under the cutter, resulting in an underestimation of the total SWE [46]. The ideal cutter area was about 30 cm^2, demonstrated by the low error percentage of the ESC30 sampler, which ranged from a 5% overestimation to a 2% underestimation [47]. The uncertainty of density measurements in non-ideal snow conditions is approximately within 10 to 15% [48]. As a control measure, random validation tests were carried out for manual samples and measurement protocols were followed [46].

Errors in TNM measurements can occur due to non-environmental issues such as instrument malfunction and incorrect instrument calibration (or calibration drift), CRN uncertainties due to changes in mid-season soil moisture levels and the undervaluation of precipitation and gaps or false null data from other meteorological variables. In this regard, TNM data are periodically calibrated with manual sampling during late snow conditions [42].

2.4. Analysis Methodology

A previous screening process was carried out, with the identification of outliers (a range check for reasonable values between zero and the maximum possible SDEN for the site), gaps and null data, discarding sites with little information or information that was not representative.

TNM measurements are fully automated and, even though they are frequently calibrated, are not quality controlled. Thus, the calculated SDEN values that significantly exceeded the expected maximum and minimum values at each site were removed. The number of samples for each TNM is given after quality-control procedures. All negative and null values were eliminated from the records, for both the SWE and SD, which are necessary to estimate SDEN. Consequently, TNMs numbers 8, 14 and 15 (Salenques, Sarrios-Formigal and Besurta) were discarded.

Manual samples, much less prone to uncertainties [37], underwent a similar screening process. On-site manual sample sites with enough data in the same location as TNM sites were selected and pooled. The previous screening process reduced 35 on-site manual sites with 841 samples to five on-site manual sites matching TNM sites with 284 samples. SDEN statistics were calculated for both manual samples and automatic measurements during the entire year (annual period), as well as for the accumulation period (winter snow, until 21 March) and for the melting period (spring snow, from 21 March).

Automatic TNM sites with a significant correlation between SDEN and the day of the year (time evolution) were selected and grouped (the set of TNMs) for automatic TNM measurements, where day 1 corresponds to 1 October. The results were compared with the SDEN–day of the year correlation for manual samples.

Independent variables were analysed for the selected automatic TNM sites. The dominant climatological drivers of annual SDEN variability were extracted by establishing single linear regressions between each of the predictor terms and SDEN. The selected climate and spatial predictors include the time evolution, precipitation, accumulated precipitation, SD and average temperature.

Multiple linear regressions (MLRs) between SDEN and these predictors were studied for automatic measurements and compared with manual samples. The effect of elevation on the grouped series (the set of TNMs) was evaluated. Predictors were added progressively in the MLR model from more to less dominant with a significance threshold of 0.05.

3. Results

In this section, the SDEN results are analysed, identifying dominant climatological variables and studying MLR models for SDEN. Results from both the manual and automatic measurements are presented.

3.1. SDEN Statistics

Table 3 shows a summary of the SDEN statistics obtained by on-site manual data for two annual periods, winter or early season (until 21 March) and spring or late season (21 March–30 June). The word "set" refers to all grouped data.

Table 3. SDEN statistics for the most representative manual samples in the same location as TNM sites and for the set of samples.

Name	Average (Annual)	C. V. (Annual)	Average (Winter)	C. V. (Winter)	Average (Spring)	C. V. (Spring)
4. Bachimaña	0.396	1.82%	0.351	1.82%	0.442	0.90%
6. Ordiceto	0.396	1.72%	0.349	1.23%	0.451	0.93%
7. Renclusa	0.368	1.96%	0.306	0.88%	0.437	0.71%
10. Airoto	0.382	1.60%	0.344	1.69%	0.427	0.68%
11. Aixéus	0.386	1.53%	0.337	0.92%	0.427	1.05%
Set of Manual Samples	0.394	1.75%	0.348	1.47%	0.443	0.93%

The average SDEN and coefficient of variation (C.V.) were very similar among sites for every period, without spatial patterns from east to west locations. Renclusa showed the lowest average SDEN and the highest C.V. due to a very low winter average SDEN and very marked differences between early and late season snow. Bachimaña and Ordiceto showed the highest average SDEN. As expected, the average SDEN value was greater for the late season (spring) than for the early season (winter). The C.V. is small for all sites studied and the set of samples, being the greatest during the early season (winter).

Table 4 shows a summary of the SDEN statistics obtained from TNM data for two annual periods, winter or early season (until 21 March) and spring or late season (21 March–30 June). The set of TNMs refers to TNMs numbers 1, 2, 4, 6, 7 and 9.

Table 4. SDEN statistics for TNM data and for data from the set of TNMs.

Name	Average (Annual)	C. V. (Annual)	Average (Winter)	C. V. (Winter)	Average (Spring)	C. V. (Spring)
1.Quimboa	0.389	3.80%	0.344	3.17%	0.511	1.04%
2. Izas	0.36	1.97%	0.309	1.04%	0.435	0.80%
3. Canal Roya	0.348	1.67%	0.325	1.32%	0.400	1.40%
4. Bachimaña	0.368	2.53%	0.332	2.11%	0.455	0.95%
5. Lapazosa	0.364	3.13%	0.334	2.81%	0.438	1.92%
6. Ordiceto	0.385	4.60%	0.312	2.66%	0.512	1.29%
7. Renclusa	0.365	2.52%	0.326	1.47%	0.462	1.43%
9. Eriste	0.435	2.23%	0.398	1.61%	0.508	1.63%
10. Airoto	0.383	3.55%	0.357	3.31%	0.449	2.67%
11. Aixeus	0.386	3.83%	0.360	4.36%	0.440	1.95%
Set of TNMs	0.384	3.07%	0.337	2.26%	0.480	1.44%

As for manual samples, except for Eriste, the TNM data showed very similar SDEN averages among sites for every period, without spatial patterns from east to west locations. Eriste showed the highest average SDEN, while Canal Roya's average SDEN was the lowest; the C.V. is again small, with all TNMs below 5%, but there were some differences among sites, since the amount of data between them is variable. The Ordiceto TNM showed

the greatest C.V. Once again, the C.V. was usually greater for the early season (winter) than for the late season (spring).

A comparison of statistics between manual and automatic data (see Table 5) showed small differences in terms of the average SDEN, although the C.V. values are higher for the automatic data. The set of manual samples and the set of TNM data show small differences for the average SDEN, especially for the annual and early-season periods. Renclusa showed the lowest annual SDEN average for both the manual and automatic data, while the highest annual average SDEN was represented by different locations for each technique.

Table 5. SDEN statistics comparison between automatic data for TNM sites in the same location as manual samples.

Name	Average (Annual)	C. V. (Annual)	Average (Winter)	C. V. (Winter)	Average (Spring)	C. V. (Spring)
4. Bachimaña	107.6%	71.9%	105.7%	86.3%	97.1%	94.7%
6. Ordiceto	102.9%	37.4%	111.9%	46.2%	88.1%	72.1%
7. Renclusa	100.8%	77.8%	93.9%	59.9%	94.6%	49.7%
10. Airoto	99.7%	45.1%	96.4%	51.1%	95.1%	25.5%
11. Aixeus	100.0%	39.9%	93.6%	21.1%	97.0%	53.8%
Set of TNMs	102.6%	57.0%	103.3%	65.0%	92.3%	64.6%

3.2. Most Representative Automatic TNM Sites

The most representative automatic TNM sites were selected and grouped (the set of TNMs) for the automatic TNM data, with a significant correlation between SDEN and the day of the year (intra-annual time dependence), where day 1 corresponds to 1 October. An intra-annual time dependence for SDEN was found using Equation (2):

$$SDEN = A \cdot day + B \quad (2)$$

The coefficients A and B are given in Table 6 along with the site elevation of each TNM and the average elevation of the set of TNMs, with the coefficient of determination (R^2) being computed in each case. The relationship found is important as it describes SDEN when data from other climatic variables are not available. The coefficient A represents the densification rate, ranging from 0.7×10^{-3} kg/L/day to 2×10^{-3} kg/L/day; the coefficient B represents the initial SDEN, ranging from 0.1 kg/L to 0.3 kg/L. Neither of the two parameters shows a spatial pattern.

Table 6. SDEN intra-annual time dependence for automatic measurements. Bold letters are used for selected sites for the Set of TNMs.

Name	A (day)	B	Elevation (m)	R^2	Sampling Period (Years)
1.Quimboa	0.0020	0.112	1810	0.61	2008–2021
2. Izas	0.0012	0.177	2080	0.64	2008–2021
3. Canal Roya	0.0007	0.252	1971	0.18	2008–2021
4. Bachimaña	0.0011	0.224	2220	0.4	2008–2021
5. Lapazosa	0.0009	0.242	2140	0.17	2008–2021
6. Ordiceto	0.0020	0.090	2380	0.73	2008–2021
7. Renclusa	0.0018	0.1	2175	0.15	2008–2020
9. Eriste	0.0009	0.303	2350	0.27	2009–2021
10. Airoto	0.0008	0.280	2380	0.13	2008–2021
11. Aixeus	0.0007	0.285	2400	0.10	2008–2021
Set of TNMs	0.0013	0.196	2187	0.44	2008–2020

Automatic TNM sites with a significant coefficient of determination (R^2) were selected and grouped (the set of TNMs) for automatic TNM measurements. The densification rate for the data from the set of TNMs is set to 1.3×10^{-3} kg/L/day, with an initial SDEN of 0.196 kg/L. Ordiceto, placed in the central Pyrenees, showed the highest densification rate and coefficient of determination (R^2) and the lowest initial SDEN. Aixeus, in the eastern part of the Pyrenees, showed the lowest densification rate and coefficient of determination (R^2), while the highest initial SDEN was found in Eriste. Canal Roya, Bachimaña, Lapazosa, Eriste, Airoto and Aixeus showed low densification rates and high initial SDENs, while Quimboa, Izas, Ordiceto and Renclusa showed the opposite behaviour. Therefore, no spatial pattern can be observed.

Regarding (R^2), TNMs numbers 1, 2, 4, 6, 7 and 9 are selected. TNM number 9 (Eriste) is selected as the most representative of the eastern part of the Pyrenees. Figure 6 shows the SDEN intra-annual time dependence for the selected TNMs and the trend line for the set of TNMs.

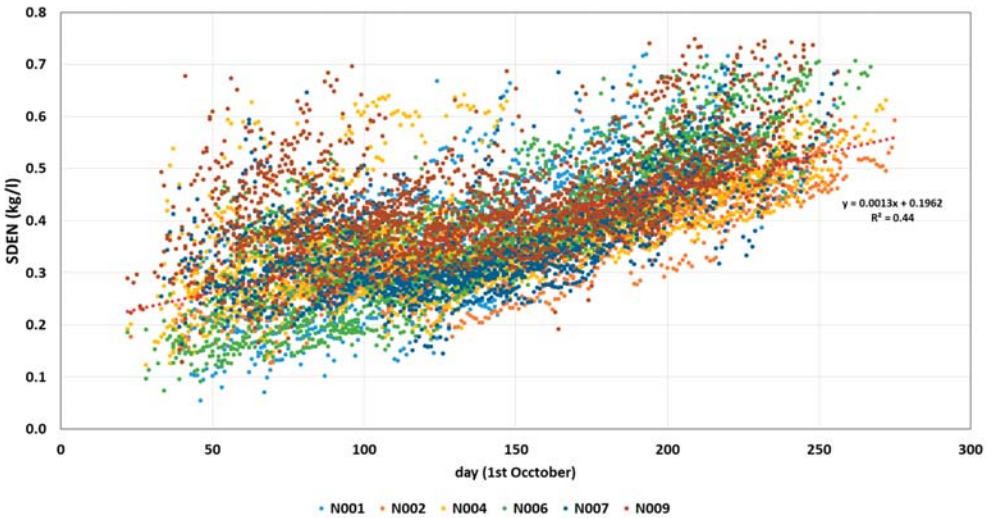

Figure 6. SDEN intra-annual time dependence for selected TNM measurements. Red trend line for the set of TNMs.

Table 7 shows the values of the coefficients A and B for manual sampling in the most representative TNM sites and the set of manual samples, which enables the establishment of the intra-annual time dependence of SDEN using Equation (2). The average elevation for the set of manual samples and the coefficient of determination (R^2) are shown, too. For manual samples, the densification rates and an initial SDEN range have less variability than the automatic measurements, from 1.1×10^{-3} kg/L/day to 1.8×10^{-3} kg/L/day and from 0.13 kg/L to 0.19 kg/L, respectively. The densification rate from the set of manual samples is set to 1.2×10^{-3} kg/L/day, with an initial SDEN of 0.189 kg/L, showing values very similar to but lower than the values of the automatic measurements. Common sites for both manual and TNM data are Bachimaña, Ordiceto and Renclusa. Bachimaña showed the same coefficient of determination but a higher densification rate and a lower initial SDEN for manual samples than for automatic data. Ordiceto showed a lower coefficient of determination and densification rate, but a higher initial SDEN for the manual samples than for the automatic data. Renclusa had a higher coefficient of determination and the same densification rate, but a lower initial SDEN.

Table 7. SDEN intra-annual time dependence for manual sampling in the most representative TNM sites and the set of manual samples. Bold letters are used for manual samples in the same locations as selected TNM sites.

Name	A (day)	B	Elevation (m)	R^2	No. Samples
4. Bachimaña	0.0013	0.157	2220	0.4	61
6. Ordiceto	0.0016	0.126	2380	0.57	65
7. Renclusa	0.0018	0.054	2180	0.73	32
10. Airoto	0.0011	0.188	2380	0.35	60
11. Aixéus	0.0011	0.180	2400	0.34	66
Set of Manual samples	0.0012	0.189	2268	0.34	840

Figure 7 displays the linear time dependence of SDEN for the set of manual samples.

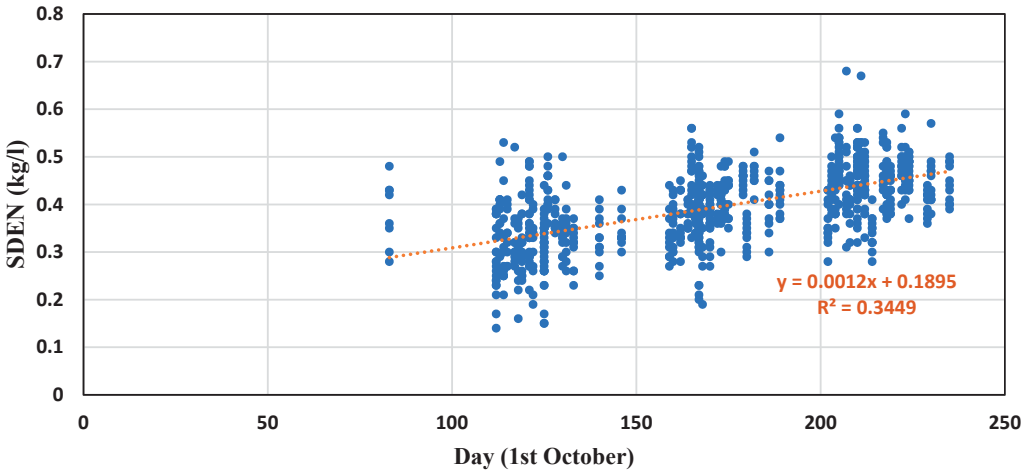

Figure 7. SDEN time dependence for on-site manual sampling. Trend line for the set of manual samples.

3.3. Identification of Dominant Variables

In addition to the time dependence, the selected predictors included the SD (cm), seasonal accumulated daily precipitation (PPacum (mm)) and 7-day average temperature (Tave7d) (°C/7 days). The seasonal accumulated precipitation was taken into account from the first day that snow accumulation starts and presented a more dominant influence than the daily precipitation, as SDEN depends on historical intra-annual evolution. The 7-day average temperatures have shown the best fitting to SDEN. SDEN depends on punctual temperatures for the accumulation process, but during melting cycles, average temperatures may describe it better [33]. The effects of the maximum and average daily temperatures were similar, while the minimum daily temperature was less dominant. Average daily temperatures were chosen, as they may be more available. Table 8 shows the correlation values, with the intra-annual time dependence and seasonal accumulated precipitation being the most dominant variables.

Table 8. SDEN correlation coefficients (R^2) for TNM selected sites.

Name	Time Dependence (day)	PPacum (mm)	Tave7d (°C/7 days)	SD (cm)
1. Quimboa	0.61	0.58	0.18	0
2. Izas	0.64	0.47	0.37	0.03
4. Bachimaña	0.4	0.21	0.20	0
6. Ordiceto	0.73	0.44	0.21	0.14
7. Renclusa	0.15	0	0.38	0
9. Eriste	0.27	0.13	0.19	0.07
Set of TNMs	0.44	0.25	0.19	0

For the Quimboa TNM, the PPacum driver was the most dominant, while Tave7d was the most dominant for the Renclusa TNM. For the rest of the selected TNMs (Izas, Bachimaña, Ordiceto and Eriste), the intra-annual time dependence was the main variable.

The SDEN linear correlation with SD is almost negligible, except for the Ordiceto and Eriste TNMs. However, it may give useful information, as the significance threshold of SDEN is reduced for high SD values. Figure 8 represents SDEN's variability on SD for the set of TNMs, divided into an early-mid season snowpack and mid-late season snowpack. As observed, SDEN has a wide range of values with low SD, especially for the early season snowpack, reducing SDEN variability as SD increases.

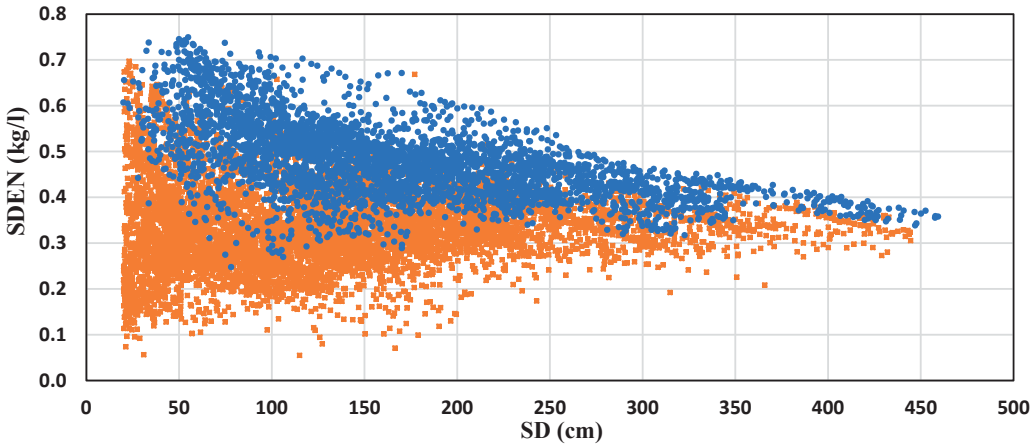

Figure 8. SDEN variability with SD for the set of TNMs. Blue, front—Late season snowpack (21 March–21 June); Orange, back—Early season snowpack (21 October–21 March).

3.4. Multiple Linear Regressions (MLRs)

The MLRs between SDEN and the evaluated predictors were studied for the automatic measurements and compared with the manual samples. Those MLRs follow Equation (3):

$$SDEN = A_1 \cdot day + A_2 \cdot PPacum + A_3 \cdot Tave7d + A_4 \cdot SD + B \quad (3)$$

The coefficients A_i are given in Table 9 for each site studied. As mentioned before, predictors were added progressively in the MLR model from more to less dominant, indicating the incrementally adjusted correlation coefficient (adjusted R^2). Moreover, the

effect of elevation for the data from the set of TNMs was also evaluated as a driver, thus the MLR followed Equation (4):

$$SDEN = A_1 \cdot day + A_2 \cdot PPacum + A_3 \cdot Tave7d + A_4 \cdot SD + A_5 \cdot elevation + B \quad (4)$$

Table 9. Optimum SDEN multiple linear regression model for TNM selected sites and the set of TNMs (TNMs Nos. 1, 2, 4, 6, 7 and 9). Regression coefficients [A_i, B] and the incrementally adjusted correlation coefficient (R_i^2). Bold letters are used for the final adjusted correlation coefficient (R^2) for Equations (3) and (4).

Name	A_1 (day)	A_2 (PPacum)	A_3 (Tave7d)	A_4 (SD)	A_5 (Elevation)	B
1.Quimboa	$[1.056 \times 10^{-3}]$ (0.606)	$[0.205 \times 10^{-3}]$ (0.648)	$[4.783 \times 10^{-3}]$ (0.681)	$[-0.190 \times 10^{-3}]$ **(0.691)**	-	[0.187]
2. Izas	$[0.788 \times 10^{-3}]$ (0.641)	$[0.078 \times 10^{-3}]$ (0.652)	$[5.520 \times 10^{-3}]$ (0.732)	$[-0.057 \times 10^{-3}]$ **(0.735)**	-	[0.218]
4. Bachimaña	$[1.282 \times 10^{-3}]$ (0.396)	$[0.020 \times 10^{-3}]$ (0.414)	$[2.317 \times 10^{-3}]$ (0.468)	$[-0.480 \times 10^{-3}]$ **(0.542)**	-	[0.257]
6. Ordiceto	$[2.295 \times 10^{-3}]$ (0.733)	$[0.035 \times 10^{-3}]$ (0.780)	$[3.287 \times 10^{-3}]$ (0.803)	$[-0.440 \times 10^{-3}]$ **(0.825)**	-	[0.096]
7. Renclusa	$[1.267 \times 10^{-3}]$ (0.152)	-	$[7.242 \times 10^{-3}]$ (0.514)	$[-0.694 \times 10^{-3}]$ **(0.631)**	-	[0.271]
9. Eriste	$[1.263 \times 10^{-3}]$ (0.271)	$[0.0475 \times 10^{-3}]$ (0.280)	$[2.505 \times 10^{-3}]$ (0.356)	$[-1.005 \times 10^{-3}]$ **(0.600)**	-	[0.365]
Set of TNMs	$[1.268 \times 10^{-3}]$ (0.459)	$[0.0685 \times 10^{-3}]$ (0.460)	$[4.266 \times 10^{-3}]$ (0.503)	$[-0.352 \times 10^{-3}]$ **(0.562)**	$[0.0482 \times 10^{-5}]$ **(0.568)**	[0.130]

Therefore, (R^2) for A_4 (SD) represents the adjusted correlation coefficient for the MLR model and Equation (3), while (R^2) for A_5 (Elevation) represents the adjusted correlation coefficient for the MLR model and Equation (4).

The MLR models improve the correlation compared with the single linear regression for intra-annual temporal dependence (A_1), especially for those with a low adjusted R^2, such as the Renclusa and Eriste TNMs. The adjusted R^2 ranges from 0.54 for the Bachimaña TNM to 0.83 for the Ordiceto TNM. The seasonal accumulated precipitation (PPacum) improves the correlation for the Quimboa and Ordiceto TNMs. The 7-day average temperature (Tave7d) plays a key role in describing SDEN for the Renclusa TNM and influences SDEN moderately for the Izas and Eriste TNMs. SD had an important effect in describing SDEN for the Bachimaña, Renclusa and especially the Eriste TNMs, and consequently, in the overall set of TNMs. The set of TNMs shows an adjusted R^2 of 0.57. However, adding elevation showed very little improvement, as the SD and elevation had a great collinearity.

4. Discussion and Conclusions

The temporal and spatial variability of snow density (SDEN) were studied in this paper, using the biggest SDEN data bank for on-site manual samples and automatic measurements in the Spanish Pyrenees. More than 375 manual samples and 21,000 automatic TNM data from the ERHIN program and Ebro Water Authority were used to define SDEN variability in the Spanish Pyrenees. Single and multiple linear regressions were conducted, relating SDEN with the time dependence and other drivers such as the seasonal accumulated precipitation, average temperatures, snow depth (SD) and elevation.

The automatic measurements (TNMs) provided a better description of SDEN variability than the manual SDEN sampling, as the data volume was about 20 times larger.

For both the manual samples and the TNM data, the average SDEN values and the C.V. were very similar, not following a spatial pattern. This similarity was proven as well for the set of manual samples and the set of TNM measurements. Additionally, the C.V. for the winter snow was usually larger than that of the spring snow. The Izas TNM showed similar SDEN values compared with previous works, with 0.2 and 0.3 kg/L during the

first months and increasing to 0.6 kg/L at the end of the season [30]. However, it should be noted that similar values for the average and the C.V. are not representative of SDEN variability, either temporally or spatially.

Intra-annual time dependence was shown to be the predominant driver for almost all TNM sites. The densification rates ranged widely from 0.7×10^{-3} kg/L/day to 2×10^{-3} kg/L/day, without showing a spatial pattern, being 1.3×10^{-3} kg/L/day for the data from the set of TMNs. The densification rate for the set of manual samples was set to 1.2 kg/L/day, which is very similar to the automatic measurements. The densification rates were higher than those estimated for alpine regions in the former Soviet Union and the US, with average spring SDENs (kg/L) and snow densification rates (kg/L/day) of 0.25 kg/L and 0.79×10^{-3} kg/L/day, respectively, for the former Soviet Union and 0.31 kg/L and 1.07×10^{-3} kg/L/day, respectively, for the US. [37].

The seasonal accumulated precipitation presented a more dominant influence than daily precipitation, being the second most dominant SDEN driver for all sites except two. Historical behaviour showed a greater influence than daily behaviour. The third most important driver was the temperature. The 7-day average temperatures showed the best fitting to SDEN. Snow densification depends on punctual temperatures for the accumulation process, but during melting cycles, average temperatures may describe it better [33]. SD was found to be less significant. For low SD, both low and high SDEN can be found, depending on an early season dominated by accumulation processes or a late season dominated by melting processes [33,36]. For the early season, SDEN will depend on the proportion of precipitation falling as rain and snow, so it is also possible to reach high SDEN values. However, the significance threshold of SDEN is distinctly reduced for high SD values. SDEN for the late-season snow shows higher values than the early-season snow for maximum SD as densification continues, even though the SD may keep similar values for a certain period.

The established significance order for the drivers matched with previous studies, where precipitation was the dominant climate variable at most sites, followed by the average temperature and melt-refreeze (MRF) events [37].

Multiple Linear Regression (MLR) models were created for the automatic TNM measurements and were compared with the manual samples. The predictors were added progressively from more to less dominant. Elevation was added as a predictor for the set of TMNs series, showing that the SD was enough to describe that component of SDEN variability. The adjusted R^2 ranged from 0.54 for the Bachimaña TNM to 0.83 for the Ordiceto TNM, and the set of TNMs showed an adjusted R^2 of 0.57.

These correlation coefficients were higher than the adjusted R^2 found for single linear regressions based on its time evolution, both for the manual samples and the automatic TNM data, with the adjusted R^2 ranging from 0.27 for Eriste to 0.73 for Ordiceto and 0.44 for the set of TNMs. This greater correlation means the existence of variability in SDEN can be explained by meteorological drivers, which are highly variable in time and space.

The R^2 values are similar to those obtained in the central Spanish Pyrenees, although the scale of work was different [40], and to those for spring snow in Alpine regions of the former Soviet Union and the US (R^2 = 0.68) [37]. These R^2 were obtained using MLR models with five variables (Precipitation, interactive SDmax * Temp, Cooling Degree Day, Latitude and Elevation). In the Swiss Alps, according to three elevation range classes ($\geq$2000 m, $\geq$1400 and <2000 m, <1400 m) and 12 seasonal classes (months), SDEN was fitted to the SD with the R^2 values ranging from 0.02 to a maximum of 0.58 [36].

The results presented in Table 6 show that, in order to increase the available data and reduce uncertainties to enlarge the knowledge of SDEN in the Spanish Pyrenees, further revision and calibration should be carried out on TNMs 3 (Canal Roya), 5 (Lapazosa), 10 (Airoto) and 11 (Aixeus). The last two are essential to represent spatial variability due to the Mediterranean climate. Other TNMs, such as numbers 8 (Salenques), 14 (Sarrios-Formigal) and 15 (Besurta), should enlarge their data bank to be representative and contribute to

similar studies. Good maintenance of the meteorological network is crucial for reducing outliers, gaps or false nulls and the undervaluation of precipitation.

The validation of these SDEN regressions could be done in other Spanish mountainous areas or other regions with similar or different climates. Results regarding the eastern locations should fit better for the Atlantic Climate (the Quimboa TNM), while those regarding western locations should fit better for the Mediterranean Climate (Eriste), although no spatial patterns were observed.

The results contribute to enlarging the knowledge of SDEN in the Pyrenees and enable it to be described in a more accurate way. The SDEN regression models that are given in this work may allow us in the future to estimate SDEN, and consequently SWE, using an economical and extensive SD and meteorological network, although the high spatial variability that has been found must be taken into account. Additionally, these SDEN regression models can be implemented in hydrological snow models to describe more complex snow transport or forced-convection phenomena now that wind velocities are increasingly more available. Estimating a relationship between SDEN and several climate drivers allows for the impact of climate variability on SDEN to be taken into account.

Supplementary Materials: The following are available online at https://www.mdpi.com/article/10.3390/w13111598/s1.

Author Contributions: Conceptualization, E.L. and G.C.; methodology, E.L.; project administration, G.C.; software, E.L.; validation, G.C.; formal analysis, E.L.; writing—original draft preparation, E.L. and J.G.-R.; writing—review and editing, E.L. and G.C.; visualization, F.J.T.; supervision, F.J.T. All authors have read and agreed to the published version of the manuscript.

Funding: This research received no external funding.

Institutional Review Board Statement: Not applicable.

Informed Consent Statement: Not applicable.

Data Availability Statement: Data is contained within article and supplementary material.

Acknowledgments: The authors acknowledge F. Pastor and F. J. Sánchez (Spanish Ministry for Ecological Transition and the Demographic Challenge); M. L. Moreno (Ebro Water Authority); the Ebro Water Authority and field engineers A. Pedrero-Muñoz and M. Motes (SPESA Ingenieria). The authors fully acknowledge the financial support provided by the Department of Geological and Geotechnical Engineering of the UPV.

Conflicts of Interest: The authors declare no conflict of interest.

References

1. Morán-Tejeda, E.; Fassnacht, S.R.; Lorenzo-Lacruz, J.; López-Moreno, J.I.; García, C.; Alonso-González, E.; Collados-Lara, A.-J. Hydro-Meteorological characterization of major floods in Spanish mountain rivers. *Water* **2019**, *11*, 2641. [CrossRef]
2. López-Moreno, J.I.; García-Ruiz, J.M. Influence of snow accumulation and snowmelt on streamflow in the central Spanish Pyrenees/Influence de l'accumulation et de la fonte de la neige sur les écoulements dans les Pyrénées centrales espagnoles. *Hydrol. Sci. J.* **2004**, *49*. [CrossRef]
3. Morán-Tejeda, E.; Lorenzo-Lacruz, J.; López-Moreno, J.I.; Rahman, K.; Beniston, M. Streamflow timing of mountain rivers in Spain: Recent changes and future projections. *J. Hydrol.* **2014**, *517*, 1114–1127. [CrossRef]
4. Mandal, S.T.; Sharma, M.C. Spatial changes in glaciers between 1965 and 2018 in Tirungkhad Watershed, Upper Sutlej Basin, Himachal Pradesh. *Earth Syst. Environ.* **2020**, *4*, 427–438. [CrossRef]
5. Corripio, J.G.; López-Moreno, J.I. Analysis and predictability of the hydrological response of mountain catchments to heavy rain on snow events: A case study in the Spanish pyrenees. *Hydrology* **2017**, *4*, 20. [CrossRef]
6. Mellor, M. *Snow and Ice on the Earth's Surface*; Report II—C1; Cold Regions Research and Engineering Laboratory: Hanover, NH, USA, 1964.
7. Sommerfeld, R.A.; LaChapelle, E. The classification of snow metamorphism. *J. Glaciol.* **1970**, *9*, 3–17. [CrossRef]
8. Gartska, W.U. Snow and snow survey. In *Handbook of Applied Hydrology*; Chow, V.T., Ed.; McGraw-Hill: New York, NY, USA, 1964; Section 10; pp. 10–12.
9. Anderson, E.A. *A Point Energy and Mass Balance Model of a Snow Cover*; US Department of Commerce, National Oceanic and Atmospheric Administration, National Weather Service, Office of Hydrology: Silver Spring, MA, USA, 1976.

10. Gray, D.M.; Male, D.H. *Handbook of Snow, Principles, Processes, Management & Use*; Pergamon Press, Inc.: Westchester County, NY, USA, 2004.
11. Dingman, L. *Physical Hydrology*, 2nd ed.; Prentice Hall: Hoboken, NJ, USA, 2002.
12. Colbeck, S.C. An overview of seasonal snow metamorphism. *Rev. Geophys. Space Phys.* **1982**, *20*, 45–61. [CrossRef]
13. Akitaya, E. Studies on depth hoar. *Contrib. Inst. Low Temp. Sci.* **1974**, *26*, 1–67.
14. Armstrong, R.L. An analysis of compressive strain in adjacent temperature-gradient and equi-temperature layers in a natural snow cover. *J. Glaciol.* **1980**, *26*, 283–289. [CrossRef]
15. Anderson, E.A. Development and testing of snow pack energy balance equations. *Water Resour. Res.* **1968**, *4*, 19–37. [CrossRef]
16. Anderson, E.A. *Snow Accumulation and Ablation Model—SNOW 17*; US Department of Commerce, National Oceanic and Atmospheric Administration, National Weather Service, National Weather Service River Forecast System: Newburyport, MA, USA, 2006; p. 61.
17. Lantarón, J.H. Modelo Físico de Acumulación y Fusión de la Nieve. Aplicación en Sierra Nevada (España). Ph.D Thesis, University of Granada, Granada, Spain, November 2007.
18. Brun, E. Investigation on wet-snow metamorphism in respect of liquid-water content. *Ann. Glaciol.* **1989**, *13*, 22–26. [CrossRef]
19. Bilello, M.A. *Regional and Seasonal Variations in Snow-Cover Density in the U.S.S.R. [Microform]/Michael A. Bilello (No. CRREL Report RR 84-22)*; US Army Corps of Engineers, Cold Regions Research & Engineering Laboratory: Washington, DC, USA, 1984.
20. Onuchin, A.A.; Burenina, T.A. Climatic and geographic patterns in snow density dynamics. *North. Eurasia. Arct. Alp. Res.* **1996**, *28*, 99–103. [CrossRef]
21. Sturm, M.; Holmgren, J. Differences in compaction behavior of three climate classes of snow. *Ann. Glaciol.* **1998**, *26*, 125–130. [CrossRef]
22. Kershaw, G.P.; McCulloch, J. Midwinter snowpack variation across the Arctic treeline, Churchill, Manitoba, Canada. *Arct. Antarct. Alp. Res.* **2007**, *39*, 9–15. [CrossRef]
23. Meløysund, V.; Leira, B.; Høiseth, K.V.; Lisø, K.R. Predicting snow density using meteorological data. *Meteorol. Appl.* **2007**, *14*, 413–423. [CrossRef]
24. Paquet, E.; Laval, M.; Basalaev, L.M.; Belov, A.; Eroshenko, E.; Kartyshov, V.; Struminsky, A.; Yanke, V.L. An application of cosmic-ray neutron measurements to the determination of the snow water equivalent. In Proceedings of the 30th International Cosmic Ray Conference, Merida, Mexico, 3–11 July 2007; Universidad Nacional Autónoma de México: Mexico City, Mexico, 2008.
25. Kodama, M.; Nakai, K.; Kawasaki, S.; Wada, M. An application of cosmic-ray neutron measurements to the determination of the snow-water equivalent. *J. Hydrol.* **1979**, *41*, 85–92. [CrossRef]
26. Kinar, N.J.; Pomeroy, J.W. Automated determination of snow water equivalent by acoustic reflectometry. *IEEE Trans. Geosci. Remote Sens.* **2009**, *47*, 3161–3167. [CrossRef]
27. Alonso, R.; del Pozo, J.M.G.; Buisán, S.T.; Álvarez, J.A. Analysis of the snow water equivalent at the AEMet-formigal field laboratory (Spanish Pyrenees) during the 2019/2020 winter season using a stepped-frequency continuous wave radar (SFCW). *Remote Sens.* **2021**, *13*, 616. [CrossRef]
28. Collados-Lara, A.J.; Pulido-Velázquez, D.; Pardo-Igúzquiza, E.; Alonso-González, E. Estimation of the spatiotemporal dynamic of snow water equivalent at mountain range scale under data scarcity. *Sci. Total Environ.* **2020**, *41*, 140485. [CrossRef]
29. López-Moreno, J.I.; Nogués-Bravo, D. Interpolating local snow depth data: An evaluation of methods. *Hydrol. Process.* **2006**, *20*, 2217–2232. [CrossRef]
30. López Moreno, J.I.; Quirós, B.A.; Latron, J.; Fassnacht, S.R. Instalación y uso de un colchón de nieve para la monitorización del manto de nieve, cuenca experimental de Izas (Pirineo Central). *Geogr. Res. Lett.* **2010**, *36*, 73–82. [CrossRef]
31. Anderton, S.P.; White, S.M.; Alvera, B. Evaluation of spatial variability in snow water equivalent for a high mountain catchment. *Hydrol. Process.* **2004**, *18*, 435–453. [CrossRef]
32. Elder, K.; Dozier, J.; Michaelsen, J. Snow accumulation and distribution in an Alpine watershed. *Water Resour. Res.* **1991**, *27*, 1541–1552. [CrossRef]
33. Mizukami, N.; Perica, S. Spatiotemporal characteristics of snowpack density in the mountainous regions of the western United States. *J. Hydrometeorol.* **2008**, *9*, 1416–1426. [CrossRef]
34. Rohrer, M.; Braun, L.N.; Lang, H. Long-term records of snow cover water equivalent in the Swiss Alps: 1. analysis. *Nord. Hydrol.* **1994**, *25*, 53–64. [CrossRef]
35. Brown, R.D. Northern Hemisphere snow cover variability and change, 1915–1997. *J. Clim.* **2000**, *13*, 2339–2355. [CrossRef]
36. Jonas, T. Estimating the snow water equivalent from snow depth measurements in the Swiss Alps. *J. Hydrol.* **2009**, *378*, 161–167. [CrossRef]
37. Bormann, K.J.; Westra, S.; Evans, J.P.; McCabe, M.F. Spatial and temporal variability in seasonal snow density. *J. Hydrol.* **2013**, *484*, 63–73. [CrossRef]
38. Alonso-González, E.; López-Moreno, J.I.; Gascoin, S.; García-Valdecasas Ojeda, M.; Sanmiguel-Vallelado, A.; Navarro-Serrano, F.; Revuelto, J.; Ceballos, A.; Esteban Parra, M.J.; Essery, R. Daily gridded datasets of snow depth and snow water equivalent for the Iberian Peninsula from 1980 to 2014. *Earth Syst. Sci. Data* **2018**, *10*, 303–315. [CrossRef]
39. Essery, R. A factorial snowpack model (FSM 1.0). *Geosci. Model Dev.* **2015**, *8*, 3867–3876. [CrossRef]

40. López-Moreno, J.I.; Fassnacht, S.R.; Heath, J.T.; Musselman, K.N.; Revuelto, J.; Latron, J.; Morán-Tejeda, E.; Jonas, T. Small scale spatial variability of snow density and depth over complex alpine terrain: Implications for estimating snow water equivalent. *Adv. Water Resour.* **2013**, *55*, 40–52. [CrossRef]
41. Navarro-Serrano, F.M.; López-Moreno, J.I. Spatio-temporal analysis of snowfall events in the Spanish Pyrenees and their relationship to atmospheric circulation. *Geogr. Res. Lett.* **2007**, *43*, 233–254.
42. Cobos, G.; Frances, M.; Arenillas, M. Le programme ERHIN. Modélisation nivo-hydrologique pour la gestion de l'eau du Bassin De l'Ebre. The ERHIN programme. Hydrological-nival modelling for the management of water resources in the Ebro Basin. *La Houille Blanche* **2010**, *3*, 58–64. [CrossRef]
43. Serreze, M.C.; Clark, M.P.; Armstrong, R.L.; McGinnis, D.A.; Pulwarty, R.S. Characteristics of the western United States snowpack telemetry (SNOTEL) data. *Water Resour. Res.* **1999**, *35*, 2145–2160. [CrossRef]
44. Arenillas, M.; Cobos, G.; Navarro, J. Datos sobre la nieve y los glaciares en las cordilleras españolas. In *El Programa ERHIN (1984 a 2008)*; Ministerio de Obras Públicas y Transporte—MOPT: Madrid, Spain, 2008.
45. Dixon, D.; Boon, S. Comparison of the SnowHydro snow sampler with existing snow tube designs. *Hydrol. Process.* **2012**, *26*, 2555–2562. [CrossRef]
46. World Meteorological Organization. *Guide to Instruments and Methods of Observation. Volume II: Measurement of Cryospheric Variables, 2018 ed.*; WMO: Geneva, Switzerland, 2018.
47. Farnes, P.F.; Goodison, B.E.; Peterson, N.R.; Richards, R.P. Metrication of manual snow sampling equipment. In Proceedings of the 50th Annual Meeting, Western Snow Conference, Reno, NV, USA, 19–23 April 1982.
48. López-Moreno, J.I.; Leppänen, L.; Luks, B.; Holko, L.; Picard, G.; Sanmiguel-Vallelado, A.; Alonso-González, E.; Finger, D.C.; Arslan, A.N.; Gillemot, K.; et al. Intercomparison of measurements of bulk snow density and water equivalent of snow cover with snow core samplers: Instrumental bias and variability induced by observers. *Hydrol. Process.* **2020**, *34*, 3120–3133. [CrossRef]

Appendix 3 – Analysis of Climate Change's Effect on Flood Risk. Case Study of Reinosa in the Ebro River Basin

Lastrada, E.; Cobos, G.; Torrijo, F.J. Analysis of Climate Change's Effect on Flood Risk. Case Study of Reinosa in the Ebro River Basin. Water 2020, 12, 1114. https://doi.org/10.3390/w12041114

water

MDPI

Article

Analysis of Climate Change's Effect on Flood Risk. Case Study of Reinosa in the Ebro River Basin

Eduardo Lastrada *, Guillermo Cobos and Francisco Javier Torrijo

Department of Geotechnical Engineering, Universitat Politècnica de València, 46022 Valencia, Spain; gcobosc@trr.upv.es (G.C.); fratorec@trr.upv.es (F.J.T.)

* Correspondence: edlasmar@aaa.upv.es

Received: 27 February 2020; Accepted: 7 April 2020; Published: 14 April 2020

Abstract: Floods are one of the natural hazards that could be most affected by climate change, causing great economic damage and casualties in the world. On December 2019 in Reinosa (Cantabria, Spain), took place one of the worst floods in memory. Implementation of DIRECTIVE 2007/60/EC for the assessment and management of flood risks in Spain enabled the detection of this river basin with a potential significant flood risk via a preliminary flood risk assessment, and flood hazard and flood risk maps were developed. The main objective of this paper is to present a methodology to estimate climate change's effects on flood hazard and flood risk, with Reinosa as the case study. This river basin is affected by the snow phenomenon, even more sensitive to climate change. Using different climate models, regarding a scenario of comparatively high greenhouse gas emissions (RCP8.5), with daily temperature and precipitation data from years 2007–2070, and comparing results in relative terms, flow rate and flood risk variation due to climate change are estimated. In the specific case of Reinosa, the MRI-CGCM3 model shows that climate change will cause a significant increase of potential affected inhabitants and economic damage due to flood risk. This evaluation enables us to define mitigation actions in terms of cost–benefit analysis and prioritize the ones that should be included in flood risk management plans.

Keywords: climate model projections; flood risk; flood hazard; Reinosa; climate change prioritization

1. Introduction

Floods are natural hazards that produce great material damage and human losses worldwide [1]. The increasing population density and infrastructure on river banks contribute to increased floodplain vulnerability, which can result in severe social, economic and environmental damage [2].

The fourth of the nine essential rules of flood risk management indicates that it should be taken into account that "The future will be different from the past. Climate and societal change as well as changes in the condition of structures can all profoundly influence flood risk" [3].

For all these reasons, it is essential to design methodologies that enable one to estimate flow regime variations and evaluate flood risk modification due to climate change. [4–6].

The technical document of the IPCC IV forecasts a probable increase in the frequency and intensity of precipitation episodes, as well as a decrease in average values in summer for mid-latitudes countries as Spain. The Fifth Assessment Report (AR5) of the IPCC (2013–14), points out that it is probable that the frequency or intensity of intense rainfall has increased in Europe, and in relation to future changes, that extreme precipitation events over most of the mid-latitude lands will most likely be more intense and more frequent [7]. Additionally, climate change can specially affect those regions in which the snow phenomenon is relevant in hydrological behavior.

As a matter of these facts, the 2019 flash flood European notifications beat the last 7 years of notifications clearly [8], and Reinosa (Cantabria, Spain) suffered two important floods on January and

December 2019, the second one being one of the worst floods in memory. This flood was caused by the Elsa storm, on December 19 and 20, which came from the southwest and was accompanied by very strong winds and very high temperatures for that time of the year, causing the melting of the snow-cover in the highest part of the catchment. A203 gauging station, recorded on 20 December 2019 at 1:00 a.m., 246 m^3/s instant (15 minutes period) flow, while the maximum ever recorded was 100 m^3/s (27 February 2010). The daily flow rate recorded by A203 for this event was 83 m^3/s and the return period has been estimated approximately as Tr = 300 years. This flood caused great damage in Reinosa, affecting residential areas (Figure 1).

Figure 1. Reinosa (Cantabria, Spain). 20th December 2019.

Reinosa (Cantabria, Spain) is located in the north of the Iberian Peninsula, in the junction of Hijar, Ebro and Izarilla rivers, immediately upstream the Ebro reservoir. Hijar catchment, with 27.6 km length and 147.6 km^2 surface, drains the highest area of Cantabrian mountain range that belongs to the Ebro river basin. The catchment height ranges between 865 and 2023 m above sea level, with a mean height of 1351 m. A203 gauging station is located in Hijar River, immediately upstream of Reinosa, with a time of concentration of approximately 15 hours.

The average rainfall of the head of the Ebro for the period 1920–2002 was 1190 mm/year, concentrated in autumn and winter, characteristic of an Atlantic climate, with some continental patterns producing 33 $L/s/km^2$. The average annual temperature is 8.9 °C in Reinosa. The main land uses in the catchment are forest and scrub. Figure 2 shows Hijar river basin overall and site map.

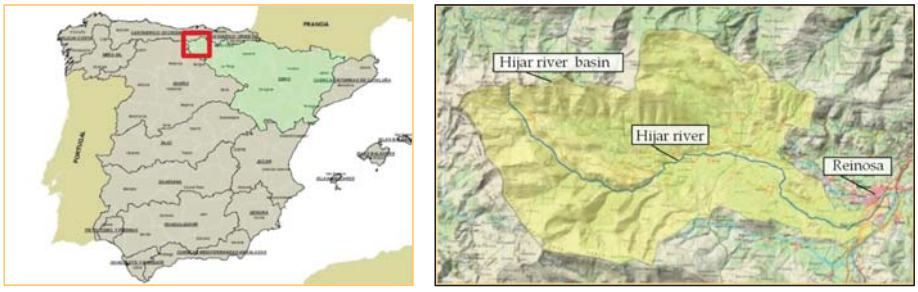

(**a**) (**b**)

Figure 2. Hijar river basin. (**a**) Overall Site map. (**b**) Detailed Site map.

Reinosa belongs to the Hijar river basin, and had potential significant flood risk (ES091_HIJ_01_02_04_05_06) during the implementation of DIRECTIVE 2007/60/EC, as shown in Figure 3.

Figure 3. Hijar potential significant flood risk (ES091_HIJ_01_02_04_05_06). http://iber.chebro.es/SitEbro/sitebro.aspx.

DIRECTIVE 2007/60/EC implies an objective quantification of flood risk, for low (500 years return period), medium (100 years return period) and high probabilities (10 years return period), that will allow the efficient development of flood risk management plans by implementing a set of combined actions to reduce floods' consequences [9].

To evaluate different climate change scenarios, the Spanish Meteorological Agency (AEMET) regionalized a set of global climate models, by using two statistical downscaling methods. The usefulness of this regionalization was assessed by their fitting to the observed data in the control period (1961–2000). A comparison based on a set of statistics show that although the fit is good for annual mean values, annual maximum values for both regionalization methods are not adequately simulated, since they provide lower extremes with a smaller variability. However, different fitting was observed depending on the Spanish region [10].

Although results might show a decrease in the magnitude of extreme floods for climate model projections downscaled by AEMET [11], a different pattern might be concluded, when taking into account snowmelt, if the melting flow rate's increase due to higher temperatures is bigger than the decrease caused by less snow accumulation.

The main aim of the work is to estimate flow and flood risk variation due to climate change by using different climate models regarding a scenario of comparatively high greenhouse gas emissions (RCP8.5), with daily temperature and precipitation data.

2. Materials and Methods

2.1. Overall Methodology

According to DIRECTIVE 2007/60/EC, Spanish hazard and flood risk maps can be downloaded at https://sig.mapama.gob.es/snczi/, regarding the following scenarios: (a) floods with a low probability, or extreme event scenarios (return period ≥ 500 years); (b) floods with a medium probability (likely return period ≥ 100 years); (c) floods with a high probability (return period ≥ 10 years).

By relating flow rates in A203 gauging station with hazard and risk maps, correlations with flooding surface, economic damage and casualties can be achieved.

In order to evaluate climate change, projections of a series of climatic variables are entered as input data in a calibrated hydrological model in the study basin. The ASTER®model is a distributed hydrological model that calculates snowmelt and accumulation regarding energy balance [12,13]

Two global climate models (GCM), downscaled by the Spanish Meteorological Agency (AEMET), have been selected; we validated them with real flow rates from the control period (1961 to 2000) and used under the highest greenhouse gas emissions pathway (RCPs 8.5) from the Fifth Assessment Report of the Intergovernmental Panel on Climate Change.

The relationship between calculated daily flow rates and instant (15 minutes period) flow rates is not necessary for these downscaled climate models, as climate change's effect will be calculated in relative terms comparing climate models in the calculation period in two equal length stages (2007–2038) and (2039–2070).

Once the flow rate variation for the climate projection is estimated and applied on real flow, new impacts on hazard and risk maps can be established. Figure 4 shows the overall methodology scheme.

Figure 4. Overall methodology scheme.

2.2. *Hazard and Risk Maps*

Hazard maps are the result of two-dimensional hydraulic models, indicating flooded area, flood depths and flood velocities. Return periods were given by Spanish Authority in the framework of DIRECTIVE 2007/60/EC implementation by "Maximum Flow Maps" software, based on a regionalized gauging station study [14].

Flood risk maps shall show the potential adverse consequences associated with flood scenarios, and express, among other things, terms of the indicative numbers of inhabitants potentially affected and the type of economic activity of each area potentially affected. Additionally, economic damage can be estimated.

According to DIRECTIVE 2007/60/EC, these maps serve as a tool for establishing priorities and for making additional technical, economic and political decisions related to flood risk management. Measures to be implemented in the at-risk areas can be prioritized, depending on the results of the cost-benefit analysis. They also allow us to evaluate climate change's effects. The risk associated with flood events is established based on the vulnerability of the threatened element and the hazard to which it is exposed. The estimation of indicative number of inhabitants potentially affected depends on updated census data. The Spanish Water Authority has also established a methodology to estimate the economic value of flood damage partially based on the PREEMPT project [15,16].

Finally, a relationship, as shown in Table 1, between flow rates for different return periods in Hijar, A203, and hazard and risk maps can be estimated, and subsequently a trend line, as shown in Figure 5, can be fitted:

Table 1. Instant (15 minute) flow rate, flood surface, inhabitants potentially affected and economic damage [1].

Instant Flow Rate (m^3/s)	Return Period (years)	Surface (km^2)	Inhabitants	Economic Value (€)
138	10	2.783	346	29,194,901
214	100	3.843	982	56,806,383
273	500	4.620	1484	90,791,074

[1] Obtained for overall ES091_HIJ_01_02_04_05_06 potential significant flood risk area, including the Spanish Public Water Domain (RDPH).

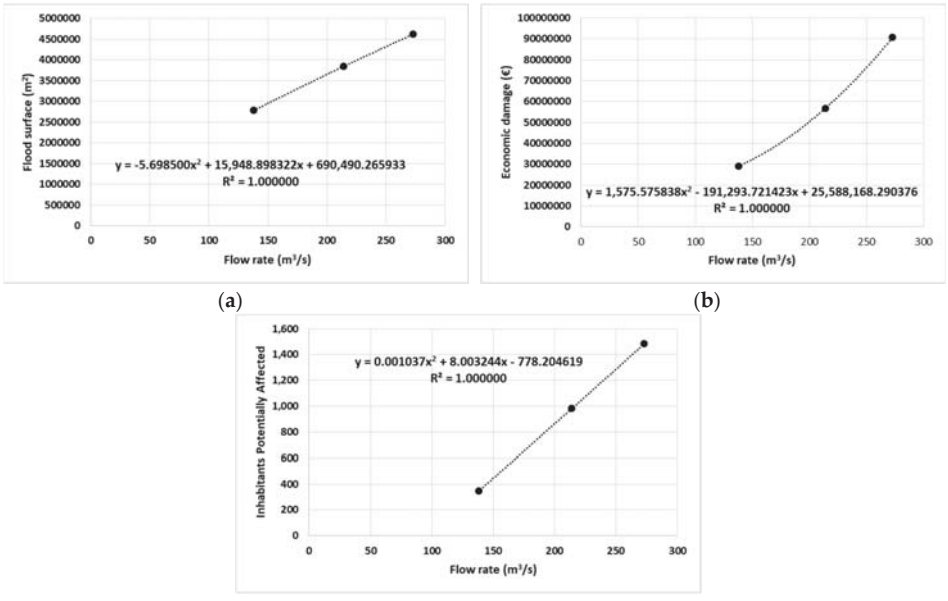

Figure 5. (**a**) Flood surface, (**b**) inhabitants potentially affected and (**c**) economic damage value in terms of flow rate in A203 gauging station.

2.3. Hydrological Model

2.3.1. Hijar Basin Model

A 500 by 500 m grid and daily time resolution distributed hydrological model has been built for the Hijar river basin (Figure 6), with A203 gauging station in Reinosa as the outlet and calibration point, 2014–2016 as the calibration period and 2017–2019 as the validation period.

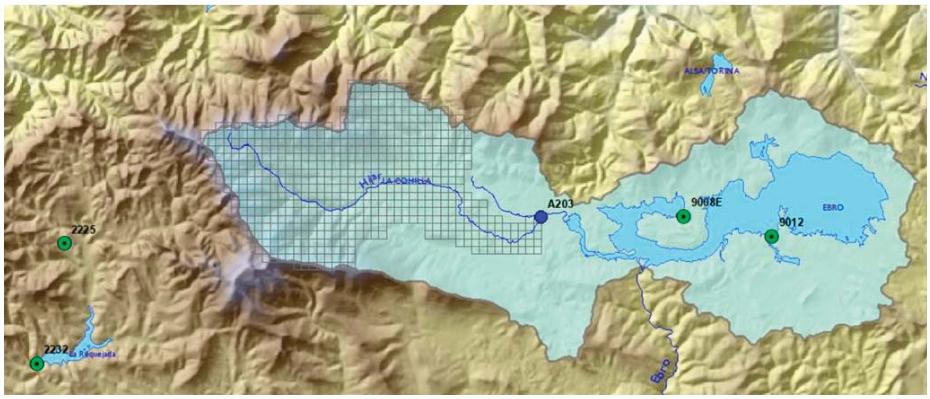

Figure 6. ASTER hydrological model. Hijar river basin mesh (grey grid), Gauging Station (A203), rainfall stations (9008E, 9012) and temperature stations (2225, 2232).

ASTER®is a distributed hydrological model that calculates streamflow in a river using rainfall, temperature, windspeed and radiation as climate inputs. It has been applied in several countries and implemented by Spanish water authorities as an accurate model in river basins with strong snow phenomena, as in our case study (Hijar catchment) [17,18]. Figure 7 shows the snow–water equivalent for two consecutive days in Hijar model.

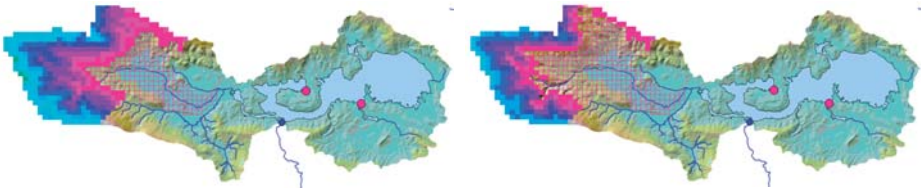

(**a**) (**b**)

Figure 7. ASTER hydrological model snow accumulation (snow–water equivalent) (**a**) Day 1, (**b**) Day 2. Hijar model (ranging from 1 mm–pink to 215 mm–cyan).

2.3.2. Snow Accumulation Routine

Precipitation will be snow or water form at different temperatures depending on several atmospheric conditions. This range of temperatures can vary between −2 and 2 °C. The model sets a temperature, named rain/snow temperature, at which 50% of precipitation is snow, with a bilineal increase and decrease of snow form up to −2 and 2 °C.

2.3.3. Snowmelt Routine

As aforementioned, snowmelt is calculated using the energy balance equation. Melting takes place when air temperature is below a specific temperature (T_{mi}—snowmelt temperature). Snowmelt can be divided into two types: (a) rainfall snowmelt; (b) no rainfall snowmelt.

Rainfall Snowmelt

It is the snowmelt produced by rainfall energy. Assuming that the snow surface temperature is equal to 0 °C (273 K), snowmelt caused by energy from rainfall is [19]:

$$M_r = 0.0125 \cdot P \cdot f_r \cdot T_r, \quad (1)$$

where:

P = Precipitation (mm)
f_r = fraction of precipitation in the form of rain
T_r = temperature of rain (°C)

In addition to energy from rainfall, other secondary terms as radiation and condensation energy must be added to calculate snowmelt when rain takes place.

No Rainfall Snowmelt

It is the snowmelt on a dry day. Due to difficulties estimating wind speed, hydrological models usually use non-forced convection or other empirical relations depending on air temperature. The following equation is used to estimate no rainfall melt M_c (mm) [20]:

$$M_c = M_f \cdot (T_a - T_{mi}) \quad (2)$$

where:

M_f = melt factor (mm/°C)
T_a = air temperature (°C)
T_{mi} = snowmelt temperature (°C)

This melt factor (M_f) indicates the seasonal variation, and can be represented with a sine function [21,22].

$$M_f = \frac{MFMAX + MFMIN}{2} + \sin\left(\frac{n * 2\pi}{366}\right) * \frac{MFMAX + MFMIN}{2} \quad (3)$$

where:

MFMAX = maximum melt factor on June 21st (mm/°C/24hrs)
MFMIN = minimum melt factor on December 21st (mm/°C/24hrs)
n = number of days from March 21st.

2.3.4. Model Calibration and Validation

Calibration and validation have been carried out, comparing real daily flow rates, in A203 Hijar in Reinosa Gauging Station with the ASTER model daily flow rates being calculated with real meteorological data. The available continuous period for the observed daily flow rate ranges from 2014 to 2019, defining the calibration period as October 1st 2014 to September 30th 2016 and the validation period from October 1st 2017 to December 22nd 2019, including the aforementioned extraordinary event.

Figure 8, shows results during the calibration period, with a correlation coefficient of 0.90 and a Nash index (NSE) of 0.78. The maximum observed daily flow rate was 23.6 m^3/s, and the maximum calculated daily flow rate was 23.5 m^3/s. Total observed runoff was 189 hm^3 and calculated runoff was 200.7 hm^3, with 27 hm^3 of overall snow–water equivalent accumulation.

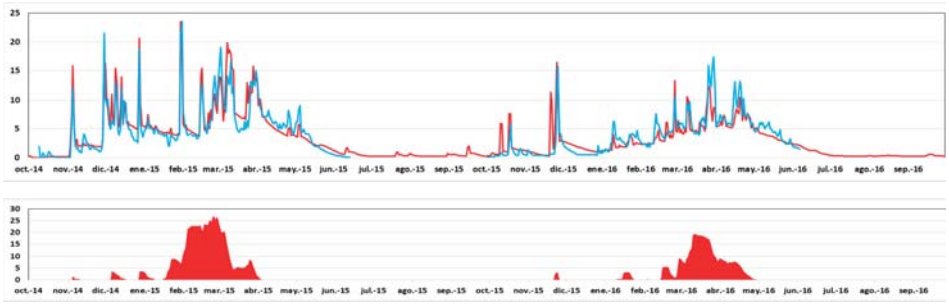

Figure 8. Upper level. Real (blue) and calculated (red) daily flow rates in A203. Lower level. Snow water equivalent in the catchment for the calibration period.

The main calibration parameters of the model are:

- MFMAX = 5.5 (mm/°C/24 h);
- MFMIN = 1.46 (mm/°C/24 h);
- T_{mi} = −0.35 (°C);
- Rain/Snow temperature = −0.53 (°C);
- Altimetry temperature gradient = −3.1 (°C/1000 m).

Figure 9 shows results during the validation period, with a correlation coefficient of 0.90 and a Nash index (NSE) of 0.80. The maximum observed daily flow rate was 83 m^3/s, and the maximum calculated daily flow rate was 69 m^3/s. Total observed runoff was 231 hm^3 and calculated runoff was 289 hm^3, with 20 hm^3 of overall snow–water equivalent accumulation.

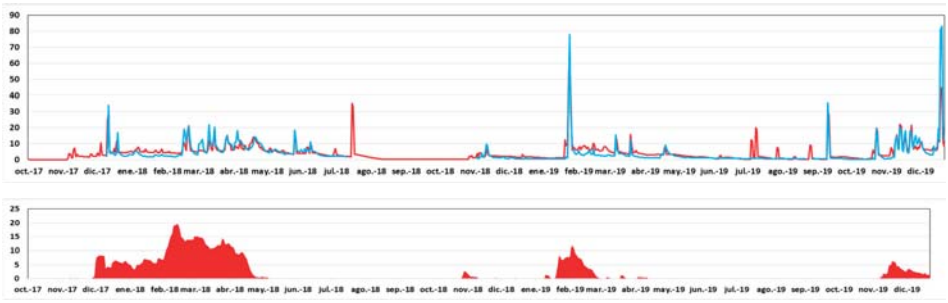

Figure 9. Upper level. Real (blue) and calculated (red) daily flow rates in A203. Lower level. Snow water equivalent in the catchment for the validation period.

2.4. Climate Projection

Daily rainfall and temperature data from two regionalized climate models (analog method—ANA and statistical regionalization method—SDSM) can be obtained from AEMET website (http://www.aemet.es/es/serviciosclimaticos/cambio_climat) for RCP 8.5.

Two climate models have been selected from 24, to analyze the combination of rainfall and temperature:

- ANA—BCC-CSM1-1-m (BCC);
- ANA—MRI-CGCM3 (MRI).

These two models have been pre-selected as generating the highest rainfalls. To evaluate their suitability, daily flow rates for the control period (1961–2000) have been calculated with ASTER for real

meteorological data and both climate models. Figure 10a shows that annual maximum real daily flow rates are above climate models, and the trend line shows a higher increase as well. Figure 10b shows that annual mean real daily flow rates fit the MRI better at the beginning of the control period, while a fit better with BCC is shown at the end of the control period. Supplementary Materials for rainfall stations (9008E, 9012) and temperature stations (2225, 2232) is given.

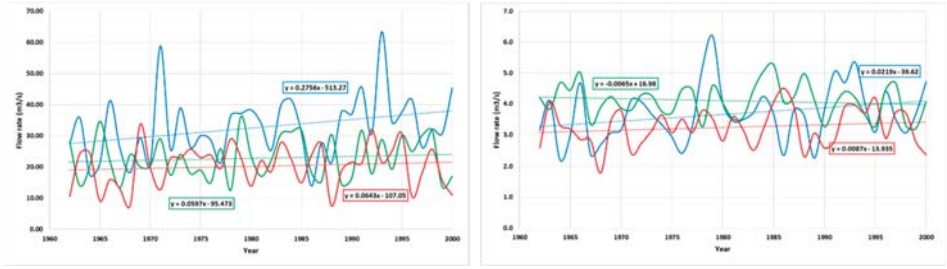

(**a**) (**b**)

Figure 10. Daily flow rate evolution during control period (1961–2000) for real data (blue), BCC (green) and MRI (red). (**a**) Annual maximum, (**b**) annual mean.

2.5. Calculation of Flow Rates for Different Return Periods

Daily flow rates for the calculation period (2007 to 2070) have been estimated with ASTER model for both climate projections (BCC and MRI). Calculation period has been divided in two equal length stages (2007 to 2038) and (2039–2070) and a probability distribution of extreme values has been estimated using the Gumbel distribution, presenting the best fit goodness:

$$X = u - \beta \cdot Ln\left(-Ln\left(\frac{Tr - 1}{Tr}\right)\right) \quad (4)$$

where:

u = location parameter;
β = scale parameter;
Tr = Return period.

Finally, daily flow rates and instant (15 minute period) flow rates observed in A203 can be fitted in a linear relationship. As climate projections flow rates are being studied in relative terms with observed flow rates, transformation from daily flow rates into instant flow rates is not necessary.

3. Results

3.1. Flow Rate Evolution (RCP 8.5)

Table 2 and Figure 11 show results and trend lines from percentile analysis for both calculated climate models. For BCC-CSM1-1-m a small decrease in flow rate projection due to climate change is estimated, with small variability for different probabilities, while for MRI-CGCM3 bigger increase is predicted, showing a smooth variability for different probabilities, describing a more extreme climate.

Table 2. Return period, daily flow rate projection, 1st Stage (2007–2038); daily flow rate projection ratio, 2nd Stage (2039–2070); and flow rate ratio (2nd Stage/1st Stage).

ANA—BCC-CSM1-1-m			
Tr (years)	**Flow Rate Projection 2007–2038 (m^3/s)**	**Flow Rate Projection 2039–2070 (m^3/s)**	**2039–2070/ 2007–2038 [1] (%)**
10	28.13	27.00	96.0%
25	31.92	30.62	95.9%
50	34.73	33.30	95.9%
100	37.52	35.96	95.9%
500	43.96	42.11	95.8%
ANA—MRI-CGCM3			
Tr (years)	**Flow Rate Projection 2007–2038 (m^3/s)**	**Flow Rate Projection 2039–2070 (m^3/s)**	**2039–2070/ 2007–2038 [1] (%)**
10	27.36	31.05	113.5%
25	31.99	36.51	114.1%
50	35.43	40.57	114.5%
100	38.85	44.59	114.8%

[1] Column 3 divided by column 2.

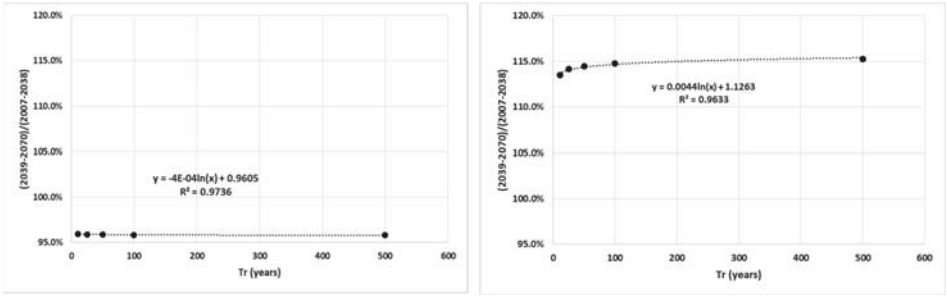

(**a**) (**b**)

Figure 11. Flow rate projection ratio (2nd Stage (2039–2070)/1st Stage (2007–2038)) trend line in terms of return periods. (**a**) Analog method (ANA)—BCC-CSM1-1-m; (**b**) ANA—MRI-CGCM3.

3.2. Hazard and Risk Maps

After calculating the projected flow rate by entering for each return period (2nd Stage (2039–2070)/1st Stage (2007–2038)) the flow rate ratio in the trend line fitted for flood surface, economic damage and inhabitants potentially affected (Figure 5), new climate change estimations show similar results as for flow rate (Table 3).

As for flow rate, the MRI-CGCM3 climate model shows an increase in flood risk effects due to climate change, while BCC-CSM1-1-m shows a decrease. Results are enlarged for economic value and inhabitants potentially affected, while flooded surface decreases.

A logarithmic trend line is the one that best fits, and represents how the atmosphere behaves that shows in Figures 12–14.

Table 3. Projection ratio 2nd Stage (2039–2070)/1st Stage (2007–2038) for the flow rate, flood surface, inhabitants potentially affected and flood damage's economic value.

ANA—BCC-CSM1-1-m					
Flow Rate (%)	**Instant Flow Rate (m^3/s)**	**Return Period (years)**	**Flood Surface (%)**	**Inhabitants (%)**	**Economic Value (%)**
−4.0	132.4	10	−2.9	−13.3	−4.5
−4.1	205.1	100	−3.1	−7.6	−7.3
−4.2	261.5	500	−3.2	−6.6	−8.2
ANA—MRI-CGCM3					
Flow Rate (%)	**Instant Flow Rate (m^3/s)**	**Return Period (years)**	**Flood Surface (%)**	**Inhabitants (%)**	**Economic Value (%)**
13.5	156.7	10	9.6	44.8	17.4
14.8	245.6	100	11.0	27.3	29.7
15.3	314.7	500	11.4	24.2	33.7

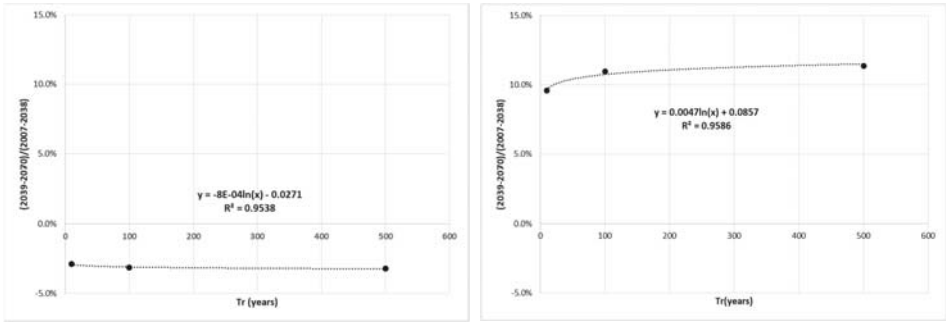

(**a**) (**b**)

Figure 12. Second Stage (2039–2070)/1st Stage (2007–2038) flood surface ratio trend line in terms of return periods. (**a**) ANA—BCC-CSM1-1-m; (**b**) ANA—MRI-CGCM3.

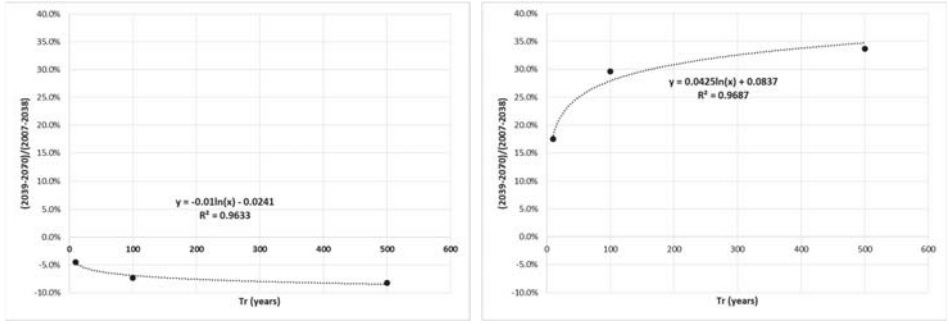

(**a**) (**b**)

Figure 13. Second Stage (2039–2070)/1st Stage (2007–2038) economic damage ratio trend line in terms of return periods. (**a**) ANA—BCC-CSM1-1-m; (**b**) ANA—MRI-CGCM3.

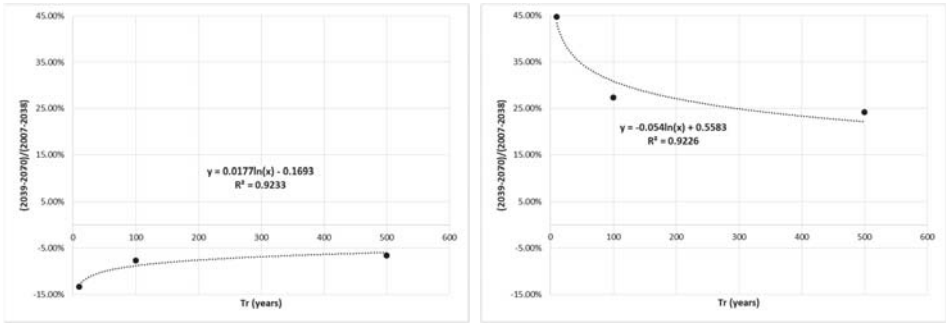

(**a**) (**b**)

Figure 14. Second Stage (2039–2070)/1st Stage (2007–2038) inhabitants potentially affected ratio trend line in terms of return periods. (**a**) ANA—BCC-CSM1-1-m; (**b**) ANA—MRI-CGCM3.

Flooded surface, inhabitants potentially affected and flood economic damage value can be calculated in absolute terms and are shown in Table 4 for ES091_HIJ_01_02_04_05_06.

Table 4. Absolute terms for the flow rate, flood surface, inhabitants potentially affected and flood damage's economic value for selected climate change projections [1].

ANA—BCC-CSM1-1-m				
Flow Rate (m^3/s)	**Return Period (years)**	**Surface (km^2)**	**Inhabitants**	**Economic Value (€)**
132.4	10	2.703	300	27,887,407
205.1	100	3.722	907	52,640,944
261.5	500	4.472	1386	83,327,840
ANA—MRI-CGCM3				
Flow Rate (m^3/s)	**Return Period (years)**	**Surface (km^2)**	**Inhabitants**	**Economic Value (€)**
156.7	10	3.049	501	34,286,399
245.6	100	4.263	1250	73,649,691
314.7	500	5.145	1843	121,426,897

[1] Obtained for overall ES091_HIJ_01_02_04_05_06 potential significant flood risk area, including the Spanish Public Water Domain (RDPH).

4. Discussion

4.1. Climate Change Effect

Comparison between observed meteorological data and projections of climate scenarios, for a common time interval, has revealed a significant difference between the series. This means that the results must in any case be interpreted in relative terms, evaluating trends and not absolute values.

Results for both selected climate models show important differences between each other in absolute and relative terms, indicating that there is significant uncertainty in the projections, especially due to rainfall; and they suggest that for local impact studies, further analysis to regionalize outputs from global climate models still needs to be done. For the results to be reliable, climate models must adequately represent extreme phenomena, as most of them are suitable for evaluating water resource evolution.

There is a large uncertainty in climate projections that influences the estimation of future flood risk. The crucial action in the case of adaptation to floods is to carry out a detailed analysis to choose

the best climate model and use results in relative terms between the short term (1st Stage) and long term (2nd Stage) of the projection period [4].

The proposed methodology allows one to determine in terms of hazard and flood risk, the effect that climate change has on a given territory, considering both variable rainfall and temperature, and enables a fast evaluation of various climate models and a comparison of their differences.

This evaluation enables one to define actions in terms of a cost–benefit analysis and prioritize the ones that should be included in flood risk management plans due to climate change, as these management plans must contain effective actions in the short, medium and long term and cannot ignore the effect of climate change.

In the specific case of Híjar River Basin, and Reinosa, MRI-CGCM3 model trend analysis shows that climate change will increase damage to society, both economic and personal, while BCC-CSM1-1-m shows a small decrease. As the MRI-CGCM3 model fits better with annual maximum real daily flow rates than BCC-CSM1-1-m, it can be concluded that climate change will cause a significant increase of potential affected inhabitants and economic damage due to flood risk that will require mitigation actions.

This assumption might match with previous years' observations, especially given the high number of low probability events recorded in Spain. This is the specific case of the Hijar River that in 2019 registered two floods, the one on December 2019 being the largest ever registered in Reinosa Gauging Station and related with a low probability event (300 years return period). This conclusion is consistent with the Fifth Assessment Report (AR5) of the IPCC (2013–14), which points out that it is likely that the frequency or intensity of intense rainfall has increased in Europe.

4.2. Future Research

As already mentioned, this methodology could be applied in every potential significant flood risk area through a water authority flood risk management plan in order to prioritize actions.

Firstly, all available regional climate models could be selected and evaluated. Finally, a sensitive RCP analysis with RCP 4.5 scenario could be carried out.

Supplementary Materials: The following are available online at http://www.mdpi.com/2073-4441/12/4/1114/s1. Spreadsheet1: Climate_Models_Input_Data.xlsm.

Author Contributions: Conceptualization, E.L. and G.C..; methodology, E.L. and G.C.; project administration, G.C.; software, E.L.; validation, G.C.; formal analysis, E.L.; writing—original draft preparation, E.L.; writing—review and editing, E.L. and G.C.; visualization, F.J.T.; supervision, F.J.T. All authors have read and agreed to the published version of the manuscript.

Funding: This research received no external funding.

Acknowledgments: The authors acknowledge ASTER model developer J. A. Collado (SPESA Ingenieria); F. J. Sanchez and M. Aparicio (Spanish Ministry for Ecological Transition and the Demographic Challenge); M. L. Moreno and L. Polanco (Ebro Water Authority); and the Ebro Water Authority.

Conflicts of Interest: The authors declare no conflict of interest.

References

1. EEA. *Mapping the Impacts of Natural Hazards and Technological Accidents in Europe*; EA Technical Report No 13/2010; European Environment Agency: Copenhagen, Denmark, 2010; Available online: http://www.eea.europa.eu/publications/mapping-the-impacts-of-natural (accessed on 10 January 2020).
2. Planes de Gestión del Riesgo de Inundación. Ministerio para la Transición Ecológica y el Reto Demográfico. Available online: https://www.miteco.gob.es/es/agua/temas/gestion-de-los-riesgos-de-inundacion/planes-gestion-riesgos-inundacion/ (accessed on 15 December 2019).
3. Yuanyuan, L.; Sayers, P.; Yuanyuan, L.; Galloway, G.; Penning-Rowsell, E.; Fuxin, S.; Kang, W.; Yiwei, C.; Quesne, T.L.; Asian Development Bank; et al. Flood Risk Management: A Strategic Approach. Available online: https://unesdoc.unesco.org/ark:/48223/pf0000220870 (accessed on 16 January 2020).

4. Doroszkiewicz, J.; Romanowicz, R.J.; Kiczko, A. The Influence of Flow Projection Errors on Flood Hazard Estimates in Future Climate Conditions. *Water* **2019**, *11*, 49. [CrossRef]
5. Zhu, T.; Lund, J.R.; Jenkins, M.W.; Marques, G.F.; Ritzema, R.S. Climate change, urbanization, and optimal long-term floodplain protection. *Water Resour. Res.* **2007**, *43*, 122–127. [CrossRef]
6. Nyaupane, N.; Thakur, B.; Kalra, A.; Ahmad, S. Evaluating Future Flood Scenarios Using CMIP5 Climate Projections. *Water* **2018**, *10*, 1866. [CrossRef]
7. Intergovernmental Panel on Climate Change. Available online: https://archive.ipcc.ch/ (accessed on 20 December 2019).
8. European Flood Awareness System (EFAS). Available online: https://www.efas.eu/en/news/summary-efas-notifications-2019 (accessed on 3 January 2020).
9. European Commission. Directive 2007/60/Ec of the European Parliament and of the Council of 23 October 2007 on the assessment and management of flood risks. *Off. J. L 288/27* **2007**, *8*, 27–34.
10. Garijo, C.; Mediero, L. Influence of climate change on flood magnitude and seasonality in the Arga River catchment in Spain. *Acta Geophys.* **2018**, *66*, 769–790. [CrossRef]
11. Garijo, C.; Mediero, L.; Garrote, L. Usefulness of AEMET generated climate projections for climate change impact studies on floods at national-scale (Spain). *Ingeniería del Agua* **2018**, *22*, 153–166. [CrossRef]
12. Cantarino, I. *Modelo *Aster. Fundamentos y Aplicación*; Ministerio de Medio Ambiente: Madrid, Spain, 1998.
13. Cobos, G.; Collado, J.A. ASTER. Modelo Hidrológico De Simulación Y Previsión Aplicado A Cuencas Donde El Fenómeno Nival Es Relevante. Manual De Usuario. Available online: http://www.spesa.es/paginas/basededatos/ASTER_Manual_Usuario.pdf (accessed on 27 December 2019).
14. Jiménez, A.; Montañés, C.; Mediero, L.; Incio, L.; Garrote, J. El Mapa De Caudales Máximos De Las Cuencas Intercomunitarias. *Revista De Obras Públicas* **2012**, *3533*, 7–32. Available online: https://www.miteco.gob.es/es/agua/temas/gestion-de-los-riesgos-de-inundacion/snczi/Mapa-de-caudales-maximos/ (accessed on 28 December 2019).
15. Propuesta de mínimos para la realización de los mapas de riesgo de inundación. *Directiva de inundaciones – 2° ciclo*; Ministerio para la Transición Ecológica: Madrid, Spain, 2019. Available online: https://www.miteco.gob.es/en/agua/temas/gestion-de-los-riesgos-de-inundacion/Metodologia%20mapas%20de%20riesgo%20Dir%20Inundaciones%20JULIO%202013_tcm38-98530.pdf (accessed on 29 December 2019).
16. Policy-Relevant Assessment of Socio-Economic Effects of Droughts and Floods, To Establish a Damage-Water Depth Relationship. Available online: http://www.feem-project.net/preempt/ (accessed on 29 December 2019).
17. Cobos, G. Cuantificación De Las Reservas Hídricas En Forma De Nieve Y Previsión En Tiempo Real De Los Caudales Fluyentes De La Fusión. Aplicación Al Pirineo Español: Cuenca Alta Del Río Aragón. Ph.D. Thesis, Universitat Politècnica de València, Valencia, Spain, 2004.
18. Cobos, G.; Frances, M.; Arenillas. The ERHIN Programme. Hydrological-Nival Modelling for the Management of Water Resources in the Ebro Basin. *La Houille Blanche* **2010**, *3*, 58–64. [CrossRef]
19. Anderson, E.A. Development and Testing of Snow Pack Energy Balance Equations. *Water Resour. Res.* **1968**, *4*, 19–37.
20. Anderson, E.A. *National Weather Service River Forecast System. Snow Accumulation and Ablation Model*; US Department of Commerce, National Oceanic and Atmospheric Administration, National Weather Service: Silver Spring, MA, USA, 1973.
21. Anderson, E.A. *A Point Energy and Mass Balance Model of a Snow Cover*; US Department of Commerce, National Oceanic and Atmospheric Administration, National Weather Service, Office of Hydrology: Silver Spring, MA, USA, 1976.
22. Anderson, E.A. *Snow Accumulation and Ablation Model—SNOW 17*; US Department of Commerce, National Oceanic and Atmospheric Administration, National Weather Service, National Weather Service River Forecast System: Newburyport, MA, USA, 2006; p. 61.